Western Norway University of Applied Sciences

Experimental and numerical investigation of the thermal ceiling jet thickness

Master Thesis in Fire Safety

Author: Nichlas Lyche	 Author sign.
Selected: Fall 2016	Open assignment
Supervisors: Bjarne Christian Hagen David Renè Ursin Johansen	

Keywords: Ceiling jet Ceiling jet thickness Experiment FDS Fire	Pages: 78 + Annex: 23 Haugesund, 01. June, 2017 Place/Date/Year

PREFACE

This thesis has been the final work in a master degree in Fire safety at the Western Norway University of applied sciences and is credited 60 ETC points.

The idea for this thesis came from my supervisor Dr. Bjarne Christian Hagen. The combination of experimental work and simulations was something I had wanted to do for a long time. The work on this thesis has been challenging and educational.

I would like to say special thanks to my two supervisors Dr. Bjarne Christian Hagen and PhD. student David René Ursin Johansen for their support and valuable guidance in this work. I would also like to thank fellow student for the past five years, Ruben Dobler Strand, for our great discussions and collaboration throughout the years and especially this last year.

SUMMARY

The ceiling jet is an important parameter associated with detection- and suppression systems in case of fires. The ceiling jet is often the first encounter with smoke for these systems. Properties in the ceiling jet such as temperature, velocity and ceiling jet thickness are therefore important properties to quantify.

In this study the thermal ceiling jet thickness have been investigated. Previous work has been specifically targeting weak driven ceiling jets, where the flame height is less than 30 % of the ceiling height. This investigation targeted the ceiling jet thickness of mainly strong driven ceiling jets, and how the thicknesses change as functions of the radial distance from the centerline of the fire plume. The behavior of the ceiling jet thickness was studied for different heat release rates, ceiling heights and burner sizes.

The ceiling jet thickness was investigated by conducting full scale experiments under a 2.44 m $\times$ 2.44 m ceiling. Based on a temperature criterion of 36.8 % of the maximum temperature in the ceiling jet thickness was measured by a total of 45 thermocouples at six different radial positions. A similar arrangement was simulated in FDS to see if simulations can be used for deciding the ceiling jet thickness.

From experiments the ceiling jet thickness was found to increase as the heat release rate of the fire increased. When the ceiling height was increased, the ceiling jet thickness was also found to increase. Simulation in FDS was found to support these trends. It was found that simulations in FDS underestimate the ceiling jet thickness from experiments. As the radius increase from 0.4 m to 1.65 m the ceiling jet thickness was found to increase 2 % of the ceiling height. Simulations in FDS showed that the ceiling jet thickness decreased by 2 % over the radial distance.

SAMMENDRAG

Røykjeten er en viktig faktor i forhold til deteksjon og slokkesystemer i forbindelse med brann. Den er ofte det første møte med røyk for disse systemene og det er derfor viktig å kvantifisere egenskaper som temperatur, hastighet og tykkelse på røykjeten.

I denne oppgaven har tykkelsen på den horisontale røykjeten blitt studert. Tidligere arbeid har blitt gjort på svak drevne røykjeter, der flammehøyden er mindre enn 30 % av takhøyden. Hovedsakelig har den sterk drevne røykjeten, flammehøyde > 30 %, blitt studert i denne oppgaven og hvordan denne oppfører seg som funksjon av radius fra senterlinjen av røyksøylen. Tykkelsen på røykjeten ble studert for ulike energifrigjøringer, takhøyder og brennerstørrelser.

For å kunne gjøre studier på tykkelsen av røykjeten, ble det satt opp fullskala forsøk under ett 5,9 m² tak. Basert på et temperatur kriteria på 36, 8 % av maksimal temperatur i røykjeten, ble tykkelsen målt ved hjelp av 45 termo elementer fordelt på seks radiale posisjoner. Lignende oppsett ble simulert i FDS for å se om simuleringer kan brukes for å bestemme tykkelsen på røykjeten.

Basert på eksperimentet ble det funnet at tykkelsen på røykjeten øker når energifrigjøringen øker, og når takhøyden øker, blir tykkelsen på røykjeten større. Resultater fra simulering støttet disse funnene. Det ble også funnet at resultat fra simulering i FDS underestimerte resultat fra eksperiment. Tykkelsen på røykjeten viste en økning på 2 % av takhøyden på den radiale forflytningen fra 0,4 m til 1,65 m. Simuleringer i FDS viste motsatt trend, at tykkelsen på røykjeten ble redusert med 2 % på den totale radiusen.

Table of content

List of figures

List of tables

LIST OF SYMBOLS

A_f	Area of the fire	[m^2]
b	Plume radius	[m]
c_p	Specific heat at constant pressure	[kJ/m²K]
D	Diameter	[m]
D^*	Characteristic diameter	[-]
D_α	Diffusion coefficient of species α	[m^2/s]
e	Euler's constant (2.718…)	[-]
E	Entrainment function	[-]
E_j	Entrainment function constant	[-]
g	Gravitational force	[m/s²]
h	Ceiling jet thickness	[m]
h_s	Sensible enthalpy	[kJ/m²]
H	Height	[m]
ΔH_c	Heat of combustion	[kJ/kg]
k	Thermal conductivity	[W/mK]
L	Flame height	[m]
$\dot{m}''$	Mass loss rate	[kg/s m^2]
$\dot{m}_b'''$	Mass production rate per unit volume	[kg/s m^3]
$\dot{m}_\alpha'''$	Mass production rate per unit volume of species α by chemical reaction	[kg/s m^3]
$\dot{m}_{b,\alpha}'''$	Mass production rate per unit volume of species α by evaporating droplets/particles	[kg/s m^3]
$\tilde{p}$	Background pressure	[Pa]
Pr	Prandtl number	[-]
$\dot{Q}$	Heat release rate	[kW]
$\dot{Q}_c$	Convective heat release	[kW]
$\dot{q}'''$	Heat release rate per unit volume	[kW/m³]
$\dot{q}''$	Heat flux vector	[kW/m²]
r	Radial distance	[m]
Ri	Richardsson number	[-]

$\boldsymbol{Re}$	Reynolds number	[-]
$\boldsymbol{t}$	Time	[s]
$\boldsymbol{T}$	Temperature	[K]
$\boldsymbol{T_p}$	Centerline temperature in the plume at the height of the ceiling	[K]
$\boldsymbol{T_0}$	Centerline temperature	[K]
$\boldsymbol{T_\infty}$	Ambient temperature	[K]
$\boldsymbol{u}$	Velocity	[m/s]
$\boldsymbol{u_\infty}$	Velocity of the flow	[m/s]
$\boldsymbol{u_\tau}$	Friction velocity	[-]
$\boldsymbol{v_{jet}}$	Characteristic velocity of the jet	[m/s]
$\boldsymbol{Y_\alpha}$	Mass fraction of species α	[-]
$\boldsymbol{Y^+}$	Non-dimensional distance from the wall expressed in viscous units	[-]
$\boldsymbol{z}$	Height of interest	[m]
$\boldsymbol{z_0}$	Height of virtual origin	[m]

Greek letters

$\boldsymbol{\alpha}$	Entrainment coefficient / thermal diffusivity (eq. 2.9)	[-] /[m²/s]
$\boldsymbol{\delta}$	Flow boundary layer	[m]
$\boldsymbol{\delta_T}$	Thermal boundary layer	[m]
$\boldsymbol{\delta_n}$	Wall normal cell dimension	[m]
$\boldsymbol{\delta_v}$	Local viscous length scale	[m]
$\boldsymbol{\delta_x}$	Grid cell size	[m]
$\boldsymbol{\ell_T}$	Thermal thickness of the ceiling jet	[m]
$\boldsymbol{\rho}$	Density	[kg/m³]
$\boldsymbol{\tau}$	Stress tensor	
$\boldsymbol{\mu}$	Dynamic viscosity	[Pa ·s]
$\boldsymbol{\upsilon}$	Momentum diffusivity	[m²/s]
$\boldsymbol{\chi}$	Combustion efficiency	[-]
$\boldsymbol{\nabla}$	Nabla-operator	[-]

1 INTRODUCTION

1.1 BACKGROUND

During the initial stages of an enclosure fire, the combustion product from the fire forms a buoyant plume of hot gases rising towards the ceiling. As the buoyant plume impinges on the ceiling, the hot gases turn radially to form a thin jet of hot gases that flows along the ceiling, the ceiling jet [1]. As the ceiling jet flow continues away from the turning region, air is entrained at the lower boundary and the thickness of the ceiling jet increases. Entrainment of air reduces the temperature and increases the thickness of the ceiling jet.

The ceiling jet associated with a fire is important because most of the hardware associated with detection and suppression of fires is located close to the ceiling surface [1]. This hardware is dependent on properties within the ceiling jet thickness, such as temperature, velocity and species. Finding the optimal spacing, placement under ceiling and sensitivity for the detection and suppression systems for all ceiling heights and geometries can be a difficult problem. The magnitude of the ceiling jet and temperature of the ceiling jet flow often determine the response time of the equipment for detection and suppression [2]. It is therefore important to quantify such parameters. One such important parameter is the thickness of the ceiling jet and how it changes with radial distance from the fire plume.

Ceiling jet and its behavior have been studied since the 1950s [3]. Pickard, Hird and Nash [3] found that the temperature profile in the ceiling jet was influenced by the heat release rate of the fire, the ceiling height and the radial distance from the centerline. In the 1970's Alpert [1] [4] did large scale experiments with ceiling heights of 8-15 meters and liquid pool fires ranging from 500 kW to 100 MW. The ceiling jet thickness was determined by thermocouple rakes at three radial positions. You's [5] small scale experiments on both weak and strong plume driven ceiling jets, where in agreement with Alpert's results.

In 1991, Marks and Motevalli [6] introduced a correlation for predicting the ceiling jet thickness for a fire under an unconfined ceiling. The correlation is based on small-scale experiments on weak plume driven ceiling flows. The experiments were conducted on fire effects of 0.75, 1.0 and 2.0 kW and measurements were done at two different ceiling heights, 0.5 and 1.0 meter. However, if the flame height is large compared to the ceiling height, the ceiling flow is driven by a strong-plume and new correlation must be investigated.

In this work, the thermal thickness of weak and strong plume driven ceiling jets will be investigated for medium scale fires.

1.2 PURPOSE AND RESEARCH QUESTION:

The purpose of the current work is to investigate the thickness of the ceiling jet that is created when a fire plume impinges on an unconfined ceiling by doing a medium-scale experiment.

The current work will investigate the following questions

> How does the thermal thickness of the ceiling jet change as a function of the radial distance from the centerline of the impinge plume? How is the change dependent on ceiling height, heat release rate and burner size?
>
> Can simulations in Fire Dynamic Simulator be used to approximate the ceiling jet thickness?
>
> How is the ceiling jet thickness affected as the ceiling jet transitions from a weak driven ceiling jet to a strong driven ceiling jet?

2 THEORETICAL BACKGROUND

In the initial stages of an enclosure fire, the combustion products from the fire form a buoyant plume of hot gases rising towards the ceiling. As the fire plume impinges on the horizontal ceiling, the hot gases turn radially to form a thin jet of combustion products. Three main regions are developed; the fire-plume, the turning region and the ceiling jet [5], see figure 1. This chapter will describe the three regions, with an emphasis on the ceiling jet.

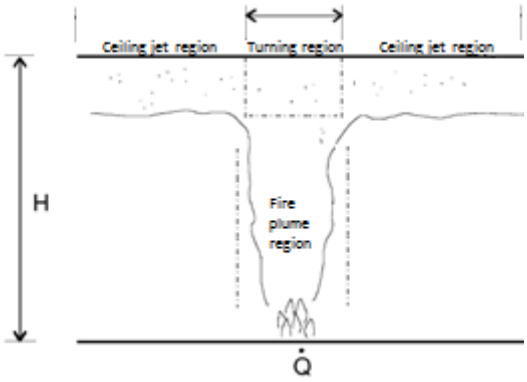

Figure 1 When the fire plume impinges on to the ceiling, three main regions are developed; the fire plume region, the turning region and the ceiling jet region.

2.1 ENCLOSURE FIRES

The development of a fire in an enclosure can be influenced by the enclosure itself and by the fuel. Factors as the geometry of the enclosure, size and location of openings and material properties of the enclosure boundaries are examples of how the enclosure itself can influence the fire development [2]. Type, amount, position, spacing, orientation and surface area are all fuel dependent factors that will influence the development of the enclosed fire [2]. In the early stages of an enclosed fire the growth of the fire is dependent on the characteristics and geometry of the fuel, the fire is said to be fuel controlled.

Heat release rate (HRR) is a term often used to express the size of the fire. The term describes the rate of energy released from combustion of different materials. The rate of energy released ($\dot{Q}$) can be calculated from

$$\dot{Q} = \dot{m}'' A_f \chi \Delta H_c \tag{2.1}$$

Where $\dot{m}''$ is the mass loss rate of the burning material, A_f is the area of the fuel, χ is the combustion efficiency and ΔH_c is the heat of combustion.

The luminous part of combustion is the flames. There are two types of flames, depending on the nature of the mixing of fuel and oxidizer in the combustion zone. If the gases from fuel and air mix inside the combustion zone, the resulting flame is a diffusion flame [2]. In the pre-mixed flame the gases from fuels and air are pre mixed before entering the combustion zone [7]. Common in fire safety engineering is the turbulent diffusion flame.

The height of the flames depends on the HRR and the diameter of the fire area, see eq. 2.2. Flames are turbulent, due to instability between the hot flame and cold air [2]. These instabilities roll up alongside the fire plume periodically as large eddies and creates shedding of the flame tip [2]. Because of the turbulent nature of the flames and periodically shedding of turbulent structures at the tip, the flame fluctuates. Therefore it is difficult to determine a specific flame height, because the flame height is always changing with time. The term of mean flame height is therefore introduced. At the lower end of the flame where flame is present all the time, it is continuous, while at the upper end the flame is fluctuating, intermittent, see figure 2. The mean flame height is within the intermittent zone, and is defined by where the flame is present 50 % of the time [1] and is given by

$$L = 0.235\,\dot{Q}^{2/5} - 1.02D \tag{2.2}$$

Products from combustion, besides energy, are the release of particles and gases into the surrounding air [7]. These particles and gases are collectedly called smoke and because of temperature differences the smoke will rise. The continuous flame, intermittent flame and the buoyant plume of smoke are all a part of the fire plume, see figure 2.

2.2 THE FIRE PLUME

The axisymmetric fire plume is the most common fire plume in fire safety engineering [2], where an axis of symmetry exists through the vertical centerline of the plume. It assumes that the fuel source is circular and that the plume is free from interference from walls and other surfaces. The fire plume consists of three zones, the continuous flame, the intermittent flame and the buoyant plume, as shown in figure 2. In the continuous flame zone, the temperature is at the highest and has relatively constant mean flame temperature. In the intermittent flame and the buoyant plume, the

temperature decreases and mass flow increases with height due to entrainment of ambient air into the plume [2].

The buoyant plume describes the convective column that rises above a heat source. The buoyant plume has properties which are important to fire detection, smoke movement and smoke control [7]. The force of buoyancy is the result density difference between the hot fluid in the plume, and the adjacent fluid at ambient temperature. The difference in density will cause the less dense fluid in the plume to rise, with respect to the surrounding fluid [2]. The buoyant plume can be described mathematically by two different methods, the ideal plume and the strong plume.

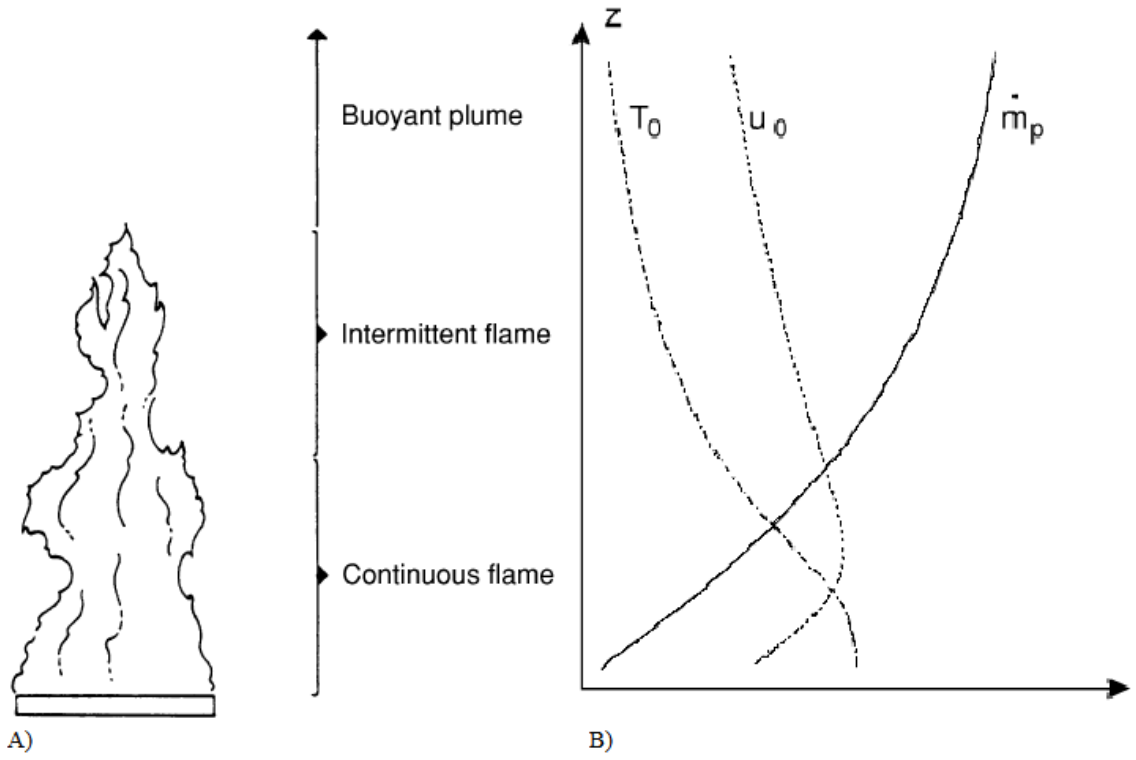

Figure 2 A) The zones of the axisymmetric fire plume; the continuous flame, the intermittent flame and the buoyant plume. B) Temperature, velocity and mass flow rate distribution in the fire plume [3].

2.2.1 IDEAL PLUME

The ideal plume theory describes the buoyant plume mathematically, giving an analytical solution for the mass flow, velocity and temperature in the plume, based on the fundamental equations of continuity and momentum. To arrive at these analytical solutions, several assumptions are made for the plume properties as described underneath [2].

The heat released into the ideal plume is assumed to come from a point source, and all the energy is assumed transported into the plume. This assumption means that heat loss due to radiation is not taken into account, typically heat loss from radiation consists of 20 – 40 % of the energy [2] [7].

The density variations throughout the height of the plume are small and are only considerable when the difference in density appears directly. Due to entrainment of air, the plume temperature is only fractional higher than the ambient temperature. At certain heights above the point source in the derivation of the mathematical terms, the ambient density is assumed to be approximately the same as the plume density $\rho_\infty \approx \rho$. This approximation is referred to as the Boussinesq approximation. However, when considering the buoyancy force, which is caused by the density difference, this approximation does not apply [2].

The velocity, temperature and force profile are assumed to follow so-called top hat profiles. Temperature and velocity within the radius of the plume is assumed to be constant over the radius of the plume at a given height. Temperature outside the radius of the plume is assumed constant at ambient temperature, $T = T_\infty$, and the velocity is assumed to be zero, $u = 0$ [2].

Entrainment of air into the plume is proportional to the local gas velocity in the plume. The horizontal entrainment velocity is assumed to $v = \alpha \cdot u$, where the entrainment coefficient α is found from experiments to correspond reasonably with 0.15 [2].

When the Boussinesq approximation is included in the Navier-Stokes equation for motion of the fluid, the equation is solved without solving for the full compressible formulation. The Navier-Stokes equations are solved in combination with the equation for continuity. With no or small density difference, this equation reduces to solve the continuity of an incompressible fluid [8].

In practical terms, the Boussinesq approximation cannot be used at heights near the fire source, where the temperature in the fire plume are much higher, causing a large density difference with adjacent fluid of ambient air. However, above the fire source, entrainment of air into the plume will cause the temperature to decrease and density differences to be negligible [2].

2.2.2 STRONG PLUME

The strong plume is derived from the ideal smoke plume, without the Bossinesq approximation. The strong plume does not assume that the density difference between ambient air and gas in the plume is negligible, and large density differences are taken into account [2]. In practical terms, the removal

of the Boussinesq approximation means that the plume properties close to the heat source can be evaluated.

The temperature and velocity of the strong plume are assumed to follow a more realistic Gaussian profile, see figure 3, where the temperature and velocity are larger at the centerline of the plume. The assumption that all energy from the fire comes from a point source is relaxed in the strong plume theory by introducing a virtual origin. The virtual origin depends on the heat release rate and the diameter of the fire source. A negative value, placing the virtual origin under the fuel source indicates that the fuel source is large compared to the energy released over that area [2]. The strong plume also takes into account that some of the energy from the fire is lost to radiation. 20 – 40 % of the total energy released from the fire is assumed to be lost to radiation, leaving the remaining 60 – 80 % of the energy in describing the plume properties [2].

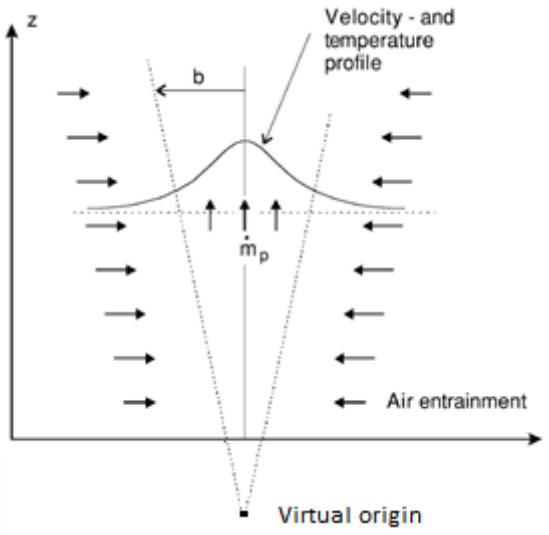

Figure 3 Gaussian temperature and velocity profile in the strong plume [3].

2.3 CEILING JET

When the buoyant plume from a fire is confined by a ceiling, the fire plume will impinge on the ceiling and the hot gases will spread out radially to form a ceiling jet [2], see figure 4. Alpert [1] refers to the ceiling jet as the relatively rapid gas flow beneath the ceiling, driven by the buoyancy of the hot combustion products from the plume.

As the hot gases spread radially away from the centerline of the buoyant plume, the thickness of the ceiling jet grows thicker due to entrainment of air at the outer boundary. The entrainment of air cools the hot gases and reduces the gas velocity of the ceiling jet [1].

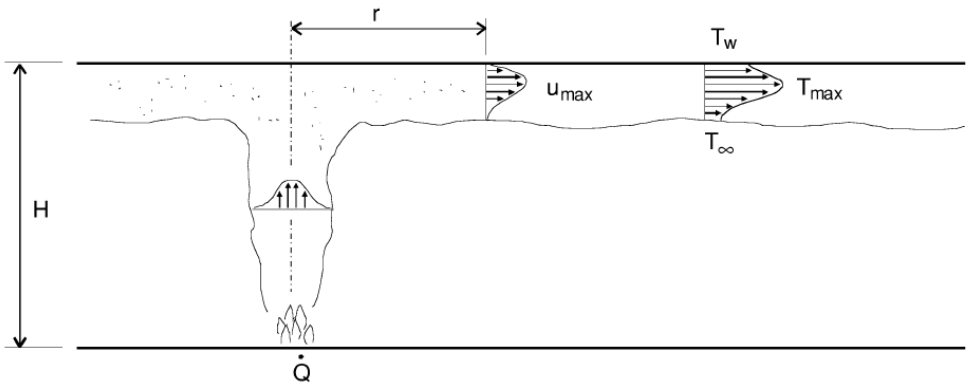

Figure 4 The ceiling jet under a ceiling height H. The velocity and temperature profiles are shown at a radius r from the centerline of the fire plume [3].

2.3.1 THE TURNING REGION

The turning region is the area where the buoyant plume impinges on to a ceiling and deflects the plume radially along the horizontal ceiling [9]. The area of the turning region extends to the edge of the buoyant plume radius, and is immediately followed by the ceiling jet region [5]. The plume radius of a buoyant plume extends approximately at an angle of about 15° to the vertical direction [2]. Karlsson and Quintiere [2] show that for an ideal plume, the radius can be expressed as

$$b = \alpha \frac{5}{6} \cdot z \tag{2.3}$$

Where α is the entrainment coefficient and z is the height above the fire.

Experiments have shown that the entrainment coefficient for a top hat velocity profile is approximately 0.15 [2]. The expression for the plume radius at a certain height reduces to give the radius as 12 % of the ceiling height.

$$b = 0.12 \cdot z \tag{2.4}$$

Heskestad examined experimental data for the strong plume and found that the radius of a strong driven fire plume obeys the following relation

$$b = 0.12\sqrt{\left(\frac{T_0}{T_\infty}\right)}(z - z_0) \tag{2.5}$$

Where T_0 is the centerline temperature in the plume, T_∞ is ambient temperature, z is the height and z_0 is the height of the virtual origin [2].

2.3.2 CEILING JET BOUNDARY LAYER

Wall jet studies by Glauert and Poreh identified the ceiling jet as a boundary layer type flow [6]. The ceiling jet can be divided into two types of thermal boundary layers describing the ceiling jets interaction with the wall and the interaction ambient air, the inner and outer boundary layer respectively.

The inner boundary layer consists of a very thin layer of fluid between the maximum temperature of the ceiling jet and the wall. The temperature within the boundary layer will decrease from the maximum temperature to the temperature of the ceiling, due to heat transfer between the hot fluid and the ceiling, see figure 5.

The outer boundary layer describes the interaction of the ceiling jets maximum temperature with the ambient fluid beyond the thickness of the jet. Marks and Motevalli [6] describes the outer boundary layer as behaving as a free jet, i.e. the outer boundary layer behaves independent of the inner boundary layer.

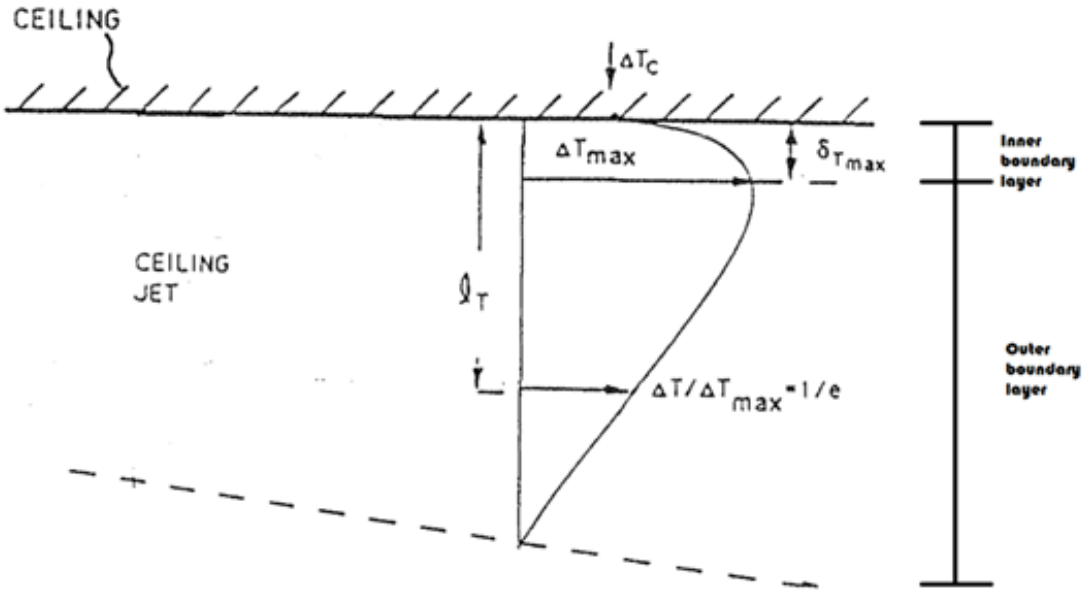

Figure 5 The thermal boundary layer in the ceiling jet, $\delta_{T_{max}}$ is within the inner boundary layer and the outer boundary layer is from the maximum temperature to the edge of the ceiling jet. [8]

The ceiling jet consists of the inner and outer boundary layers. Within these, the boundary layer can be defined by two types of flow, the hydrodynamic boundary layer flow and thermal boundary layer flow [10]. The hydrodynamic boundary layer is defined as a region within the fluid flow where viscous drag from the surface of the wall directly influences the flow patterns of the fluid [11]. The effect of the viscous force can be apparent at a large depth into the fluid, this is called the hydrodynamic boundary layer thickness. This thickness extends until the velocity is unmeasurably close to the free stream value and can be measured by balancing the wall friction with the loss in kinetic energy of the fluid [10]. The thickness of the hydrodynamic boundary layer (δ) is given by

$$\delta \approx \sqrt{8} \cdot \sqrt{\frac{\mu\, r}{\rho\, u_\infty}} \tag{2.6}$$

Where μ is the dynamic viscosity, r is the radius of the boundary layer, u_∞ is the velocity of the flow and ρ the density of the fluid. Reynolds number can be expressed by $\rho u_\infty r/\mu$, the term for the thickness of the hydrodynamic boundary layer can be rewritten in terms of the Reynolds number

$$\delta \approx \sqrt{8} \cdot \sqrt{\frac{r^2}{Re}} \tag{2.7}$$

The thermal boundary layer is similar to the hydrodynamic boundary layer, however it describes how the fluid temperature is influenced by the heating or cooling of the wall. The thickness of the thermal boundary layer, δ_T, can be described as a function of the flow boundary layer, δ, and the Prandtl number, Pr

$$\delta_T \approx \frac{1}{\sqrt[3]{Pr}} \cdot \delta \tag{2.8}$$

The expression for estimating the thermal boundary layer is found from equating the depletion of sensible enthalpy of the fluid with the heat gained at the wall [10].

The Prandtl number expresses the ratio of momentum diffusivity to thermal diffusivity [7]. At low Prandtl number (<< 1), thermal diffusivity is dominant and energy is most effectively transferred via conduction. For a large Prandtl number (>> 1), momentum diffusivity is dominant, and energy is transferred most effectively by convection [12]. The Prandtl number describes the relative thickness of thermal- and hydrodynamic boundary layer e.g. when Prandtl number is low, heat diffuses faster compared to the momentum, the thermal boundary layer will be large compared to the velocity boundary layer [12]. This can be seen from the representation of the Prandtl number

$$Pr = \frac{v}{\alpha} = \frac{\text{Viscous diffusion rate}}{\text{Thermal diffusion rate}} = \frac{\mu/\rho}{k/c_p\rho} = \frac{c_p\mu}{k} \tag{2.9}$$

Where c_p is the specific heat at constant pressure, μ is the dynamic viscosity and k is the thermal conductivity.

For most gases at different temperatures the Prandtl number is approximately constant. For air at standard temperature and pressure, the Prandtl number is 0.710 [13].

2.3.3 CEILING JET ENTRAINMENT

Entrainment of ambient air in the horizontal ceiling jet is not widely investigated [4]. Experimental data on unheated radial wall jets by Bakke and Poreh, quoted in [4], suggests that the entrainment of the wall jet is approximately the same as for the circular impinging turbulent jet. Thus, the entrainment of air into the horizontal ceiling jet is assumed as a constant equal to the magnitude of entrainment of a turbulent impinging plume. Experimental data suggests that the entrainment constant is in the range of 0.12-0.14 [4].

In general, the entrainment function into the ceiling jet depends on the Richardson number, the Reynolds number and the radial position [4]. The Richardson number is defined as the ratio of gravitational forces acting over the ceiling jet thickness, to the momentum flux in the ceiling jet [14]. The Reynolds number is a measure of the turbulent nature of the jet [7]. The Richardson's number [14] and Reynolds number [15]is respectively given as

$$Ri = \frac{\Delta\rho \; g \; h}{\rho_{jet} \; v_{jet}^2} \tag{2.10}$$

and

$$Re = \frac{\rho_{jet} v_{jet} r}{\mu} \tag{2.11}$$

Where $\Delta\rho$ is difference in density of the fluid in the jet and the adjacent fluid, h is the thickness of the ceiling jet, ρ_{jet} is the density of the fluid in the jet and v_{jet} is the characteristic velocity of the jet.

However, the work of Bakke and Poreh [4] indicated that the entrainment functions connection to radial distance and Reynolds number is weak. The entrainment function is therefore assumed to depend on the Richardson number alone. When Richardson number is large (>1) gravitational forces dominate and entrainment into the jet is suppressed [14]. Alpert's [4] showed that the Richardson number became greater than unity within the length of two ceiling heights. The increase of the Richardson number is expected to dampen the turbulence in the ceiling jet, because it is a representation of gravitational stability given as the ratio of gravitational potential energy and the flow kinetic energy [4].

The work of Ellison and Turner, quoted in [4] [5], on salt water floor-jets submerged in fresh water, demonstrates this dependency of gravitational stability, or the Richardson number on the entrainment function. It was found that the entrainment function was governed by the following expression

$$E = E_j \exp(-\alpha Ri) \tag{2.12}$$

Where E_j is a constant representing the entrainment function for the imping fire plume, α is a constant regulating the effect of the Richardson number [5].

2.3.4 CEILING JET TEMPERATURE

The temperature profile within the ceiling jet is illustrated in figure 5. It is bounded by the ceiling temperature on the one side, and the ambient temperature on the other [2]. As the ceiling jet flows radially along the ceiling, the temperature in this jet decreases. Alpert [1] has provided simple correlations, based on experimental and theoretical work, for predicting the temperature in the unconfined weak driven ceiling jet, e.g. when the flame height is much smaller than the ceiling height [7]. The correlations give the maximum temperature of the ceiling jet. Alpert found that the maximum temperature in the ceiling jet was independent of the radial distance close to the ceiling at about 1 % of the ceiling height [7] [16]. The experiment was conducted with various types of fuels, with a heat release rate ranging from 500 kW – 100 MW and ceiling height ranging from 4.6 – 15.5 meters [4] [2] [16].

Alpert correlations are separated depending on the region of interest. Near the plume, the temperature is independent of the radius and further away the temperature is influenced by entrainment [2] [16]. The two regions have been defined by the relationship between the radius of the ceiling jet, *r*, and the height of the ceiling, *H*. If the ratio between the ceiling jet radius of interest and ceiling height is greater than 0.18, $r/H > 0.18$, the temperature is influenced by the radius and entrainment of air and is given as [1]

$$T - T_\infty = \frac{5.38\ (\dot{Q}_C/r)^{\frac{2}{3}}}{H} \tag{2.13}$$

If the ratio between the ceiling jet radius of interest and ceiling height is 0.18 or less, $r/H \leq 0.18$, the maximum temperature is independent of the radius and is given by [1]

$$T - T_\infty = \frac{16.9\ \dot{Q}_C^{\frac{2}{3}}}{H^{\frac{5}{3}}} \tag{2.14}$$

Where T is the maximum temperature of the vertical temperature distribution, $\dot{Q}_C$ is the convective heat release rate, *r* is the radius of interest in the ceiling jet and *H* is the height of the ceiling. [1]

The temperature of a strong driven ceiling jet, when $L/H > 0.3$ [7], was investigated by Heskestad and Hamada [17]. In their experiments, the maximum temperature in the ceiling jet was measured for different burners, heat release rates and ceiling heights. The thermocouples for measuring the temperature were positioned at 2% of the ceiling clearance, within the anticipated layer of maximum temperature.

A correlation for the maximum excess temperature in the strong driven fire plume ceiling jet was found

$$\frac{\Delta T}{\Delta T_p} = 1.92\left(\frac{r}{b}\right)^{-1} - exp\left[1.61\left(1-\frac{r}{b}\right)\right] \qquad \text{for } 1 \leq \frac{r}{b} \leq 40 \tag{2.15}$$

Where ΔT_p is the excess temperature on the centerline of the plume at the height of the ceiling r is the radial distance in meters and b is the plume radius for strong plumes given by

$$b = \left(5.67\left(c_p\rho_\infty\right)^{4/5} T_\infty^{3/5} g^{2/5}\right)^{-1/2} \frac{\sqrt{T_p}\dot{Q}_c^{2/5}}{\Delta T_p^{3/5}} \tag{2.16}$$

Where the specific heat, c_p, density, ρ_∞, temperature, T, and gravity, g, are ambient variables. T_p is the maximum centerline temperature in the plume at the height of the ceiling and $\dot{Q}_c$ is the convective heat release rate.

2.3.5 Ceiling jet Velocity

The maximum velocity of the ceiling jet flow is typically found close to the ceiling, around 1% of the ceiling height [2]. Correlations for the ceiling jet velocity was found by Alpert [1] , and is given for $r/H < 0.15$

$$u_\infty = 0.96\left(\frac{\dot{Q}}{H}\right)^{1/3} \tag{2.17}$$

And $r/H > 0.15$

$$u_\infty = \frac{0.195\dot{Q}^{1/3}H^{1/2}}{r^{5/6}} \tag{2.18}$$

Where $\dot{Q}$ is the heat release rate, H is the ceiling height and r is radius.

2.3.6 Ceiling jet thickness

Alpert [1] defined the ceiling jet thickness as the distance from the ceiling to the point where the excess gas temperature drops to $1/e$, or 36.8 %, of the maximum gas temperature in the ceiling jet.

Oka, Oka and Imazeki [18] defined the thickness of the ceiling jet to where the temperature or velocity has dropped to 50 % of the maximum ceiling jet temperature.

In a small-scale experiment conducted by Motevalli and Marks [6], a correlation for predicting the ceiling jet thickness, ℓ_T/H was developed.

$$\frac{\ell_T}{H} = 0.112\left[1 - \exp\left(-2{,}24\frac{r}{H}\right)\right] \qquad \text{for } 0.26 \leq \frac{r}{H} \leq 2 \tag{2.19}$$

Where ℓ_T is the ceiling jet thickness, r is the radius of interest and H is the ceiling height. The correlation is based on a small scale experiment with heat release rates ranging from 0.75, 1 and 2 kW and measurements were conducted for the heights 0.5 and 1 meter at six locations different locations of r/H.

For strong driven ceiling jets, You [5] found through measurements and calculations that the initial ceiling jet thickness at the edge of the turning region, was up to twice the thickness of that predicted for a weak plume driven ceiling jet. You also found that the ceiling jet flow contracts at about 0.3 r/H from the centerline of the plume. The ceiling jet of a strong driven plume will reach its minimum at about 0.5 r/H, and increase at larger radial distances as for a weak driven ceiling jet [1].

Atkinson & Drysdale [19] suggested that the larger initial thickness of the ceiling jet were due to loss of kinetic energy in the process of impingement. Based on You's measurements, Atkinson & Drysdale suggested that 75 % of the kinetic energy of the mean flow is lost [19].

2.4 THERMOCOUPLES

The measurement of temperature is an important aspect in fire safety engineering. A thermocouple is often used as a device for measuring temperature [20]. The accuracy of the measurements is crucial to ensure the correct interpretation of the data, which is often used in creating empirical correlations used in practical fire safety engineering [2].

A thermocouple is a closed circuit consisting of two connecting wires, made out of different types of metal. The two metal wires within the thermocouple with the same length are joined together at the ends, in what is called a junction. One junction is placed in a hot environment and the other end in a cold environment as a reference junction. The different metals create a temperature dependent voltage at the connecting junction as a result of the thermoelectric effect [20]. This voltage can be interpreted to measure temperature.

.

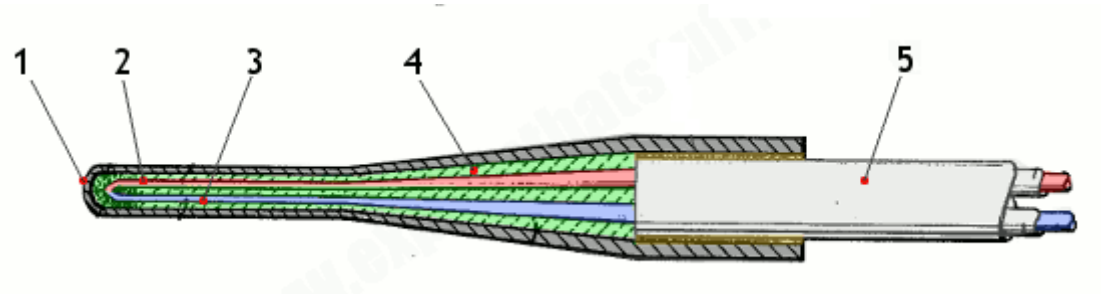

Figure 6 Schematic view of a thermocouple [21].

Figure 6 shows a schematic view, with numbered parts, of the junction that is exposed with to a hot medium. No. 1 is a protective metal sheath covering the two different metals (2) (3) that are combined in a junction at the tip. The two metals is incased in insulation (4). The measurements takes place in the tip of the thermocouple, therefore the remaining part of the thermocouple is covered with electrical insulation made from rubber or plastic. Different configurations of thermocouples can be seen in figure 7.

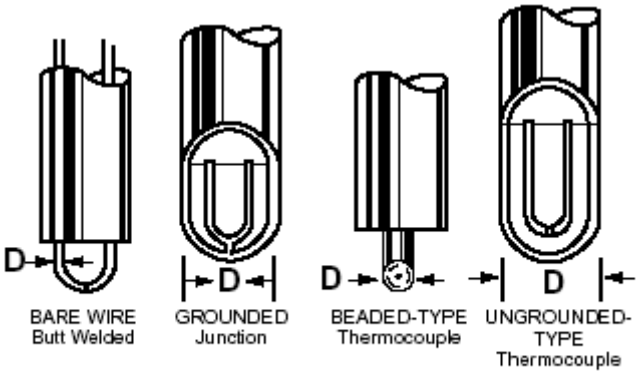

Figure 7 Different configurations of the thermocouple [22].

The response time is the most important characteristic of thermocouples. The response time of a thermocouple is defined by the time required for the sensor output to reach 63.2% of the final value following a step change in the process temperature [23], also called the time constant τ, see figure 8. The time constant is dependent on several factors, including the construction and geometry, especially the thickness of the sensor, as well as the operating conditions [24]. The response time varies with the configurations of the thermocouple. A bare wire thermocouple typically has a

response time of a few milliseconds, a grounded thermocouple about 100 milliseconds and a ungrounded thermocouple has a response time of a few hundred milliseconds [24].

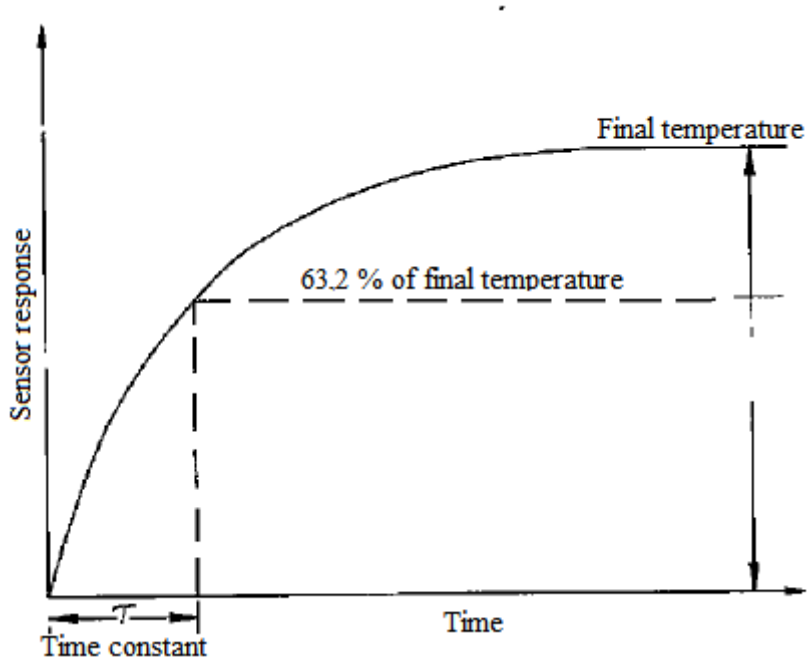

Figure 8 Response time of a thermocouple is defined by the time constant, the time to reach 63.2 % of the final temperature [23].

2.5 FIRE DYNAMIC SIMULATOR

Fire dynamic simulator (FDS) is a computational fluid dynamic model for solving fire-driven fluid flows [25]. The software solves a form of the Navier-Stokes equations designed for thermally driven flows, low mach flows, with an emphasis on smoke and heat transport from fires [25]. The equations governing the evolution of the low mach flow are continuity, species concentration, momentum, energy and ideal gas equation of state [26].

Equation of continuity

$$\frac{\partial \rho}{\partial t} + \nabla \cdot (\rho u) = \dot{m}_b''' \tag{2.20}$$

Where ρ is the density of the fluid, u is the velocity and $\dot{m}_b'''$ is the mass production rate per unit volume.

Equation of momentum

$$\frac{\partial \rho u}{\partial t} + \nabla \cdot (\rho u u) = -\nabla \tilde{p} - \nabla \cdot \tau + (\rho - \rho_0) g \tag{2.21}$$

Where ρ is the density of the fluid, u is the velocity, $\tilde{p}$ the disturbance in pressure, τ the stress tensor, g the gravitational force.

Equation of energy (sensible enthalpy)

$$\frac{\partial \rho h_s}{\partial t} + \nabla \cdot (\rho h_s u) = \frac{D\bar{p}}{Dt} + \dot{q}''' - \nabla \cdot \dot{q}'' \tag{2.22}$$

Where h_s is sensible enthalpy, ρ is the density, u is the velocity, $\bar{p}$ background pressure, $\dot{q}'''$ is the heat release rate per unit volume and $\dot{q}''$ is the heat flux vector.

Equation for species concentration

$$\frac{\partial \rho Y_\alpha}{\partial t} + \nabla \cdot (\rho Y_\alpha u) = \nabla \cdot (\rho D_\alpha \nabla Y_\alpha) + \dot{m}_\alpha''' + \dot{m}_{b,\alpha}''' \tag{2.23}$$

Where Y_α is the mass fraction for the specific species α, ρ is the density of the fluid, u is the velocity, D_α is the diffusion coefficient of species α, $\dot{m}_\alpha'''$ the mass production rate per unit volume of species α by chemical reactions, and $\dot{m}_{b,\alpha}'''$ the mass production rate per unit volume of species α by evaporating droplets/particles.

FDS is a Large Eddy Simulation (LES) code which imply that the software solves the motion of the large turbulent eddies, while the smallest are modelled. The equations for LES are derived by applying a low-pass-filter to the transport equations for mass, momentum and energy [26]. The low pass-filter in FDS has the same length scale as the grid size of the simulation mesh. The software uses an explicit predictor-corrector scheme second order accurate in time and space for solving the conservation equations [25].

In FDS the Prandtl number is a constant given by default as the value of 0.5 [26]. The value is found through comparison with experimental data [26].

The combustion model in FDS is based on mixing-controlled, infinitely-fast reaction of lumped species. In this approach, a single fuel species is reacting with oxygen in one mixing controlled step to form H_2O, CO_2, CO and soot [26]. The lumped species is representing several species grouped together as one, e.g. air is a lumped species consisting of oxygen and nitrogen. The lumped species in FDS is air, fuel (reactants) and products [25]. The reactant species within a grid cell is converted into product species, at a rate that is determined by a characteristic mixing time, τ_{mix} [26].

$$\overset{Fuel}{C_3H_8} + \overbrace{\alpha(O_2 + 3.76N_2)}^{Air} \rightarrow \overbrace{\beta CO_2 + \omega CO + \phi H_2O(vapor) + \alpha \cdot 3.76N_2 + \varphi Soot}^{\text{Products}}$$

Where β, ω and φ are user specified values for the production of CO_2 and CO and soot respectively, compared to the consumption of fuel.

2.5.1 MESH RESOLUTION

When setting up a simulation in FDS the user needs to specify a mesh. The size of the grid cells are important for the outcome of the results in FDS, depending on the scenario being simulated [25]. In general, the grid should start with coarse spacing, and gradually refine the mesh until the results converge. This is called a grid sensitivity analysis. When simulating buoyant plumes, it can be measured how well the flow field is resolved, given as the non-dimensional expression $D^*/\delta x$. D^* is the characteristic fire diameter given as

$$D^* = \left(\frac{\dot{Q}}{\rho_\infty C_p T_\infty \sqrt{g}}\right)^{\frac{2}{5}} \qquad 2.24$$

And δx is the preferred spacing of a grid cell [25]. This non- dimensional expression, $D^*/\delta x$, is a measure of how many cells cover the fire area that is calculated. The larger the number, the more cells are included in the calculation, the better resolution [25]. In the validation guide [27], the ceiling jet behavior has been validated with several different experiments. The values of the non-dimensional expression of $D^*/\delta x$ used in these simulations, range from 3 – 15 [27]. The general recommendation for adequately solving the flow field is a value of $D^*/\delta x$ between 4-16 [28].

2.5.2 NEAR WALL GRID RESOLUTION

When simulating boundary layer flows, FDS uses LES with near-wall modeling to resolve the stream wise velocity gradient normal to the wall [26]. The model used is the Werner-Wengle wall model for

smooth walls [25]. For the wall model to function properly, the grid resolution should fall within a certain value of a non-dimensional distance from the wall, Y^+, expressed in viscous units

$$Y^+ = \frac{\delta n}{2\,\delta_v}\,, \quad \delta_v = \frac{\mu}{\rho u_\tau} \tag{2.25}$$

Where δn is the wall normal cell dimension, δ_v is the local viscous length scale, μ the dynamic viscosity, ρ the density of the flow and u_τ is the friction velocity given as $\sqrt{\tau_w/\rho}$, τ_w the viscous stress evaluated by the wall, computed by the wall model.

The inner boundary layer is divided into three layers, the viscous layer ($Y^+ < 5$), the buffer layer ($5 < Y^+ < 30$) and the log law layer ($Y^+ > 30$). Wall functions are under development [25]; however, a general guideline is that the first grid cell fall within the log law layer. A Y^+ value of 30 is considered highly resolved, while for practical engineering a value of 100 is reasonable [25]. By knowing the preferable value of Y^+, the formula in 2.25 can be rearranged to give the size of the grid cell

$$\delta n = \frac{2\,\mu\,Y^+}{\rho\,u_\tau} \tag{2.26}$$

Both the criteria for mesh resolution $D^*/\delta x$ and the criteria for near wall treatments Y^+ must be fulfilled when simulating a flow where resolving the boundary layer is important.

2.5.3 THERMOCOUPLES

A thermocouple is a device in FDS that simulates temperature at a certain point in the grid. The temperature simulated at the thermocouple lags the real gas temperature by the term [25]

$$\rho_{TC} c_{TC} \frac{\delta T_{TC}}{\delta t} = \varepsilon_{TC}\left(\frac{U}{4} - \sigma T_{TC}^4\right) + h(T_g - T_{TC}) \tag{2.27}$$

Where $\rho_{TC}$is the density of the bead, $c_{TC}$the specific heat of the material, $T_{TC}$the temperature of the thermocouple, U an integrated radiative intensity, $\varepsilon_{TC}$the emissivity of the thermocouple and h the heat transfer coefficient to a small sphere $h = kNu/D_{TC}$.

By default the thermocouple bead diameter is 0.001 m, made of nickel with a density of 8908 kg/m³ and a specific heat of 0.44 kJ/ (kg/K) [25].

3 METHODS

3.1 EXPERIMENTAL SETUP

The purpose of the experiments was to measure the thickness of the horizontal ceiling jet using temperature measurements at fixed radial and vertical positions. The ceiling jet thickness was measured for different sized burners, heat release rates and ceiling heights, to get a better understanding of both weak and strong ceiling jets.

3.1.1 CEILING PLACEMENT

The experiments were conducted under a 2.4 m high smoke hood as illustrated in figure 9. Two Skamotec gypsum boards with an area of 5.9 m² (2 × 2.44 m × 1.22 m) were suspended 0.24 m inside the smoke hood, making the height from the floor to ceiling 2.64 m, as seen in figure 9. The placement of the ceiling inside the smoke hood, in addition to increasing the ceiling height, also hindered the smoke from escaping to the outside. As the smoke gathered in the top of the smoke hood it was mechanically ventilated out, preventing buildup of a smoke layer. To ensure free flow of smoke to the smoke hood, the distance from the edge of the ceiling to the smoke hood frame was approximately 0.35 meters, see figure 9.

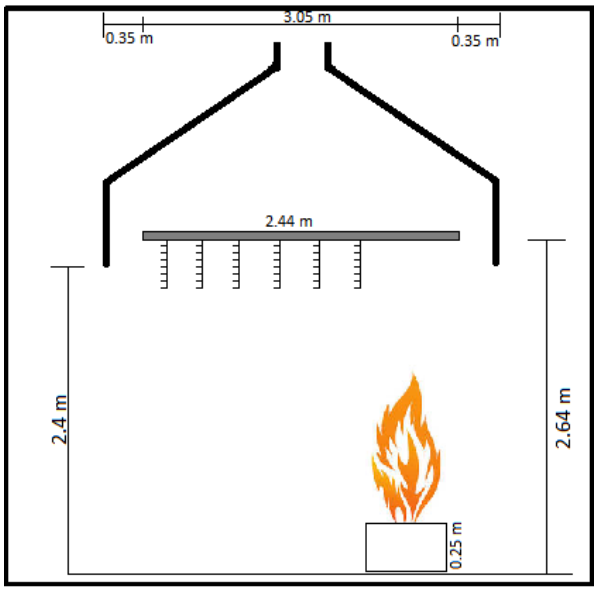

Figure 9 Setup of the experimental rig. A 2.44 m × 2.44 m Skamotec gypsum boards suspended 0.24 m inside a smoke hood, 2.64 m above the floor. The width of the smoke hood is 3.05 m. From the ceiling to the walls of the smoke hood, there is a space of 0.35 m on each side where the smoke can flow freely into the smoke hood.

3.1.2 HEAT RELEASE RATE

Previous studies [1] [6] of the weak driven ceiling jet indicate that fire effect is a variable that does not affect the ceiling jet thickness. One purpose of this study is to see how the ceiling jet thickness reacts to changes in heat release rate. Propane was distributed to a sandbox burner by a Brooks SLA 5832 S mass controller. The mass controller has an uncertainty of $\pm$ 2 % within 20 – 80 % of the max set point of 220 kW. The fire effects chosen were the upper and lower limits of the mass controller. The lower limit of the mass controller, 20 % of the max set point, is 44 kW and the upper limit, 80% of the max set point 176 kW. Three values between maximum and minimum were chosen as; 65 kW, 80 kW and 120 kW. The heat release rates are listed in table 1.

3.1.3 BURNER

The experiments were conducted using two different size propane sandbox burners. The dimensions of the burners were 0.3 m $\times$ 0.3 m and 0.5 m $\times$ 0.5 m, listed in table 1. The burners were placed near the corner of the experimental rig, with the center of the burner 0.9 meters diagonally from the corner of the ceiling, see figure 9. The placement of the burners increases the radius for which the temperature in the ceiling jet can be measured. Theoretically, the center of the fire plume at the area of impingement should be at the same location for both burners, at 0.9 meters from the edge of the setup, thus ensuring that the whole of the fire plume radius impinges on to the ceiling.

3.1.4 CEILING HEIGHTS

From previous studies [1] [6], ceiling height is the main factors for calculating the thickness of the weak driven ceiling jet. The ceiling heights in this study refer to the distance between the surfaces of the burners and the ceiling. Based on the chosen heat release rates and calculations of the flame height, the ceiling heights for the experiments were chosen. When the burners were on the floor, the ceiling clearance was 2.39 m. The smallest ceiling height is based on a calculation of the flame height for the largest heat release rate and is 1.12 m. A ceiling height of 1.94 m was chosen in the middle. Some of the ceiling heights for 44 kW and 65 kW have been specifically chosen to study the effect of strong and weak driven plumes, 1.52 m, 1.74 m and 2.14 m. When the ceiling height is 2.39 m the ceiling jet for both 44 kW and 65 kW fire is weak. At ceiling height of 1.74 m the ceiling jet from a 44 kW fire is weak, and at 1.52 m the ceiling jet has transition to a strong driven ceiling jet. The ceiling heights for experimental runs are listed in table 1.

Table 1 Summary of the variables for the experiments conducted in the fire lab and simulated in FDS

Run	$\dot{Q}$ [kW]	D [m]	H [m]	L_{flame}/H	FDS
1	44	0.5×0.5	2.39	0.21	
2	44	0.5×0.5	1.74	0.29	
3	44	0.5×0.5	1.52	0.33	
4	44	0.5×0.5	1.12	0.45	
5	44	0.3×0.3	2.39	0.30	*
6	44	0.3×0.3	1.74	0.41	*
7	44	0.3×0.3	1.52	0.47	
8	44	0.3×0.3	1.12	0.64	*
9	65	0.5×0.5	2.39	0.28	
10	65	0.5×0.5	2.14	0.31	
11	65	0.5×0.5	1.94	0.35	
12	65	0.5×0.5	1.12	0.60	
13	65	0.3×0.3	2.39	0.38	
14	65	0.3×0.3	1.94	0.46	
15	65	0.3×0.3	1.12	0.80	
16	80	0.5×0.5	2.39	0.33	
17	80	0.5×0.5	1.94	0.40	
18	80	0.5×0.5	1.12	0.70	
19	80	0.3×0.3	2.39	0.42	*
20	80	0.3×0.3	1.94	0.52	*
21	80	0.3×0.3	1.12	0.90	*
22	120	0.5×0.5	2.39	0.43	
23	120	0.5×0.5	1.94	0.53	
24	120	0.5×0.5	1.52	0.67	
25	120	0.5×0.5	1.12	0.91	
26	120	0.3×0.3	2.39	0.52	
27	120	0.3×0.3	1.94	0.64	
28	120	0.3×0.3	1.52	0.82	
29	176	0.5×0.5	2.39	0.54	
30	176	0.5×0.5	1.94	0.66	
31	176	0.5×0.5	1.52	0.84	
32	176	0.3×0.3	2.39	0.63	*
33	176	0.3×0.3	1.94	0.78	*
34	176	0.3×0.3	1.52	0.99	*

3.1.5 PLACEMENT OF THERMOCOUPLES

To determine the ceiling jet thickness, a total of 45 type K thermocouples with 1.5 mm thickness were used. The temperature was measured at six fixed radial positions from the center of where the fire plume impinges; 0.4 m, 0.65 m, 0.9 m, 1.15 m, 1.4 m and 1.65 m. The first radial position (0.4 m) was determined based on a calculation of the plume radius when the plume impinges on the ceiling.

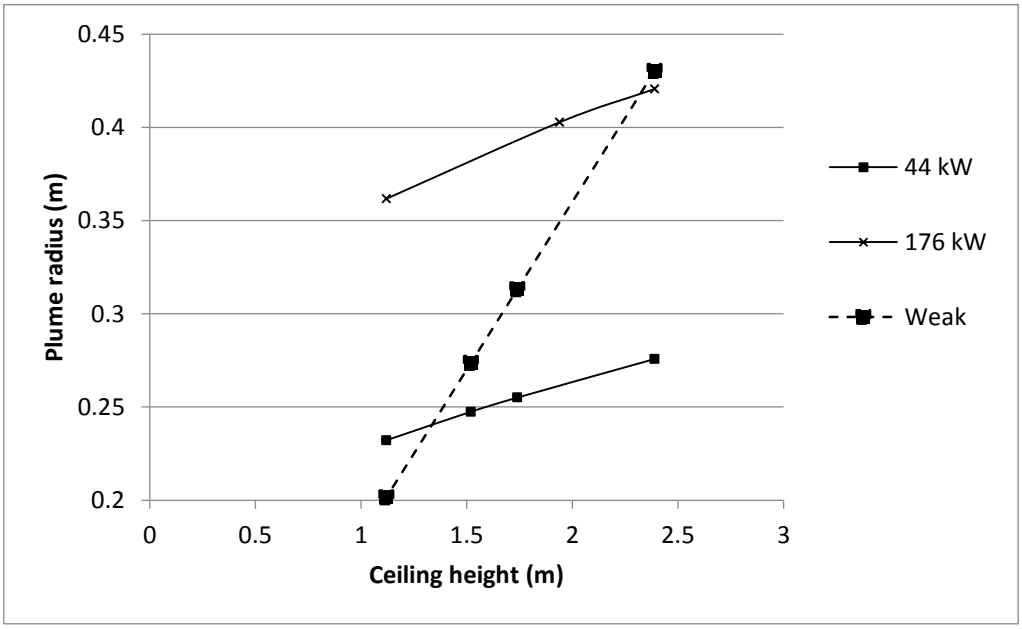

Figure 10 Radius of the fire plume as a function of ceiling height for strong- (solid lines) and weak (dashed line) driven fire plumes.

Figure 10 shows the plume radius as a function of ceiling height for different heat release rates. The dotted line shows the plume radius as a function of height for a weak driven plume (equation 2.3), the solid lines shows the plume radius for strong driven plumes (equation 2.16). For weak driven plumes, the radius of the turning region depends on the ceiling height. For strong driven plumes, the radius of the turning region depends on ambient conditions, heat release rate from the fire and temperature in the centerline of the fire plume, therefore indirectly the ceiling height. Figure 10 show that the widest fire plume radius for the weak driven fire plume where the ceiling height is 2.39 m is 0.43 m wide. The first radial position of the thermocouples was chosen to be 0.4 m based on this analysis.

At each radial position, a tree of thermocouples was positioned at different heights. The first thermocouple at all radial positions was placed at 0.02 m under the ceiling. This thermocouple was to determine the maximum temperature within the ceiling jet. Previous work [16] [17] has shown that

the maximum temperature of the ceiling jet is within 1 – 2 % of the ceiling height. The placement of thermocouples 0.02 m under the ceiling is between 0.8 -1.8 % of the ceiling heights chosen for this study. The temperature from these thermocouples is the reference temperature $\Delta T = T_{max} - T$ for calculating the ceiling jet thickness.

Calculation on the weak driven ceiling jet thickness implied that the ceiling jet grow as the radius becomes larger. The number of thermocouples was increased by one for each radial position. At the first radial position five thermocouples were positioned, at the second radial position six thermocouples were positioned and so on until the sixth radial position where ten thermocouples were placed to capture the temperature. Pre-testing showed that the height of the thermocouples needed to be individually adjusted depending on the heat release rate, burner size and ceiling height. The distance between the first thermocouple measuring maximum temperature at 0.02 m and the second thermocouple of the rest of the tree was 0.05, 0.08 or 0.013 m. The vertical distance between the rest of thermocouples in the tree was 0.025 m, see figure 11 and Appendix C.1 for more information about the placement of thermocouples.

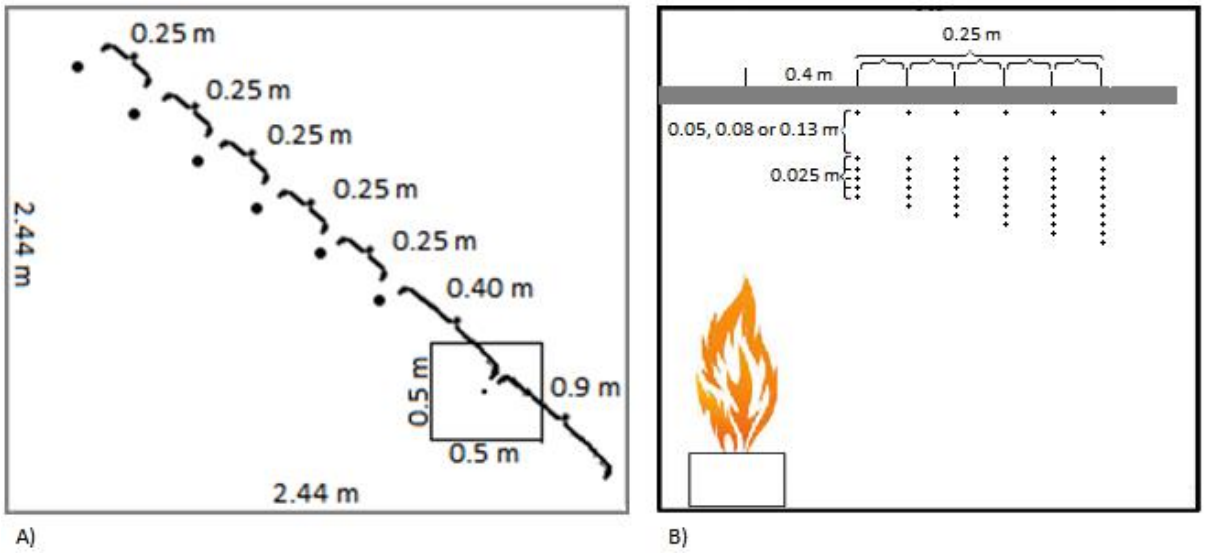

Figure 11 Laboratory setup. A) The placement of the burner in the corner of the ceiling and the thermocouples placed diagonal radius under the ceiling. B) Vertical placement of thermocouples.

To hang the thermocouples beneath the ceiling, metal wires were suspended between the floor and the ceiling. The thermocouples were the twisted around the metal wire and placed at the intended height for that particular thermocouple. Each new thermocouple was twisted around the previous.

When the string of thermocouples was complete, the heights of all thermocouples were checked and adjusted to ensure the right positions.

3.1.6 EXECUTION OF EXPERIMENT

Before doing measurements for each experiment, the fire was burning until the thermocouples gave as steady readings as possible. The fire was burning approximately 2-3 minutes before each experiment. Each experiment was conducted over 2 minutes, measuring the temperature at each thermocouple every 5 seconds.

Figure 12 Picture of the experimental setup in the laboratory. The fire has a heat release rate of 80 kW, under a ceiling height of 2.39 m. To left of the fire the arrangement of thermocouples can be seen hanging from the ceiling.

3.2 SETUP OF SIMULATIONS IN FDS

The experiments were simulated with FDS version 6.5.2, sub version Git-r21-0-g4e9103f. The simulations were performed for specific ceiling heights for a burner size of 0.3 m × 0.3 m, see table 1. The simulations were setup with the specifications described for the experiment in section 3.1. The simulation script can be found in Appendix D.1. The burner was placed in the corner of the rig, 0.9 m diagonally from the corner. The thermocouples were placed as strings at the same radial distance from the centerline of the fire plume, 0.4, 0.65, 0.9, 1.15, 1.4 and 1.65 meters. The first thermocouple in each string was placed 0.02 meters beneath the ceiling, the string of thermocouples then followed every 0.025 m. One difference in the setup between experiment and simulation in FDS is the number of thermocouples. In the experiment, the amount of thermocouples were limited and had to be adjusted for some of the runs. In FDS, there were no limitations in number of thermocouples, and more thermocouples were used. In total, 79 thermocouples were used to measure the temperature, see figure 13.

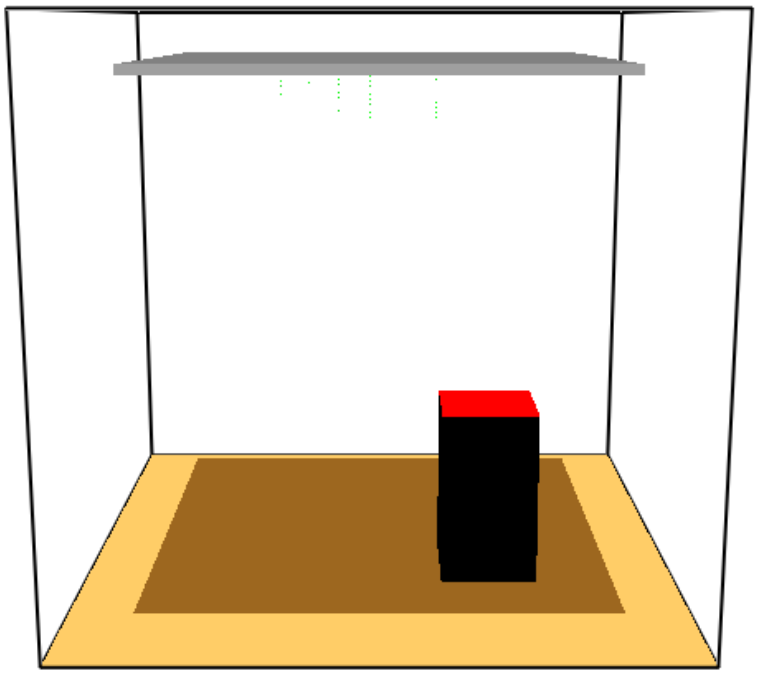

Figure 13 Screenshot of the setup in FDS from FDS visualization program smokeview. The green dots near the ceiling are the representation of thermocouples. The black box is the elevation of the red fire surface.

3.2.1 GRID RESOLUTION

When determining the grid spacing, it is important to consider what is to be investigated with the simulation. In this study, it is the ceiling jet flow under an unconfined ceiling that is to be looked at, therefor it is important to resolve the boundary layer flow at the ceiling properly. The existence of a ceiling jet is decided from a criterion of the maximum temperature. The maximum temperature is within the boundary layer of the flow.

When solving the boundary layer of a flow, the grid spacing of the simulations is of essence to the results. An important factor when determining the grid spacing is the near wall treatment and the non-dimensional criteria for viscous distance from the wall, Y^+, described in section 2.5.2 in this study. FDS user's guide [25] recommends a value of $Y^+ = 100$ for practical engineering. In order to approximate the grid spacing needed for resolving the boundary layer flow reasonably, different approximated values need to be found. From Alpert's equations for temperature (2.13) (2.14) and velocity (2.17) (2.18), the temperature and velocity of the ceiling jet can be found. From these the density (ρ), dynamic viscosity (μ) and friction velocity (u_τ) of the ceiling jet can be found. By inserting these values into eq. 2.26 the preferable grid spacing where the boundary layer is sufficiently solved ($Y^+ = 100$), could be found, see table 2.

Table 2 Calculated grid cell size based on the near wall treatment in FDS and sensitivity analysis of the grid spacing expressed as the non-dimensional expression for how well the flow field is resolved, D^*/δ_x.

$\dot{Q}$ [kW]	Ceiling height [m]	Grid cell size ($Y^+ = 100$) [m]	D^*	$\frac{D^*}{\delta_x}$ (0.025 m)	Y^+(0.025 m)
44	2.39	0.029	0.9	35.0	87.4
44	1.12	0.051	1.0	40.9	48.6
120	1.12	0.054	1.1	44.4	46.0
176	1.52	0.041	1.3	52.3	60.7
176	2.39	0.026	1.5	60.9	96.8

Table 2 shows the grid cell size for ($Y^+ = 100$), the characteristic fire diameter (D^*), the non-dimensional expression for how well the buoyant flow field is resolved with the chosen grid cell size (D^*/δ_x) and the actual value of Y^+ for the chosen grid cell size.

The grid cell size was chosen based on the calculation of eq. 2.26. Table 2 shows that when simulating with a value of $Y^+ = 100$, the fire of 176 kW and a ceiling height of 2.39 m has the smallest grid spacing of 0.026 m. Based on this analysis, the grid cell size was chosen to 0.025 m for all simulations. For some of the simulations, this means that the flow with respect to Y^+ is better resolved, i.e. for a 120 kW fire and ceiling height of 1.12 m, the value of $Y^+ = 46$, see table 2.

The grid spacing was chosen based on the Y^+ criterion to be 0.025 m. How the flow field of the buoyant plume is resolved (D^*/δ_x) is also important for this investigation. The recommended value is 4-16, however higher values only indicate that the flow field is better resolved. Table 2 show that the value of (D^*/δ_x) is much higher than the recommended value. The lowest value of (D^*/δ_x) is for 44 kW fire under a 2.39 m ceiling height at 35. A grid cell size of 0.025 m resolves the buoyant flow field better than recommended.

A grid sensitivity analysis is performed to see if the results have converged with results from using coarser and finer grid cells. The results of the chosen grid cell size of 0.025 m was compared to the results from two coarser grid cell sizes of 0.05 m and 0.08 m and one finer grid cell size of 0.02 m. Figure 14 show the result from the sensitivity analysis. The results for the grid cell size 0.02 m and 0.05 m have converged with the result from the simulation with the chosen grid cell size of 0.025 m. The results from grid cell size of 0.08 m have not converged with the results of the finer grid cell sizes. Based on these results, the necessary grid cell size for the simulations is 0.05 m. However, the criterion of Y^+ for practical engineering problems suggests a smaller grid cell size for resolving the boundary layer flow of the ceiling jet.

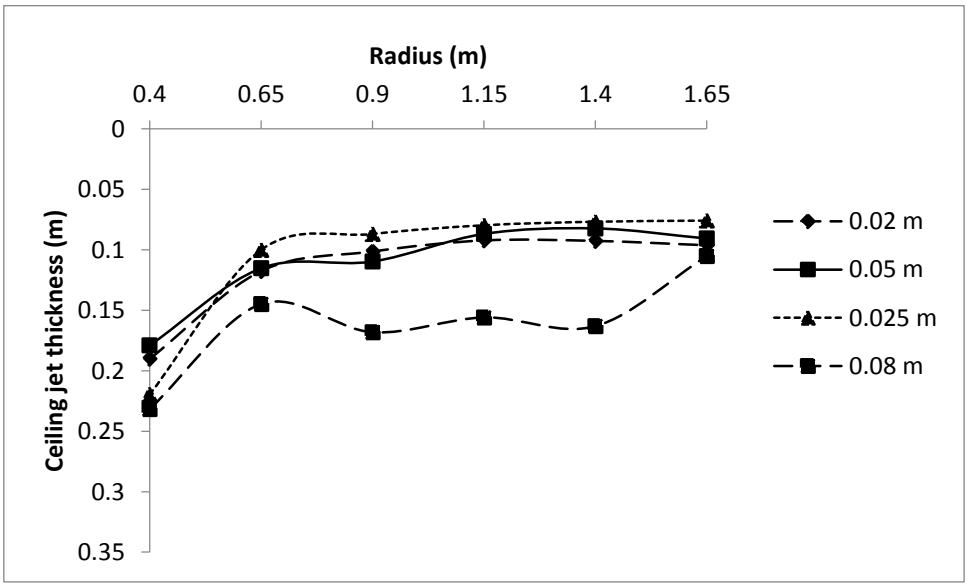

Figure 14 Sensitivity analysis of the grid spacing in the simulation. The sensitivity analysis was performed for a grid spacing of 0.025 m against a finer grid of 0.02 m, and two coarser grids of 0.05 m and 0.08 m. The sensitivity analysis was performed on a 44 kW fire under a 2.39 m ceiling height.

4 RESULTS

In this chapter the results from the experiments and FDS simulations will be presented. The results have been obtained by measuring the temperature within the thickness of the ceiling jet. In total, 33 experiments and 9 simulations were performed in this study. By using a temperature criterion of 36.8 % of the maximum temperature ($\Delta T/e$), the thermal ceiling jet thickness could be determined. All experimental results presented in this chapter are from fires from a 0.5 m $\times$ 0.5 m burner size. Experimental results from fires from a 0.3 m$\times$ 0.3 m burner size can be found in Appendix (A.1).

4.1 PROCESSING DATA

The result for the experiment and simulations in FDS is originally temperature measurements made over time at different radial positions and heights under the ceiling. The temperature measurements were conducted for 125 seconds for each experimental and simulated run.

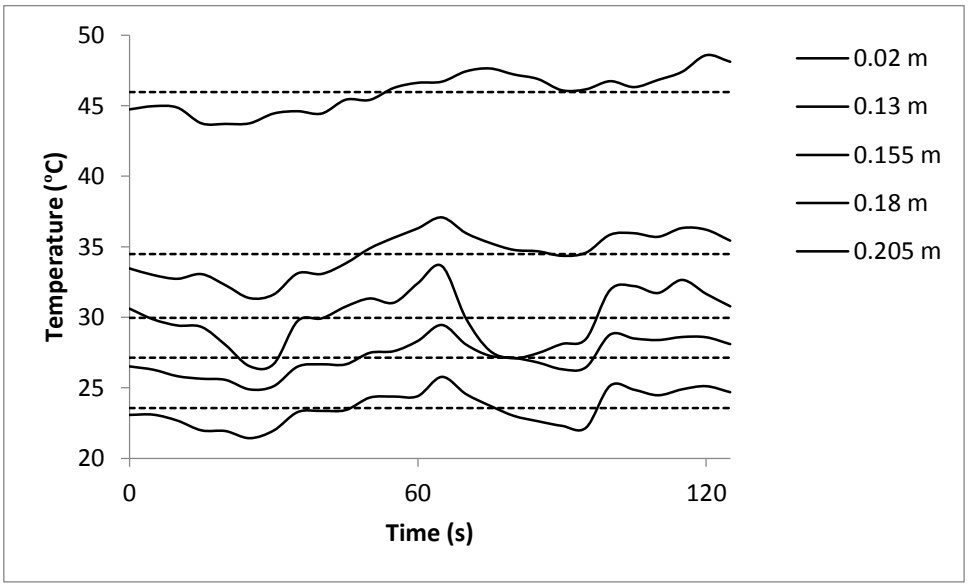

Figure 15 Temperature curves for all thermocouples at radius 0.4 m. The solid lines show the measured temperature and the dotted lines show the temperature average used to determine the ceiling jet thickness.

Figure 15 show the temperature measurements at the thermocouples at the radius 0.4 m. Before measurements were conducted, the fire had been burning for a while to stabilize the temperature in the ceiling jet, creating a steady state environment. Therefore the temperature measurements do not include a temperature rise from ambient temperature. The fluctuating values of the

temperatures (solid lines) were averaged over time (dotted lines) to get the temperature to base the ceiling jet thickness upon. The time averaged temperature for all heights at all radial positions is plotted in figure 16.

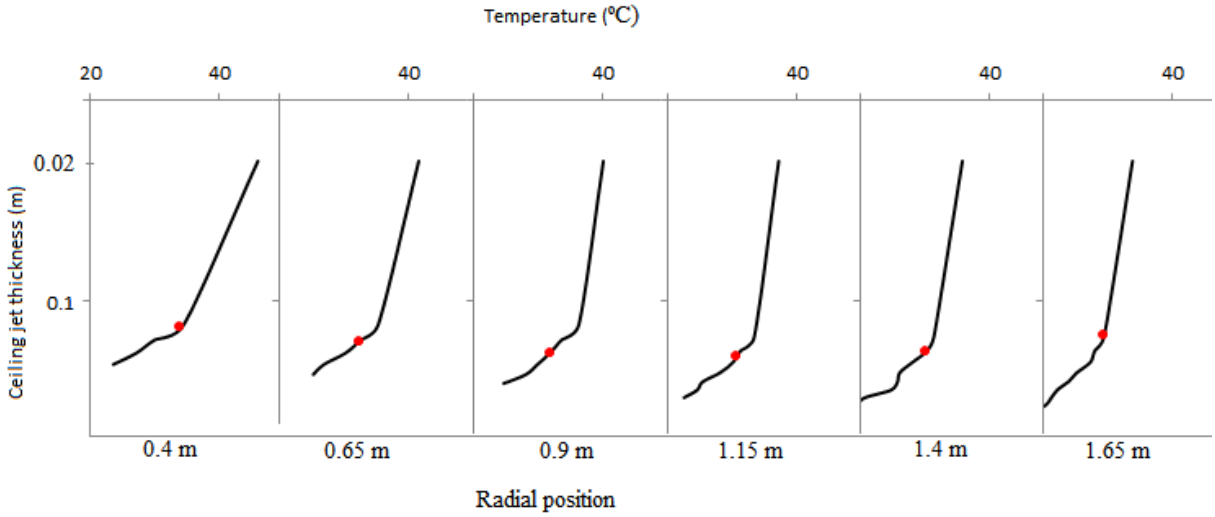

Figure 16 Temperature profile at each radial position. The dots represent the thickness of the ceiling jet.

From the thickness of 0.02 m the temperature criterion of the ceiling jet was calculated. The temperature result from the calculations can be seen as dots in figure 16 and is the temperature at a distance under the ceiling where the ceiling jet is defined to exist. The temperature criterion often fell between two measuring points giving the thickness of the ceiling jet. To decide the final thickness of the ceiling jet it was assumed that the temperature decrease linearly between the thermocouples, hence, the final value was linearly interpolated between the temperature and the thickness of the ceiling jet.

4.2 EXPERIMENTAL RESULTS

The results from the experiment performed in this study will be presented in this chapter. The presented results are of the ceiling jet thickness from fires with a large fire surface of 0.5×0.5 m. The results from where the ceiling jet thickness is measured from a fire of a small fire surface, 0.3 m $\times$ 0.3 m can be found in Appendix A.1.

4.2.1 EFFECT OF CEILING HEIGHT

In this chapter the ceiling jet thickness is given for a constant heat release rate, to see what effect changing the ceiling height will have on the ceiling jet.

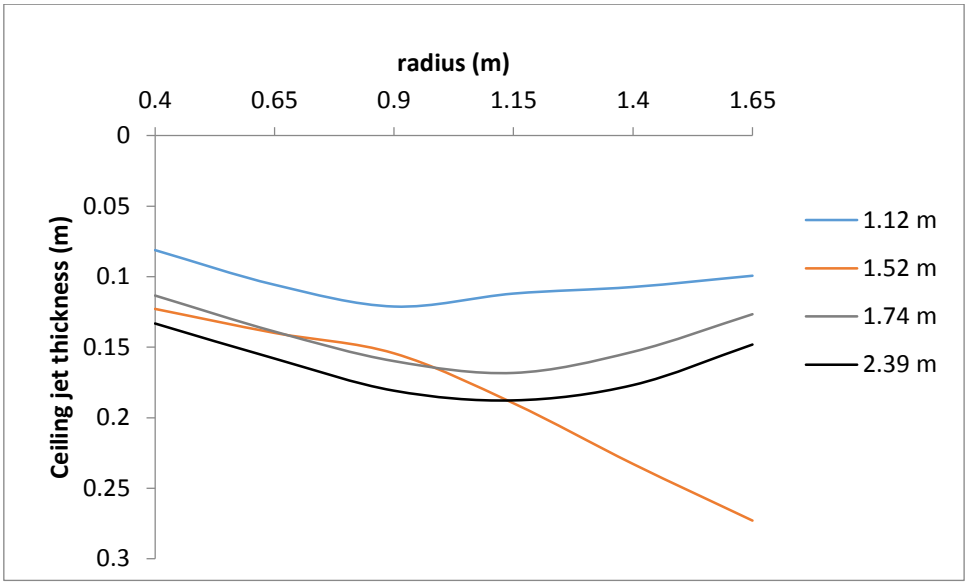

Figure 17 Ceiling jet thickness as a function of radius. A constant HRR of 44 kW fire is burnt under ceiling heights of 1.12 m, 1.52 m, 1.74 m and 2.39 m. The ceiling jet is measured over a radius of 1.25 m starting at 0.4 m.

Figure 17 show the result of the ceiling jet thicknesses as a function of radius from the centerline of the fire plume, for a 44 kW fire at ceiling heights of 1.12 m, 1.52 m, 1.74 m and 2.39 m. The ceiling height 1.52 m and 1.74 m is especially chosen to investigate the difference of a weak driven ceiling jet and a strong driven ceiling jet. The x-axis show the radius of the ceiling jet and the y-axis show the thickness of the ceiling jet. The values of the ceiling jet thickness on the y- axis are shown in opposite direction, to better illustrate the ceiling jet. The x- axis represents the ceiling and the lines, representing different ceiling heights, are the thickness of the ceiling jet.

From figure 17 it can be seen that the thickness of the ceiling jet increases as the ceiling height increases. The ceiling jet for a ceiling height of 1.12 m has a maximum thickness of 0.12 m, the maximum ceiling jet thickness under 1.74 m ceiling is 0.17 m and under a 2.39 m ceiling has the maximum thickness of 0.19 m.

The ceiling jets start at a radius of 0.4 m with different thicknesses from 0.08, 0.11 and 0.13 m. When the radius increases, the ceiling jets increase in thickness. The ceiling jets under 1.74 m and 2.39 m high ceilings increase until a radius of 1.15 m, where the ceiling jets starts to decrease until the radius

is 1.65 m from the centerline of the fire plume and the thickness 0.12 and 0.14 m. The ceiling jet thickness for the fire under a 1.52 m ceiling increases approximately as the ceiling jet under 1.74 m ceiling. However, at a radius of 0.9 m the thickness of the ceiling jet under 1.52 m ceiling plunges to a thickness of 0.27 m at a radius of 1.65 m. The ceiling jet under a 1.12 m high ceiling also increase until 0.9 m, but decrease with the radius and seem to be stabilizing at about 0.11 m at 1.65 m radius.

Curves for ceiling heights 1.74 m and 2.39 m seem to have the same shape, with a certain distance between the thicknesses of the ceiling jets. The difference in ceiling height between 1.74 m and 2.39 m ceiling height is 0.65 m and the difference separating the two ceiling jets is 0.02 m at all radial distances. The ceiling jet under 1.52 m ceiling seems to be similar to that of 1.74 m ceiling height until 0.9 m, where it separates from the others both in shape and in thickness. The curve for the ceiling jet of 1.12 m has a different shape than the other curves, because it starts to decrease at 0.9 m and has a gentler decreasing than the other curves. Difference in ceiling height between 1.12 m and 1.74 m is 0.62 m, and the difference in ceiling jet thickness between the two ceiling jets is approximately 0.03-0.04 m. At the same difference in ceiling height, the differences in separating the ceiling jet thicknesses have doubled from 0.02 to 0.03-0.04 m.

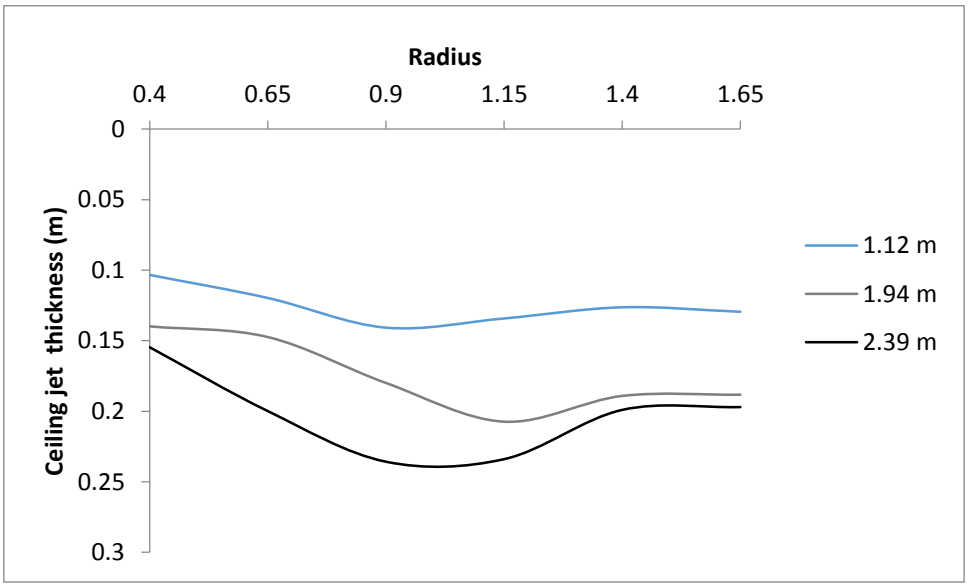

Figure 18 Ceiling jet thickness as a function of radius. A constant HRR of 65 kW fire is burnt under ceiling heights of 1.12 m, 1.94 m and 2.39 m. The ceiling jet is measured over a radius of 1.25 m starting at 0.4 m.

Figure 18 show the ceiling jet thickness for a 65 kW fire under ceiling height of 1.12 m, 1.94 m and 2.39 m. The ceiling jets thicknesses for a 65 kW fire under different ceiling heights seem to follow the

same overall trend as the 44 kW fire, the ceiling jet thickness increase with larger ceiling heights. The ceiling jet thickness under a 1.12 m ceiling has a maximum thickness of 0.14 m, under a 1.94 m ceiling the maximum thickness is 0.20 m and under 2.39 m ceiling height the maximum thickness of the ceiling jet is 0.23 m.

At a radius of 0.4 m the thickness of the ceiling jet with a ceiling height of 1.12 m is 0.1 m, 0.14 m for ceiling height 1.94 m and 0.15 m for the curve representing a ceiling height of 2.39 m. As the radius increase from 0.4 m, the ceiling jets for all ceiling heights increase. At a radius of 0.9 m the ceiling jet thickness for ceiling height 1.12 m starts to gently decrease and seems to stabilize at 0.13 m. The ceiling jet for ceiling height 1.94 m increases until 1.15 m, having a sharp decrease before stabilizing at 0.19 m. The ceiling jet thickness for ceiling height 2.39 m increases until 1.15 m radius and decreases to 0.20 m at 1.65 m radius.

The ceiling jet thicknesses for the ceiling heights of 1.94 m and 2.39 m seem to increase more, than the ceiling jet thickness when the ceiling height is 1.12 m. This can be seen form the distance separating the ceiling jet thicknesses. At 0.4 m the distance separating the ceiling jet for 1.12 m and 1.94 m ceiling height is 0.04 m. At 1.65 m radius the thicknesses of the ceiling jets are separated 0.06 m, an increase of 0.02 m. The ceiling jet for ceiling height 2.39 m has approximately, although different thickness in the radial distance, the same difference at radius 0.4 m and 1.65 m.

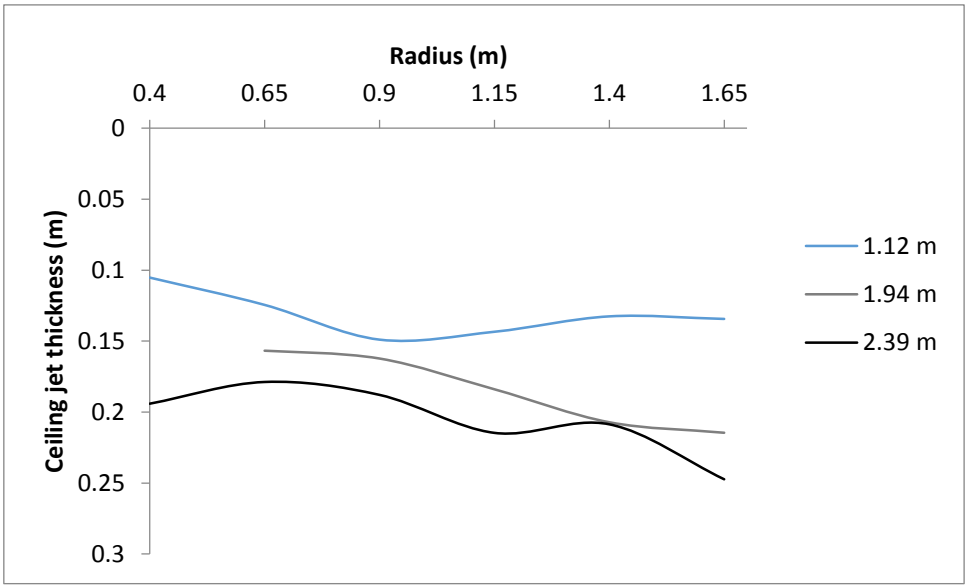

Figure 19 Ceiling jet thickness as a function of radius. A constant HRR of 80 kW fire is burnt under ceiling heights of 1.12 m, 1.94 m and 2.39 m. The ceiling jet is measured over a radius of 1.25 m starting at 0.4 m.

Figure 19 show the ceiling jet thickness for an 80 kW fire under the ceiling heights 1.12 m, 1.94 m, and 2.39 m. Figure 19 show the same as the previous figures 17 and 18, that the ceiling jet thickness increases with larger ceiling height. The maximum ceiling jet thickness is 0.15 m for the ceiling jet under 1.12 m ceiling height, 0.21 m for 1.94 m ceiling height and 0.25 m for 2.39 m ceiling height. The maximum ceiling jet thicknesses for the ceiling height 1.94 m and 2.39 m are at the largest radius measured, 1.65 m, and both ceiling jets seem to be increasing further beyond this point.

For the ceiling jet underneath a ceiling height of 1.94 m the resulting thickness at 0.4 m radius is inconclusive. The calculated temperature for the criterion for where the ceiling jet is was too low compared to the temperature measured at the thermocouples. The thickness of the ceiling jet at this radial position is larger than what could be measured. Where this is the case, it is assumed that the jet is a part in the turning region, see section 2.3.1.

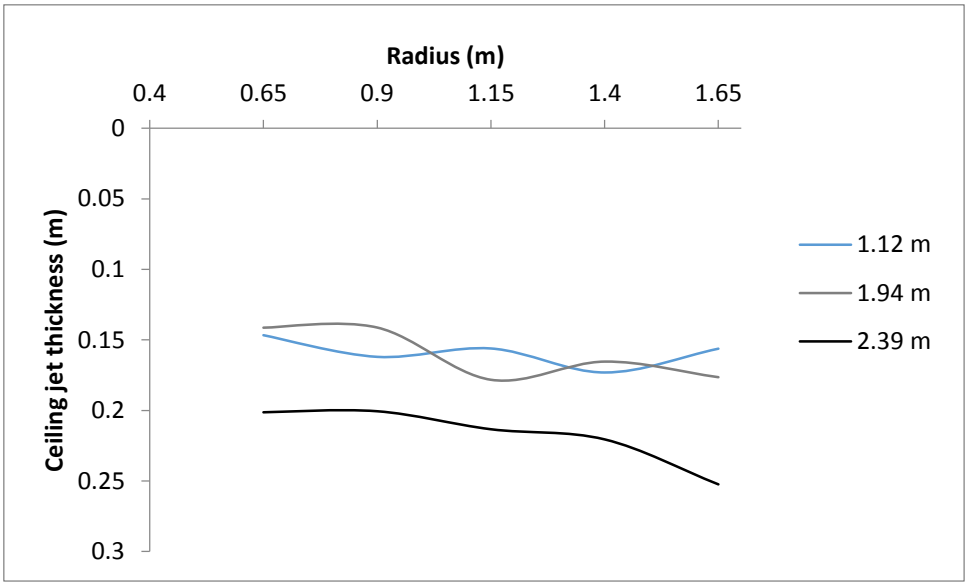

Figure 20 Ceiling jet thickness as a function of radius. A constant HRR of 120 kW fire is burnt under ceiling heights of 1.12 m, 1.94 m and 2.39 m. The ceiling jet is measured over a radius of 1.25 m starting at 0.4 m.

Figure 20 show the ceiling jet thickness for a 120 kW fire under the ceiling heights 1.12 m, 1.94 m and 2.39 m. Where the thickness of the ceiling jet for smaller heat release rate in previous figures has shown a trend of increasing with the ceiling height, it does not for the ceiling jet thickness under 1.12 m and 1.94 m ceiling height. Although the thickness is fluctuating with radius, the thickness of the two is rather similar, with an average thickness of 0.17 m. However, when increasing the ceiling height further, to 2.39 m, the ceiling jet thickness increases.

At 0.65 m radius the thickness of the ceiling jet under 1.12 m and 1.94 m ceiling is 0.14 m. As the radius gets larger, both ceiling jets increase gently to 0.17 m at 1.65 m radius. The ceiling jet under a 2.39 m high ceiling has a thickness of 0.2 m at 0.65 m radius. The thickness increases gently until 1.4 m radius and a thickness of 0.22 m, where it plunges to 0.25 m and 1.65 m radius.

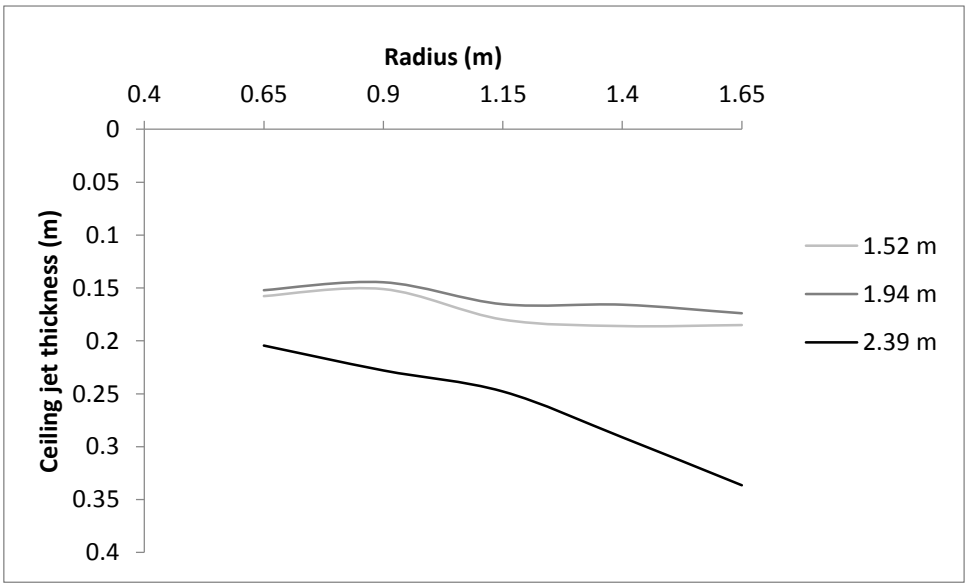

Figure 21 Ceiling jet thickness as a function of radius. A constant HRR of 176 kW fire is burnt under ceiling heights of 1.12 m, 1.94 m and 2.39 m. The ceiling jet is measured over a radius of 1.25 m starting at 0.4 m.

Figure 21 show the ceiling jet thickness for a 176 kW under the ceiling heights 1.52 m, 1.94 m and 2.39 m. Results for ceiling height 1.12 m was not conducted for the 176 kW fire because the fire was too large. The graph show that the ceiling jet thickness for the ceiling heights 1.52 m and 1.94 m are approximately the same, with a ceiling jet thickness of 0.15 m at 0.4 m radius, increasing to 0.17 m at 1.65 m radius. When the ceiling height increases to 2.39 m, the ceiling jet thickness also increases. At 0.65 m radius the thickness of the ceiling jet is 0.2 m. The thickness increases to a maximum thickness of 0.33 m at 1.65 m radius.

4.2.2 Effect of heat release rate

In this chapter the resulting ceiling jet thickness is given for a constant ceiling height, to see what the effect of changing the heat release rate will have on the thickness of the ceiling jet.

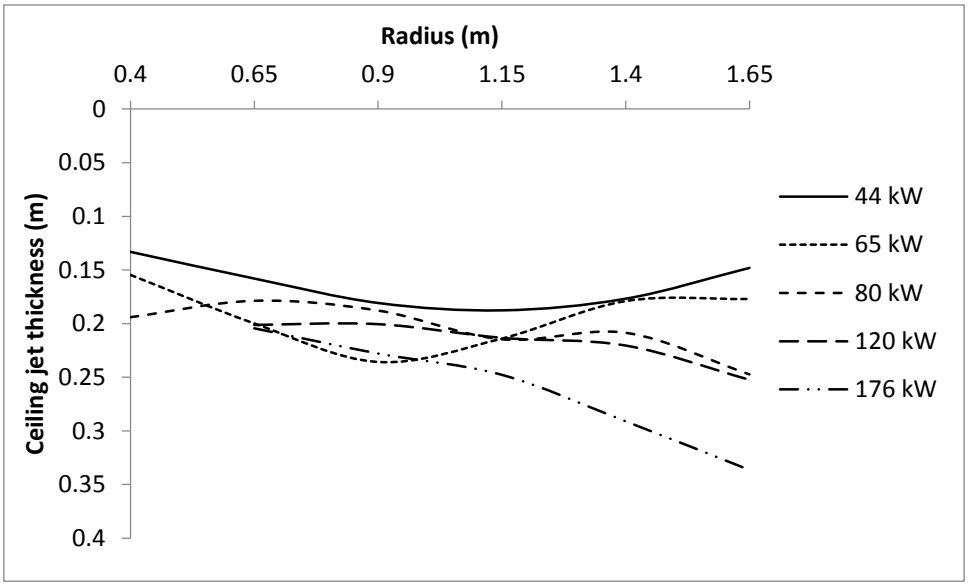

Figure 22 Ceiling jet thickness as a function of radius for a constant ceiling height of 2.39 m. Fires with HRR of 44 kW, 65 kW, 80 kW, 120 kW and 176 kW are burnt beneath a constant ceiling height of 2.39 m. The ceiling jet is measured over a radius of 1.25 m starting at 0.4 m.

Figure 22 shows the ceiling jet thickness when the ceiling height is kept constant at 2.39 m for heat release rates of 44 kW, 65 kW, 80, kW, 120 kW and 176 kW. From the figure it can be seen that there are differences in the ceiling jet thickness when the heat release rate is changed. The overall trend of the figure is that the ceiling jet increases with larger heat release rate. The ceiling jet is at its thinnest when the heat release rate is smallest, 44 kW, and thickest when the heat release rate is 176 kW.

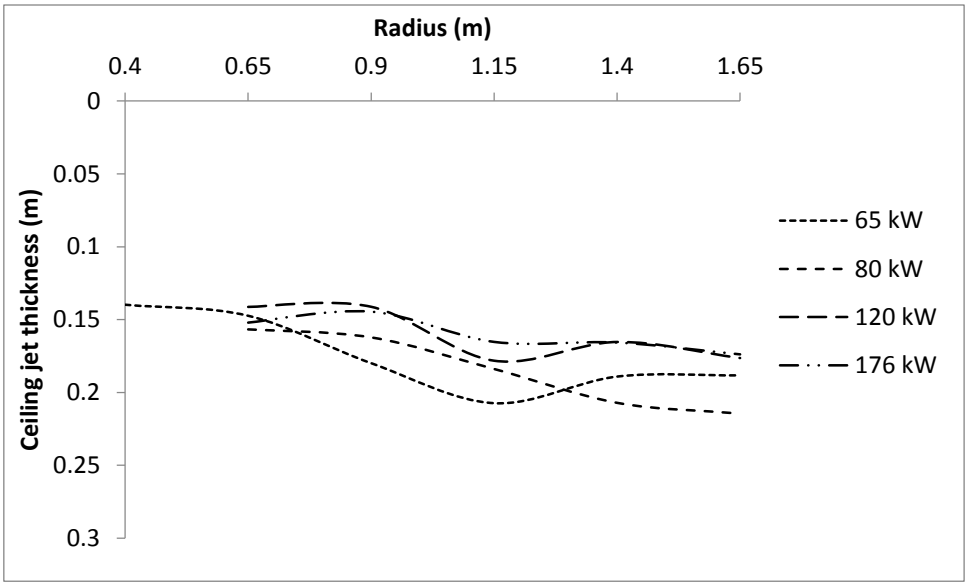

Figure 23 Ceiling jet thickness as a function of radius for a constant ceiling height of 1.94 m. Fires with HRR of 65 kW, 80 kW, 120 kW and 176 kW are burnt beneath a constant ceiling height of 1.94 m. The ceiling jet is measured over a radius of 1.25 m starting at 0.4 m.

Figure 23 shows the ceiling jet thickness when the ceiling height is kept constant at 1.94 m, for heat release rates of 65 kW, 80 kW, 120 kW and 176 kW. Experiments for 44 kW fire was not conducted for this ceiling height. The overall trend of the figure is the opposite from figure 22, the ceiling jet thickness increase for larger heat release rate.

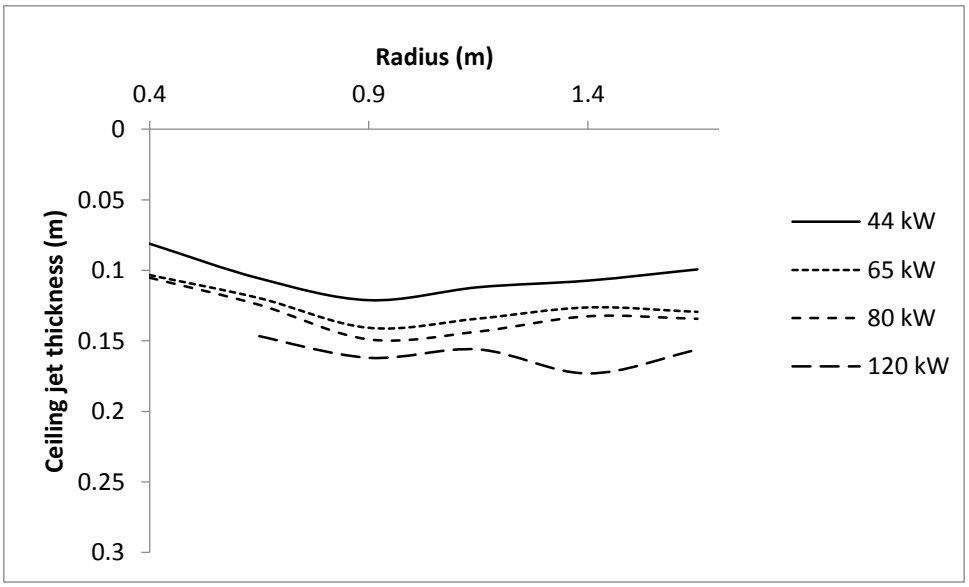

Figure 24 Ceiling jet thickness as a function of radius for a constant ceiling height of 1.12 m. Fires with HRR of 44 kW, 65 kW, 80 kW, 120 kW and 176 kW are burnt beneath a constant ceiling height of 1.12 m. The ceiling jet is measured over a radius of 1.25 m starting at 0.4 m.

Figure 24 shows the ceiling jet thickness for different heat release rates at a constant ceiling height of 1.12 m. The ceiling jets seem to have increasing thickness when there is an increase in heat release rate. The ceiling jet from a 44 kW fire has a thickness of 0.08 m at 0.4 m radius. It increases to a thickness of 0.12 m at radius 0.9 before decreasing to about 0.1 m at 1.65 m. The ceiling jet for 65 kW and 80 kW fires seems to have relatively similar ceiling jet thicknesses, with only 0.01 m separating the two. Starting at 0.1 m at a radius of 0.4 m, both of the ceiling jets increase in thickness until 0.9 m radius. Both of the ceiling jets seem to be levelling out at 0.13 -0.135 m from about 1.4 m radius.

4.2.3 CONCLUDING REMARKS

Experimental results on the ceiling jet thickness have been presented in this chapter. The thicknesses as a function of radius have been presented for varied heat release rates and ceiling heights. From the results it was found that the ceiling jet increases in thickness as the ceiling height increase. When the effect of heat release rate was studied, it was also found that the ceiling jet increased in thickness as the heat release rate increased. Overall, the thicknesses of the ceiling jet seem to increase as the radius increases under the ceiling.

4.3 RESULTS FROM SIMULATION IN FDS

The graphs below shows the result from simulations performed in FDS. The result is compared to the results from the experiment to see how well FDS can reproduce the results. Simulations have been performed on various ceiling heights and heat release rates for a burner size 0.3 m × 0.3 m. Result is shown for the effect of the ceiling height for a 44 kW fire and the effect of heat release rate for a given ceiling height of 2.39 m. The result for effect of ceiling height and effect of heat release rate show the same trend for different variables. The result showing these variables can be found in Appendix B.1.

4.3.1 EFFECT OF CEILING HEIGHT

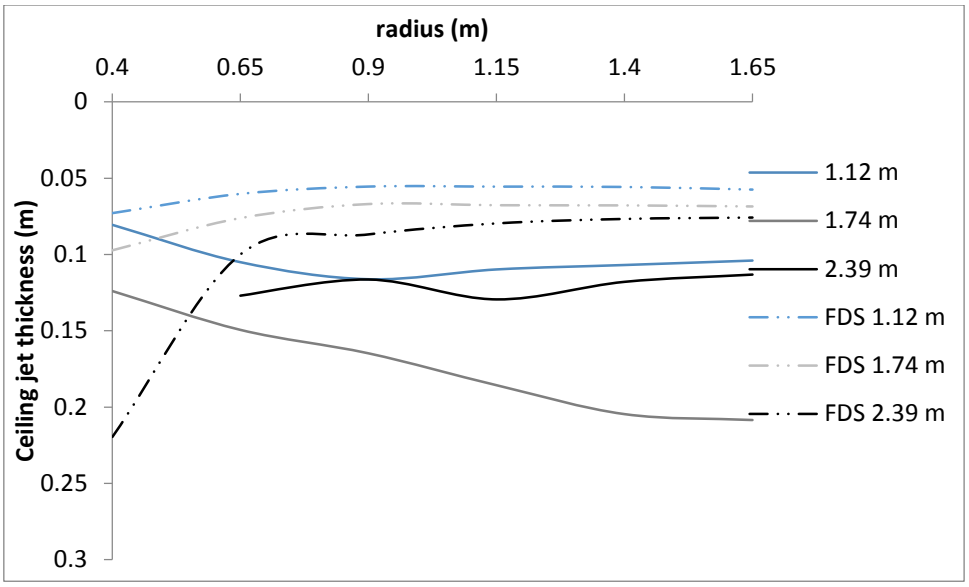

Figure 25 Ceiling jet thickness as a function of radius. A constant HRR of 44 kW fire is under ceiling heights of 1.12 m, 1.74 m and 2.39 m. The ceiling jet is measured over a radius of 1.25 m starting at 0.4 m. The dashed lines represent the result from simulation in FDS.

Figure 25 shows the results of comparing experimental results of the ceiling jet thickness for 44 kW fire beneath different ceiling heights, with the result from simulation in FDS. When looking at the entirety of figure 25, it can be seen that the simulations of the ceiling jet thickness in FDS is underestimating the results for all ceiling heights, compared to experimental results. The trend of increased ceiling jet thickness with increased ceiling height is present in the result from simulation. The distance between the ceiling jets decrease as the ceiling height increase. This is more prominent in the experimental results. However, it can be seen in the distance between the simulated thicknesses, i.e. the distance between the ceiling jet thickness under a 1.12 m ceiling and 1.74 m is twice the distance of that between 1.74 m and 2.39 m. The increase in ceiling height is approximately 0.6 m in both intervals.

4.3.2 EFFECT OF HEAT RELEASE RATE

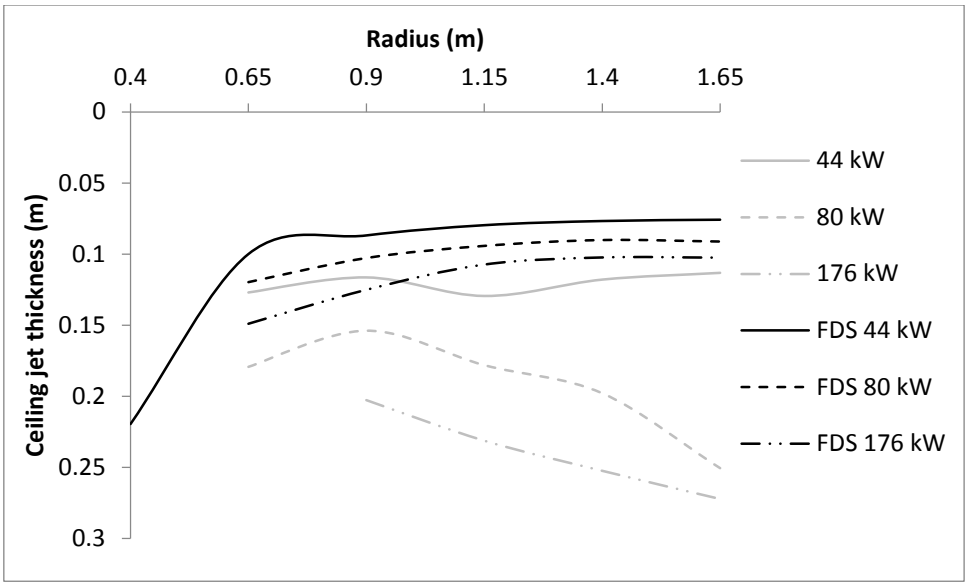

Figure 26 Ceiling jet thickness as a function of radius for a constant ceiling height of 2.39 m. Fires with HRR of 44 kW, 65 kW, 80 kW, 120 kW and 176 kW are burnt beneath a constant ceiling height of 1.12 m. The ceiling jet is measured over a radius of 1.25 m starting at 0.4 m. The faded lines are results from experiments, and the black lines are the result from simulation in FDS.

Figure 26 shows the results from simulation compared to the results from experiments. The results from FDS underestimate the experimental results. The figure shows the same trend of increased ceiling jet thickness when the heat release rate is increased for a given ceiling height, is present in results from FDS.

4.3.3 CONCLUDING REMARKS

The ceiling jet thickness simulated in FDS has been compared to the experimental results for constant heat release rates and constant ceiling heights. Generally, the simulated result on the ceiling jet thickness underestimates the experimental results. The trend of increasing ceiling jet thickness with increase in heat release rate and ceiling height is the same in results from simulation in FDS.

5 DISCUSSION

Experiment and simulations have been conducted to study the ceiling jet thickness. The ceiling jet thickness was determined using a temperature criterion equal to 36.8 % of the maximum temperature in the ceiling jet. The ceiling jet thickness have been found experimentally and estimated by simulations, with using different heat release rates and ceiling heights, to study the behavioral effect on the ceiling jet and how the thickness changes as a function of the radius.

In this study, the criterion used for the ceiling jet thickness has been from Alperts [1] definition, $1/e$ of the maximum temperature in the ceiling jet. Oka, Oka and Imazeki [18] define the ceiling jet thickness as the distance where the ceiling jet temperature has dropped to 50 % of the maximum ceiling jet temperature. Figure 27 shows the difference of the two criterions on the ceiling jet thickness. When the criterion is 50 % of the maximum temperature, the ceiling jet thickness is thinner than if the criterion is $1/e$ of the maximum temperature.

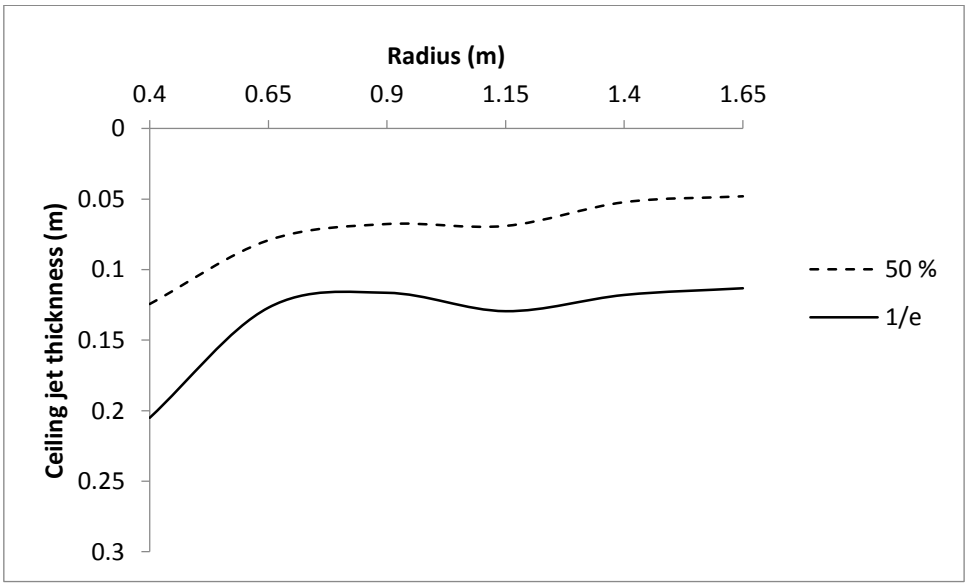

Figure 27 Ceiling jet thickness as a function of radius for different criterions for the temperature where the ceiling jet is defined. The dashed line shows the ceiling jet thickness when the criterion is 50 % of the maximum temperature in the ceiling jet. The solid line shows the criterion used in this study, $1/e$ of the maximum temperature in the ceiling jet.

5.1 EFFECT OF HEAT RELEASE RATE

The ceiling jet thickness has been studied for given ceiling heights and different heat release rates. The results from experiments show different trends for different given ceiling heights. Figure 22 and 24 where the ceiling heights are 2.39 m and 1.12 m respectively, show a trend where the ceiling jet

thickness increase with increasing heat release rates. The results in figure 23 with a ceiling height of 1.94 m show an opposite trend with decreasing ceiling jet thickness with increasing heat release rates. The result from simulation in FDS, figure 26 and figure 48 and 49 in Appendix B.1.2, supports the experimental results for ceiling heights 1.12 m and 2.39 m where the ceiling jet thickness increase as the heat release rate increases. Experimental results for both burner sizes 0.3 m $\times$ 0.3 m and 0.5 m $\times$ 0.5 m show the same trend that the ceiling jet thickness increase as the heat release rate increases, see Appendix A.1.2 and figure 38, 39 and 40.

Factors influencing the conducted experiments, could contribute to the result for the ceiling height 1.94 m of decreasing ceiling jet thickness with increase in heat release rate. Such factors could be draft from ventilation openings in the laboratory influencing the tilt of the flame and impingement zone of the fire plume. But, it is somewhat unlikely that only the result for the ceiling height of 1.94 m was influenced, especially when the experimental runs were conducted at different days and wind conditions. It could be that the result for other ceiling heights also were affected to some degree, but the results do not support this.

Previous work [6] on the ceiling jet thickness represented by eq. 2.19 is based on the ceiling height only, and the heat release rate is not included. Figure 28 shows the work of Motevalli and Marks compared to the experimental results for a given ceiling height of 1.12 m. The thick solid line shows the ceiling jet thickness as a function of radius as presented by Motevalli and Marks, and is equal for all heat release rates. From figure 28 it can be seen that for the experimental results the heat release rate do influence the ceiling jet thickness. It can also be seen that the ceiling jet thickness from Motevalli and Marks underestimates the ceiling jet thicknesses found from the experiment conducted in this study. Results comparing the work of Motevalli and Marks to the given ceiling heights of 2.39 m, 1.94 m and to burner size 0.3×0.3 can be found in Appendix A.1.2.1 and show the same trends as shown in figure 28.

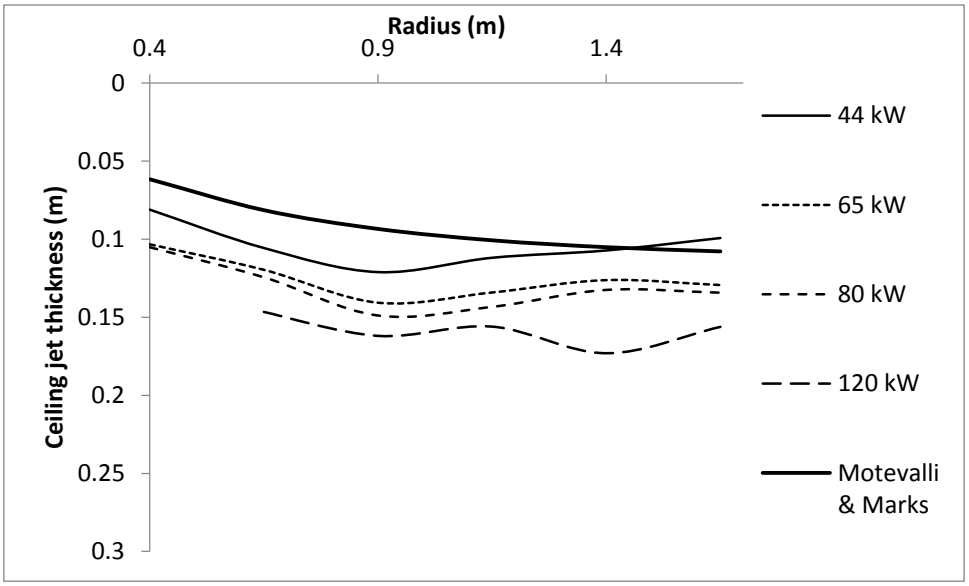

Figure 28 Ceiling jet thickness as a function of radius for the given ceiling height of 1.12 m is compared to the ceiling jet thickness from Motevalli and Marks [6].

When the heat release rate is increased, the temperature in the ceiling jet increases. From eq. 2.13 and eq. 2.14 for a weak driven ceiling jet it can be seen that by increasing the heat release rate, the maximum temperature in the ceiling jet increase. The correlation of the maximum temperature in the strong driven ceiling jet eq. 2.15 depends on the radius of the imping fire plume, eq. 2.16. The radius of the impinge fire plume increases when the heat release rate of the fire is increased. Therefore the maximum temperature of the strong driven ceiling jet is also increased by the increase of heat release rate.

Eq. 2.14 and 2.16 also show that the temperature in the ceiling jet decreases with radial distance. This reduction in temperature is due to heat transfer and vertical entrainment of air into the ceiling jet. The vertical entrainment into the ceiling jet is described by the Richardson number. An increase in fire heat release rate will increase the velocity of the jet, and decrease the Richardson number. A lower Richardson number indicates an increase of air entrainment into the ceiling jet. As the radius increase, the velocity in the ceiling jet decrease and the Richardson number increases, resulting in less entrainment of air into the ceiling jet. As the Richardson number increase to unity, the gravitational force becomes larger than the momentum flux in the ceiling jet, at this point the entrainment of air into the ceiling jet is reduced to zero and becomes independent of radius. The entrainment of air into the ceiling jet is reduced to zero because the turbulence in the ceiling jet is dampening as a result of gravitational stability in the ceiling jet. This is where the ceiling jet thickness will stabilize. According to Zukoski [14], the stabilization of the ceiling jet thickness occurs at a radial

distance from the fire plume centerline impingement point of the same value as the ceiling height. The ceiling jet thickness from experiments seems to be stabilizing as the radius increases. Not all results show that the ceiling jet thickness stabilizes. Perhaps if the ceiling jet thickness was measured over a larger radial distance, the stabilizing of the ceiling jet would become more prominent.

As the ceiling jet moves radially under the ceiling from 0.4 m to 1.65 m radius the thickness of the ceiling jet increases. From figure 22, 23 and 24 it can be seen that the majority of ceiling jet thicknesses for different heat release rates for a given ceiling height have an increase over the total radial distance. By scaling the ceiling jet thicknesses with the ceiling heights, the thickness can be expresses as a percentage of the ceiling height. Subtracting the percentage thickness at radius 0.4 m with the percentage ceiling jet thickness at 1.65 m, the result is the percentile change in ceiling jet thickness. The average increase in ceiling jet thickness is 2 % of the ceiling height. For a 2.39 m ceiling height, the ceiling jet thickness will increase by 0.05 m from 0.4 m until 1.65 m radius, for a ceiling height of 1.12 m the increase is 0.02 m. The smallest percentile increase among all the ceiling jet thicknesses is 0.5 % and the largest is 6.8 % of the ceiling height.

Results from FDS do not support these findings. The same analysis show that the ceiling jet thickness decreases by 2 % of the ceiling height from 0.4 m radius to 1.65 m radius. The largest percentile decrease is 6 % and the smallest decrease is 1.1 % of the ceiling height.

5.2 EFFECT OF CEILING HEIGHT

When the heat release rate is kept constant, and the ceiling height is varied, the effect of the ceiling height on the ceiling jet thickness can be studied. Figure 17 – 21 in section 4.2.1 show the results of the experimental ceiling jet thickness for different heat release rates and set heights. The effect of ceiling heights have been tested with five different heat release rates: 44, 65, 80, 120 and 176 kW. The figures show that as the ceiling height increase, the ceiling jet thicknesses also increase. For the heat release rates 44 kW, 65 kW and 80 kW there are clear differences in the ceiling jet thicknesses for the different ceiling heights. Here the ceiling jet thicknesses increase with increased ceiling height. For the heat release rates of 120 kW and 176 kW the ceiling jet thickness also increases with increasing height. However, the thickness only increases for the ceiling heights 2.39 m and 1.94 m. The ceiling jet thickness for ceiling heights 1.94 m and 1.12 m for 120 kW fire have the same thickness. The ceiling jet thickness for ceiling heights 1.94 m and 1.52 m for 120 kW fire, also have the same thickness. This could indicate that the ceiling jet has a minimum thickness when the heat

release rate is large, and the ceiling height is decreased. Perhaps the ceiling jet thickness for the heat releases 44, 65 and 80 kW also have a minimum thickness however, this is not found in the results.

Result from experiments when the burner size is 0.3 m × 0.3 m, see Appendix A.1.1, supports the results of increasing ceiling jet thickness with increasing ceiling height. The result for the ceiling jet thickness for a 2.39 m ceiling height is not consistent with these results in all figures. During experiments, draft from natural ventilation openings disturbed the air flow, tilting the flames away from the experimental setup. The tilting of flames was tried controlled by stopping the measuring when the flame was tilting. This could be an influencing factor to why the thickness of the ceiling jet under 2.39 m does not comply with other results. The results from simulation in FDS, figure 25 and figure 46 and 47 in Appendix B.1.1, supports the trend found in experimental results.

The results from the work of Motevalli and Marks, eq. 2.19, also support the trend of increasing ceiling jet thickness with increase in ceiling height, as shown in figure 29.

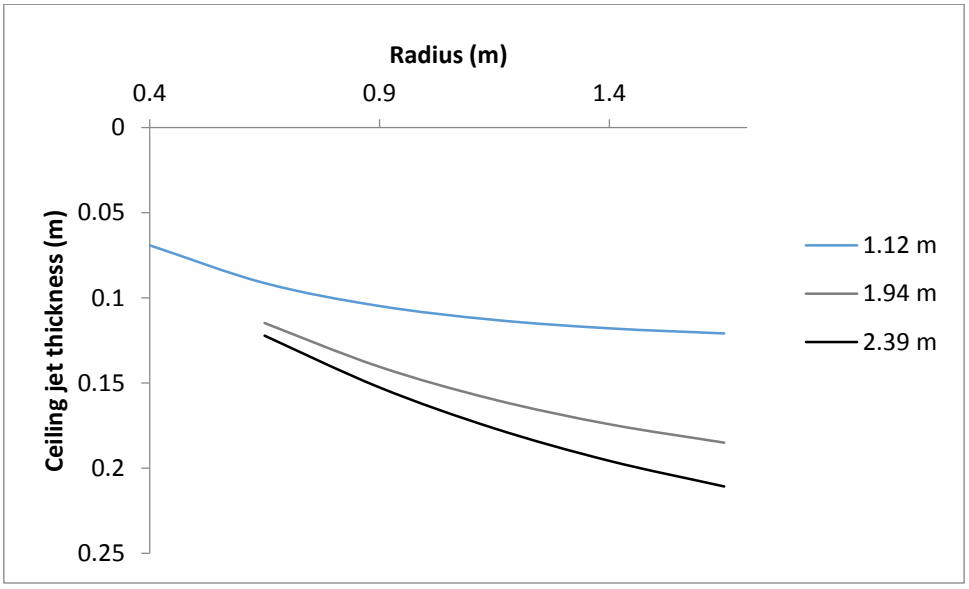

Figure 29 The results of the work presented by Motevalli and Marks on the ceiling jet thickness. The figure show that the ceiling jet increase in thickness as the ceiling height increase.

The thickness of the ceiling jet changes as the radius increases. From figures 17-21 it can be seen that for smaller heat release rates the ceiling jet thickness increases with radius until approximately 0.9-1.15 m when the ceiling jet thickness decreases and stabilizes at radius 1.65 m. However, the ceiling jet stabilizes at a thickness larger than the initial thickness at 0.4 m radius. For the two largest heat release rates the ceiling jet thickness has a steady increase from radius 0.4 m to 1.65 m where it

seems to stabilize. Over the total radius, from the initial radius of 0.4 m to 1.65 m the ceiling jet thickness increases. The largest increase in ceiling jet thickness, scaled by the height of the ceiling, was 6.9 % of the ceiling height. The smallest increase was a decrease in thickness by 0.58 % of the ceiling height. On average, the ceiling jet thickness, independent of heat release rate, had an increase of 2 % of the ceiling height. For a ceiling height of 2.39 m a 2 % increases means that the thickness will increase 0.05 m from 0.4 m radius until 1.65 m.

5.3 SIMULATIONS VS. EXPERIMENTAL RESULTS

The ceiling jet thickness has been simulated using FDS version 6.5.2. Simulations were performed for the ceiling jets from an 0.3×0.3 m burner. The simulations in FDS were setup similarly as the experimental setup. Thermocouples were used to measure the temperature and the processing of data was conducted in the same manner as for the experimental data.

Figure 25 and 26 in section 4.3 and figure 46 - 49 in Appendix B.1 show both the result from simulation and the results from experiments. In general, the result of the ceiling jet thickness from FDS is underestimating the ceiling jet thickness obtained from experiments. At 0.4 m radius, the ceiling jet thicknesses from simulations have approximately the same thickness as the ceiling jet from experiments. Experimental results have a tendency to increase in ceiling jet thickness as the radius increase. Results from FDS decrease as the radius increase, before the thickness stabilizes. The results from FDS are not affected by the draft and turbulence experienced by the experiments and was more grouped.

Figure 30 show the temperature results from the thermocouple 0.02 m under the ceiling at a radius of 0.04 m, from both experiments and simulations in FDS. The grey fluctuating curve is the temperature results from simulation in FDS and the dashed line is the time averaged temperature. The solid black line with relaxed fluctuations is the result from experiment and the dotted line is the time averaged temperature. Temperature results from FDS fluctuate more compared to that measured in experiment. Temperature measurements performed in experiments were conducted every 5 seconds. The temperature shows therefore less fluctuation than the results from FDS. In FDS the temperature is measured at every time step, and there will be several measurements per second. In figure 30 the temperature from simulation in FDS has been averaged every 5 seconds, to be comparable to temperature results from experiments. The fluctuating temperatures indicate a turbulent flow. Since measurements in the experiments were conducted every 5 seconds, turbulence is more dampen in the resulting experimental temperature. The thermocouples used in the experiments have a thermal inertia in the response time, and cannot capture the turbulent nature of

the flow properly. Had the temperature in the experiment been measured several times per second, the temperature curve would have shown turbulence by fluctuating more.

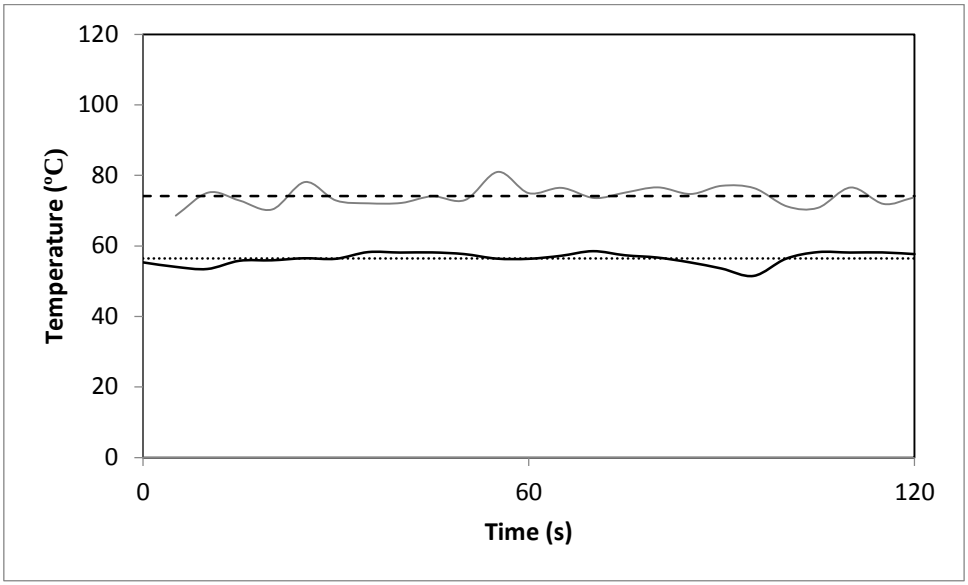

Figure 30 Temperature measurements from experiments and FDS. The temperature is from a radius of 0.4 m, 0.02 m under the ceiling of a 44 kW fire under a ceiling height of 2.39 m. The grey fluctuating line show the temperature results from simulation in FDS. The dashed line shows the time averaged temperature from simulation in FDS. The solid black line shows the temperature from experiments. The dotted line is the time averaged temperature.

Figure 30 show that the temperature in FDS is higher than the temperature measured in experiments. The average temperature in experiments is 56 °C, while the average temperature in the simulation is 73 °C. Heat in the ceiling jet is mainly lost through heat transfer to surroundings by radiation or convection, or by entrainment of air into the ceiling jet. Assuming that heat loss to the surroundings is the same in FDS and the experiments, the difference in temperature suggest that entrainment into the fire plume and ceiling jet is much greater in the experiments than simulation. The temperature in the experiments is influenced by more than entrainment. Draft from the outside will contribute to a more turbulent air flow in the laboratory, which will cool both the temperature in the flames, plume and ceiling jet. The temperature in from FDS is not exposed to this exterior factor.

It can also indicate that the maximum temperature in the ceiling jet is not at 0.02 m as assumed when determining the thickness, but could be located either higher or lower in the ceiling jet, see discussion in section 5.5.

Figure 31 show the temperature profile at different radial positions for both simulated and experimental results. The solid lines show the temperature profile for experimental results and the dashed lines show the results from simulations. The dots represent the ceiling jet thickness at each radial position.

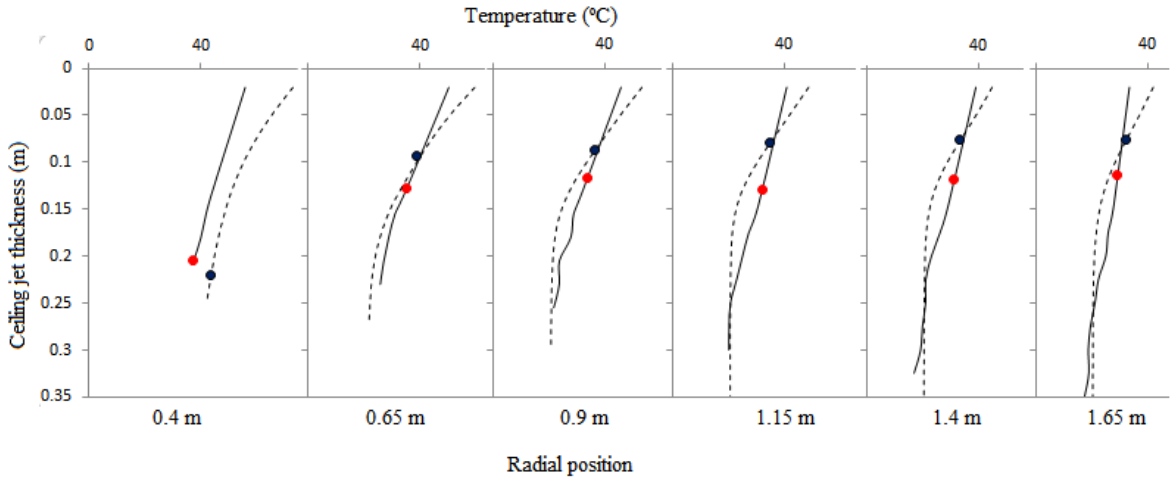

Figure 31 Temperature profile at radial positions for both results from experiments and simulation in FDS for a 44 kW fire under 2.39 m ceiling height. The solid lines represent the temperature profile from experiments. The dashed line represents the temperature profile from simulations. The dots associated with each line shows where the temperature criterion $\Delta T/e + T_\infty$ for where ceiling jet thickness is found.

In this study, the position of the thermocouple measuring the maximum ceiling jet temperature was fixed at 0.02 m under the ceiling. Since the thermal boundary layer is assumed to have a constant thickness, the ceiling jet thickness is decided by the half-Gaussian temperature profile of the outer boundary layer of the ceiling jet and the rate the temperature reduces. Figure 30 and 31 shows that the maximum temperature in FDS is higher than the maximum temperature from experiments. The rate the temperature reduces is also larger in the simulated temperature profile, which could suggest more entrainment into the ceiling jet. With higher maximum temperature and larger reduction rate of the temperature, the thickness of the ceiling jet becomes thinner than the thickness from experiments.

Simulation is not reality, it is a representation of a reality based on numerous assumptions and simplifications. The simulation consists of a domain that is discretized in numerous grid cells, for which the equations of conservation is calculated upon. These are the mathematical terms used to explain what is occurring. Depending on what is being simulated and what is being studied for in the

simulation, the grid cell size of the simulation needs to be sufficiently small for the result to be acceptable. Three tests were performed to ensure sufficiently small grid cell size for the simulations conducted in this study. The grid sensitivity analysis showed in figure 14, show that the results of the simulations are sufficiently as it converges with results for a finer grid. The analysis of the characteristic diameter $D^*/\delta x$, show how well the buoyant plume is solved. The criteria for solving the buoyant plume sufficiently, the value of should be $4 < D^*/\delta x < 16$. Table 2 in section 3.2.1 shows that values of $D^*/\delta x$ are between 30-60 for all heat release rates. The higher value outside the criteria of $D^*/\delta x$ does not mean that the buoyant plume is not sufficiently solved, but rather that the flow is better resolved, with more grid cells spanning the diameter of the fire surface. Both the grid sensitivity and $D^*/\delta x$ show that the grid cell size is smaller than what is needed to solve for the fire plume and that it could be solved with a larger cell size. The grid cell size for the ceiling jet is based on the criteria of Y^+, the non-dimensional distance from the wall expressed in viscous units. The criteria of Y^+ is a measure of how small the grid cells should be to sufficiently solve the flow interaction with the wall. According to FDS user guide [25], when the value of $Y^+ = 30$ the flow near the wall is considered highly resolved. For the simulations performed in this study, a criteria of $Y^+ = 100$ was set as the largest value. With 100 as the criteria, the grid cell size was 0.025 m. For comparison, for $Y^+ = 30$ the grid cell size of the simulation would have to be smaller than 0.0077 m. Such small grid cells would be impractical to simulate. A sensitivity analysis on the importance of Y^+ on the results from simulations should be conducted in further studies.

Accuracy of simulations can be approximated by the grid cell size. The temperature at the grid point, apply for the whole grid cell, 0.0125 m in every direction from the center of the cell for the simulations in this study. The fact that the temperature is uniform within the grid cell ads an uncertainty in the result from simulations. In the experiments and in simulations, the accuracy of the measurements of the ceiling jet thickness is 0.025 m. Another uncertainty for the measurements of the ceiling jet thickness is the assumption that the temperature reduces linearly between each measuring point. Because of this assumption, the position of the ceiling jet thickness is found through linear approximation is made between the measurement points.

During experiments draft and air flows would significantly influence the flames, fire plume and ceiling jets. The draft and air flow in the laboratory were caused by wind gusts from the outside. The draft and air flows the wind created in the fire safety laboratory, made the flame fluctuate and tilt severely towards the side of the experimental setup. As the flame tilts, the whole fire plume tilts and moving

the anticipated point of impingement in the ceiling. Under optimal conditions the area of impingement would be in the same place at all times. During experiments there are always movements in the air, and there will be some movement of the impingement zone. The effect of the fluctuations and tilting of the flame was tried controlled by stopping the measurement when the tilt was visible in the temperature measurements. When the severely tilting of the flame ceased, the measurements were resumed. In the simulations in FDS, there are no factors such as wind influencing the simulation. Specifying random behavior of draft in FDS can be very challenging and no known data exist on the subject. The conditions in terms of air flow are optimal, and the area of impingement can be expected to be in the same area. However, the turbulent nature of the flames will contribute to some movement of the impingement zone.

In the experimental setup, the thermocouples were suspended by twisting them around a wire, as described in section 3.1.4 of this study. The placement of thermocouples was double checked before starting experiments. However, there is a small chance that the thermocouples moved and the position where measurements were conducted changed. Movement of thermocouples could occur while personnel were moving around the setup, or when changing the ceiling height between experiments. The position of the thermocouples needed individual adjustments depending on ceiling height and heat release rate, due to limited number (45) of thermocouples. Pre- testing showed that the thermocouples needed to be adjusted for some ceiling heights and heat release rates. The calculated temperature, $\Delta T/e + T_\infty$ for the thickness of the ceiling jet, fell outside the height of the thermocouples. In FDS this was not a problem, the thermocouples is given a permanent position and cannot be moved, ensuring that what is measured in the simulation is correct for that simulation.

Many of the uncertainties experienced with the experimental setup can and will be removed when simulating the phenomenon. Some of the eliminated uncertainties in simulations have been discussed above. However, when using simulation tools, new and sometimes unforeseen uncertainties appear. It is important to be aware of the uncertainties that follow the use of simulation tools. The grid cell sizing as discussed above, is one such uncertainty.

5.4 WEAK AND STRONG DRIVEN CEILING JETS

The ceiling jets are divided into weak and strong driven ceiling jets depending on the ratio between the flame height and ceiling height, L/H [7]. Based on the ceiling height and the calculated flame height from eq. 2.2 the ceiling jets from a 44 kW (0.5 m × 0.5 m burner) fire under ceiling heights

2.39 m and 1.74 m, and 65 kW (0.5 m × 0.5 m burner) under 2.39 m ceiling height are weak driven ceiling jets. All other experimental and simulated ceiling jet is strong driven ceiling jets. A comparative analysis of thickness of the mentioned weak driven ceiling jets against strong driven ceiling jets was performed without finding anything separating the weak from the strong driven ceiling jet. From this analysis on the thickness of a weak and strong driven ceiling jet, it does not seem to be any major differences that separate the weak- from the strong driven ceiling jet. The difference seem to only be in the mathematical way of the describing the phenomena of the ceiling jet.

5.5 MAXIMUM TEMPERATURE IN A CEILING JET

In this study the maximum ceiling jet has been assumed to be at 0.02 m under the ceiling surface. Previous work by Alpert [16], You [5], Motevalli and Marks [6] and Heskestad and Hamada [17] assumed the maximum temperature to be at approximately 1-2 % of the ceiling height. The work in this paper assumes a permanent position of 0.02 m, which make up 0.8 - 1.8 % of the ceiling heights used in the experiments.

The maximum temperature in the ceiling jet is in the separation between the inner and the outer thermal boundary layer of the ceiling jet. The thickness of the inner thermal boundary layer can be expressed by the thickness of the inner hydrodynamic boundary layer and the Prandtl number, as shown in eq. 2.8. From eq. 2.6 the thickness of the hydrodynamic boundary layer can be expected to grow thicker with either increase in radius, decrease in free stream velocity and with increase in the dynamic viscosity in the fluid.

Figure 32 show a representation of how the thermal boundary layer looks, based on simple assumptions that the free stream velocity and temperature is equal to Alperts expressions for maximum temperature and velocity in a ceiling jet, eq. (2.13, 2.14, 2.17, and 2.18). The figure show the how the thermal boundary layer behaves when variables as the radius, ceiling height and heat release rate is changed. Change in ceiling height and heat release rate will alter the maximum temperature and velocity in the ceiling jet. Figure 32 show the calculated thermal boundary layer thickness from eq. 2.8 for the heat release rates 44 kW and 176 kW. The ceiling heights are varied between 2.39 m and 1.12 m for both heat release rates.

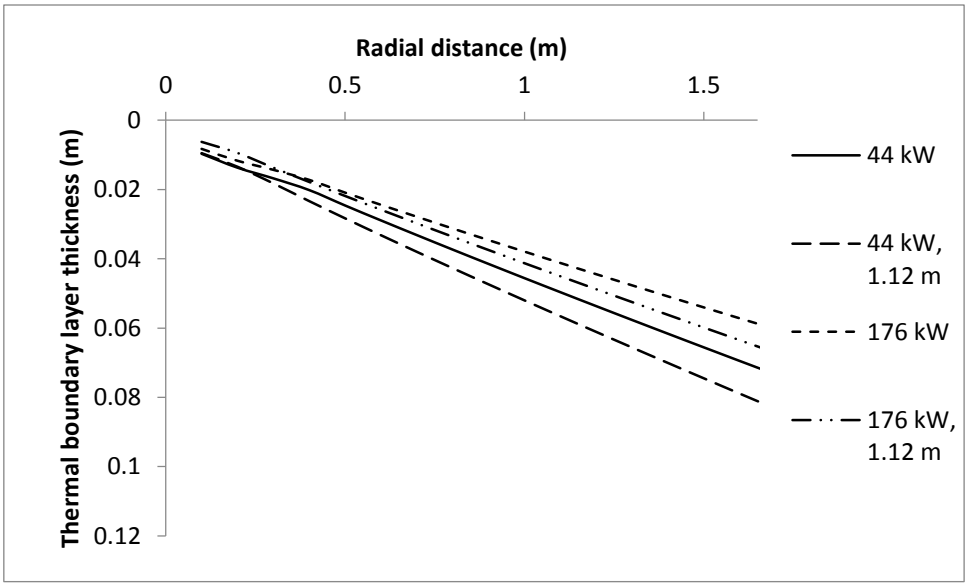

Figure 32 Thermal boundary layer of the ceiling jet under a 2.39 m ceiling height. The solid line shows the thermal boundary layer for a 44 kW fire and the dotted line shows the thermal boundary layer for a 176 kW fire. The dashed line shows the thermal boundary layer for a 44 kW fire under a 1.12 m ceiling height.

The approximation of the thickness of the thermal boundary layer in figure 32, show that the boundary layer increases with increased radius. In the beginning, the thickness of the thermal boundary layer is less than 0.01 m, increasing to 0.05 – 0.08 m depending on heat release rate and ceiling height. In percentage of the ceiling height, this corresponds to less than 0.4 – 0.9 % for ceiling heights 2.39 m and 1.12 m respectively when the thermal boundary layer is less than 0.01 m. As the radius increase to 1.65 m, the thermal boundary layer increases to 2.1 – 3.3 % and 4.4 – 7.1 % of the ceiling height for 2.39 m and 1.12 m respectively. The thermal boundary layer increase in thickness as the radius under the ceiling increase. This is not taken into account in experiments, simulations or previous work, and is perhaps something that should be studied further.

Figure 32 is a theoretical representation of the thermal boundary and not necessarily how it actually behaves. However, if the maximum temperature in ceiling jet follows the thermal boundary layer, then the placement of thermocouples at 1-2 % of the ceiling height, or at 0.02 m, will not be where the actual maximum temperature in the ceiling jet is. Figure 32 suggests that the thickness of the boundary layer is upwards of 7.1 % of the ceiling height and increasing with radius.

In the experiment performed in this study, the vertical temperature profile at radial positions was measured. The maximum temperature were assumed to be at 0.02 m, and the next temperature measurement in the profile was at 0.05, 0.08 or 0.13 m depending on the experimental run, see section 3.1.5 *Placement of thermocouples* and figure 10 B. It was not seen in the raw data that the

temperature at any of the lower thermocouples were higher than the temperature at the assumed maximum temperature position. Since the next temperature measurement in the profile is 0.03 – 0.10 m from the first thermocouple, it is possible that the maximum temperature could be found within this distance.

The placement of the thermocouple at 0.02 m was within the anticipated area of the maximum temperature based on previous work. As figure 32 show, the thermal boundary layer and the maximum temperature change with radius, heat release rate and ceiling height. The change in where the maximum temperature is means that what is being measured at 1 %, 2% of the ceiling height or in this study 0.02 m, might not be the actual maximum temperature of the ceiling jet. If the temperature is in fact higher in another place, it will influence the thickness of the ceiling jet. Since the ceiling jet thickness is based on a temperature criterion of $1/e$ of the maximum temperature, a higher maximum temperature will increase the temperature the ceiling jet thickness is measured upon and thus increase the thickness of the ceiling jet.

6 CONCLUSION

In this study the thermal ceiling jet thickness has been investigated. The behavior of the strong driven ceiling jet was investigated, and how the ceiling jet thickness changes with radial distance from the fire plume, and with change of heat release rate and ceiling height. The difference of a weak and a strong driven ceiling jet thickness have also been investigated. For this investigation full-scale experiments and simulations in FDS have been conducted.

The ceiling jet has been found to increase as the radius increase. From experimental testing it was found that the ceiling jet thickness, on average, increases 2 % of the ceiling height from the initial radius of 0.4 m to 1.65 m. Ceiling jet thicknesses simulated in FDS show the opposite trend, a decrease in ceiling jet thickness of 2 % of the ceiling jet.

In this investigation the behavior of the ceiling jet thickness has been tested when ceiling heights and heat release rates have been changed. The effect of heat release rates show that the ceiling jet increase in thickness as the heat release rate is increased. The effect of ceiling height on the ceiling jet thickness has the same effect. Increasing ceiling height leads to increasing ceiling jet thickness.

Simulation of the ceiling jet thickness in FDS, the results show that FDS under predicts the thickness of the ceiling jet. The ceiling jet thickness simulated in FDS show the same trend as the experiments. Increase in ceiling jet thickness when the heat release rate and ceiling height are increased. However, the results from simulation in FDS show a decrease in thickness as the radius become larger. This is opposite of the experimental results.

The ceiling jet is divided into weak and strong driven ceiling jets. The differences between the two mathematical terms of describing a ceiling jet have been investigated. There has not been discovered any physical differences between the two in the results of this study.

The ceiling jet thickness has been found through experiments and simulations. The ceiling jet was found to increases as the heat release rate and ceiling height increases. Simulations in FDS showed the same trend.

7 FURTHER WORK

The investigation performed in this study looked at the ceiling jet thickness over a radius of 1.25 m. As a continuation of this work, the ceiling jet thickness for a larger radius can be investigated further.

The ceiling jet thickness can be defined by the thermal thickness, as this study has investigated. However, the ceiling jet thickness can also be described by velocity, species and visual thickness. Further work on the ceiling jet thickness should include these issues.

In this study the maximum temperature of the ceiling jet was not investigated. The maximum temperature was assumed at 0.02 m. However the thickness of the thermal boundary layer, where the maximum temperature is, is not constant. Other studies have used 1-2 % of the ceiling height as guidance for where the maximum temperature of ceiling jet is. Further work on the ceiling jet could include a study on the maximum temperature of the ceiling jet.

This study has been performed for a radius close to the fire, within 1.65 m from the centerline of the plume. For some of the ceiling jet thicknesses it was difficult to see how the radius affected the thickness. In further work, the behavior of the ceiling jet thickness on a larger radius should be studied.

The ceiling jet is divided by the ratio of flame height to ceiling height as weak or strong driven ceiling jets. In this study it was attempted to find a physical difference in the thickness between the two terms dividing the ceiling jet. It seems that there is only mathematics dividing the weak from the strong ceiling jet. If there is a difference between weak and strong driven ceiling jet thicknesses needs to be investigated further.

REFERENCES

[1] The Society of fire protection engineers, SFPE Handbook of fire protection engineering, New York: Springer, 2016.

[2] B. Karlsson and J. G. Quintiere, Enclosure Fire Dynamics, Boca Raton: CRC Press LLC, 2000.

[3] R. W. Pickard, D. Hird and P. Nash, "The thermal testing of heat-sensitive fire detectors," Department of Scientific and Industrial Reasearch and Fire Offices Commitee Joint Fire Reasearch Organization, Boreham Wood, 1957.

[4] R. L. Alpert, "Turbulent ceiling-jet induced by large-scale fires," Combustion Science and technology, 11:5-6, 197-213, Norwood, 1975.

[5] H.-Z. You, "An investigation of fire-plume impingement on a horizontal ceiling: 2- Impingement and ceiling-jet region," *Fire and Materials, Vol. 9, No. 1 ,* pp. 46-55, 1985.

[6] V. Motevalli and C. Marks H, "Characterizing the unconfined ceiling jet under steady-state conditions: A reassessment," International association for fire safety science, 1991.

[7] D. Drysdale, An introduction to fire dynamics, West Sussex: John Wiley & Sons Ltd., 2011.

[8] Comsol, "Comsol.no," [Online]. Available: https://www.comsol.no/multiphysics/boussinesq-approximation. [Accessed 08 December 2016].

[9] H. W. Emmons, "The ceiling jet in fires," International association for fire safety science, Cambridge.

[10] K. A. Murty, "3.4 Heat transfer across a boundary layer," in *Introduction to combustion phenomena* , New York, Gordon and Breach, 1975, pp. 57-59.

[11] J. E. Finnmore and J. B. Franzini, Fluid mechanics- with engineering applications, New York: McGraw-Hill, 2002.

[12] F. M. White, Viscous Fluid Flow, New York: Mcgraw-Hill, Inc, 1991.

[13] J. C. Dixon, "Appendix B; Properties of air," in *The shock absorber handbook*, Wiley online library,

2007, pp. 375-378.

[14] E. Zukoski, "Fluid dynamic aspect of room fires," Karman laboratory of fluid mechanics and jet propulsion, Pasadena, 1985.

[15] J. E. Finnmore and J. B. Franzini, Fluid Mechanics with Engineering Applications, New York: McGraw- Hill, Inc, 2002.

[16] R. Alpert, "Calculation of Respons Time of Ceiling-Mounted Fire Detectors," Factory Mutual Research Corporation, 1972.

[17] G. Heskestad and T. Hamada, "Ceiling jet of stong fire plumes," Fire safety journal 21 (1993) 69-82, Norwood, 1992.

[18] Y. Oka, H. Oka and O. Imazeki, "Ceiling jet thickness and vertical distribution along flat-ceilinged horizontal tunnel with natural ventilation," Tunnelling and underground space technology Vol. 53, 01.03.2016, p. 68-77, 2016.

[19] G. T. Atkinson and D. Drysdale, "Convective heat transfer from fire gases," *Fire Safety Journal (19),* pp. 217-245, 1992.

[20] J. P. Bentley, "Thermoelectric sensing elements," in *Principles of measurement systems*, Essex, Pearson Education Limited, 2005, pp. 172-176.

[21] C. Woodford, "Explainthatstuff!," 25 November 2016. [Online]. Available: http://www.explainthatstuff.com/howthermocoupleswork.html . [Accessed 01 May 2017].

[22] Omega, "Omega Engineering," [Online]. Available: http://www.omega.com/techref/ThermocoupleResponseTime.html. [Accessed 25 May 2017].

[23] H. Hashemian, "New technology for remote testing of response time of installed thermocouples; Volume 1 - Background and general details," Analysis and measurement services Corp. , Knoxville, 1992.

[24] P. Sharma, N. Murali and T. Jayakumar, "Effect of thermocouple time constant on sensing of temperature fluctuations in a fast reactor subassembly," Journal of Sensors and Sensor Systems, 2014.

[25] National Institute of Standard and Technology, Fire Dynamic Simulator User's Guide, National Institute of Standard and Technology, 2017.

[26] National Institute of Standard and Technology, "Fire Dynamics Simulator Technical Reference Guide Volume 1: Mathematical Model," National Institute of Standard and Technology, 2017.

[27] National Institute of Standard and Technology, "Fire Dynamic Simulator Technical Reference Guide Volume 3: Validation," National Institute of Standard and Technology, 2017.

[28] National Institute of Standards and Technology, "Fire Dynamics Simulator User's Guide," National Institute of Standards and Technology, Maryland, 2015.

APPENDIX

A.1 Results for 0.3 m × 0.3 m burner

All the experiments were conducted for an 0.3 m × 0.3 m burner as well as the 0.5 m × 0.5 m burner showed in chapter 4 of this study. The experimental and simulated results for all runs with a burner size 0.3 m × 0.3 m are shown in this chapter.

A.1.1 Effect of ceiling heights

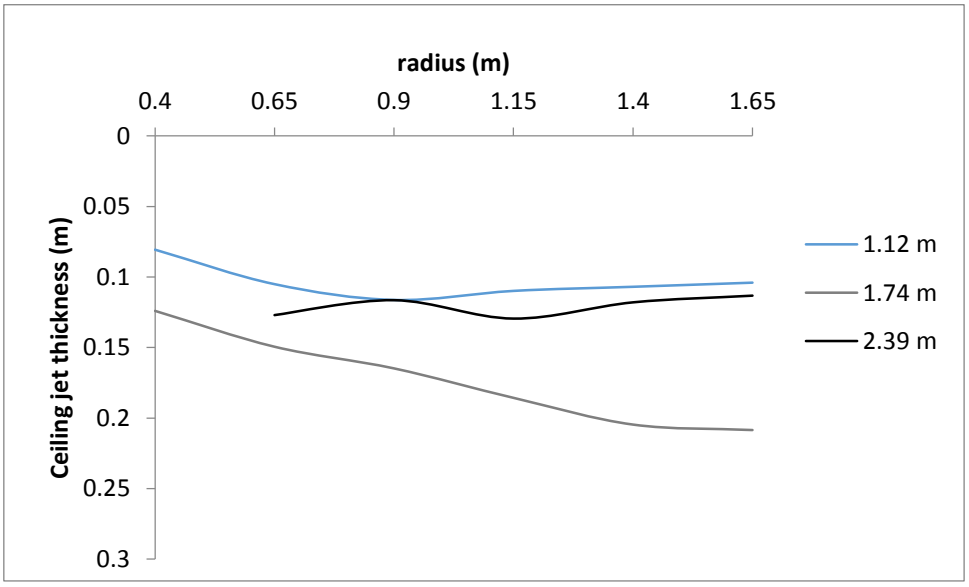

Figure 33 Ceiling jet thickness as a function of radius. A constant HRR of 44 kW fire is burnt under ceiling heights of 1.12 m, 1.74 m and 2.39 m. The ceiling jet is measured over a radius of 1.25 m starting at 0.4 m.

Figure 33 shows that the ceiling jet thickness increases as the ceiling height increase. The result from 2.39 m ceiling height is not in agreement with the trend of increasing ceiling jet thickness when the ceiling height is increased.

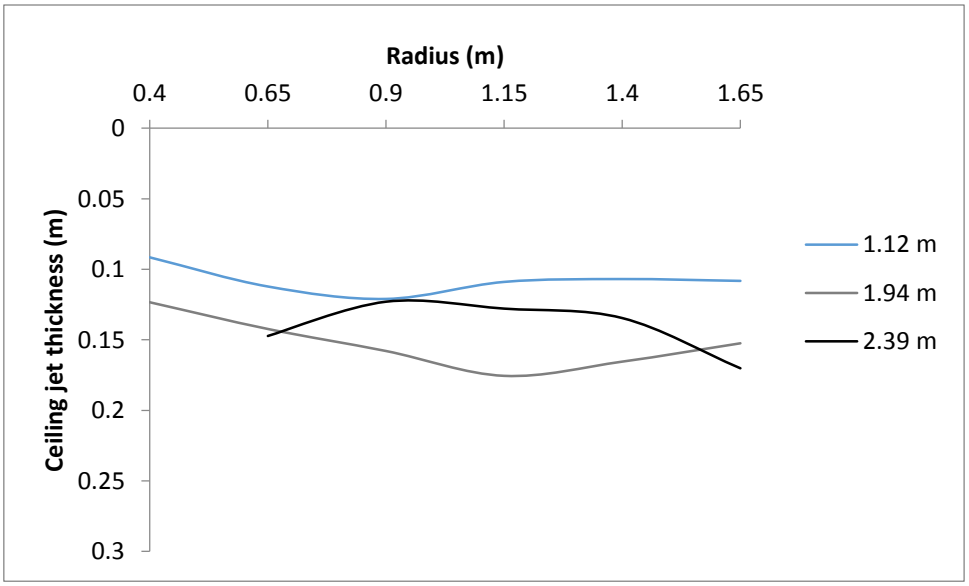

Figure 34 Ceiling jet thickness as a function of radius. A constant HRR of 65 kW fire is burnt under ceiling heights of 1.12 m, 1.94 m and 2.39 m. The ceiling jet is measured over a radius of 1.25 m starting at 0.4 m.

Figure 34 shows that the ceiling jet thickness increases as the ceiling height increase. The result from 2.39 m ceiling height is not in agreement with the trend of increasing ceiling jet thickness when the ceiling height is increased.

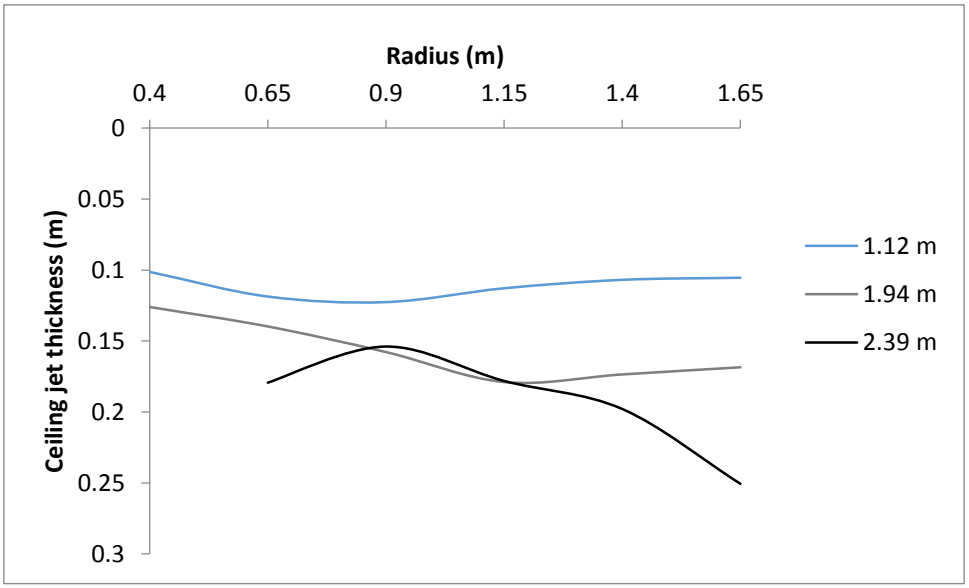

Figure 35 Ceiling jet thickness as a function of radius. A constant HRR of 80 kW fire is burnt under ceiling heights of 1.12 m, 1.94 m and 2.39 m. The ceiling jet is measured over a radius of 1.25 m starting at 0.4 m.

Figure 35 shows that the ceiling jet thickness increases as the ceiling height increase.

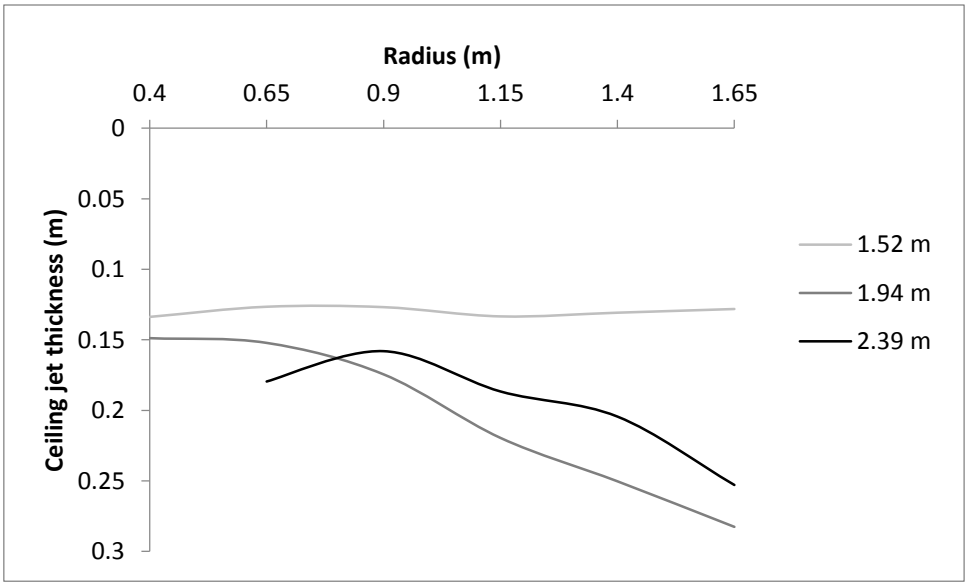

Figure 36 Ceiling jet thickness as a function of radius. A constant HRR of 120 kW fire is burnt under ceiling heights of 1.12 m, 1.94 m and 2.39 m. The ceiling jet is measured over a radius of 1.25 m starting at 0.4 m.

Figure 36 shows that the ceiling jet thickness increases as the ceiling height increase. The result from 2.39 m ceiling height is not in agreement with the trend of increasing ceiling jet thickness when the ceiling height is increased.

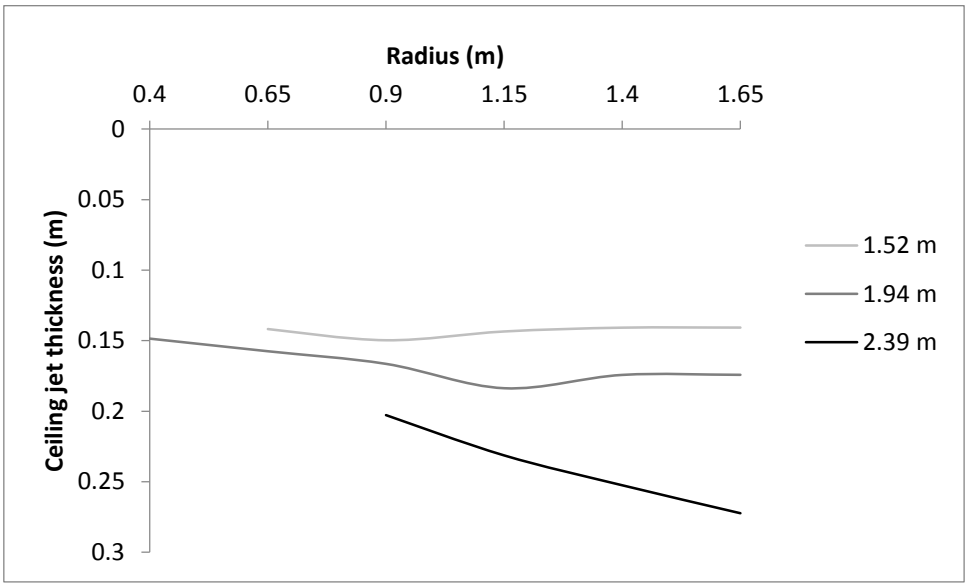

Figure 37 Ceiling jet thickness as a function of radius. A constant HRR of 176 kW fire is burnt under ceiling heights of 1.52 m, 1.94 m and 2.39 m. The ceiling jet is measured over a radius of 1.25 m starting at 0.4 m.

Figure 37 shows that the ceiling jet thickness increases as the ceiling height increase.

A.1.2 Effect of heat release rate

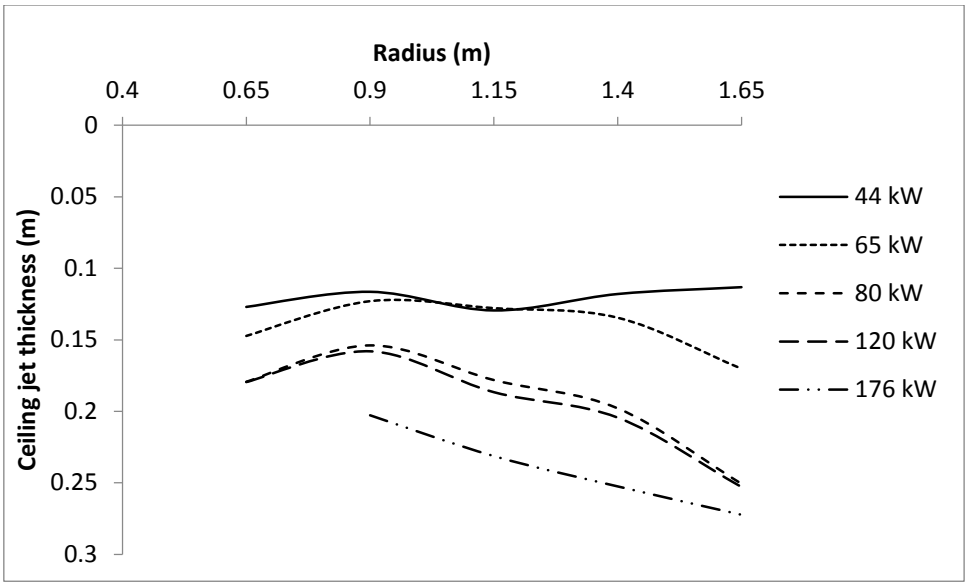

Figure 38 Ceiling jet thickness as a function of radius for a constant ceiling height of 2.39 m. Fires with HRR of 44 kW, 65 kW, 80 kW, 120 kW and 176 kW are burnt beneath a constant ceiling height of 2.39 m. The ceiling jet is measured over a radius of 1.25 m starting at 0.4 m.

Figure 38 shows that the ceiling jet thickness increases as the heat release is increased.

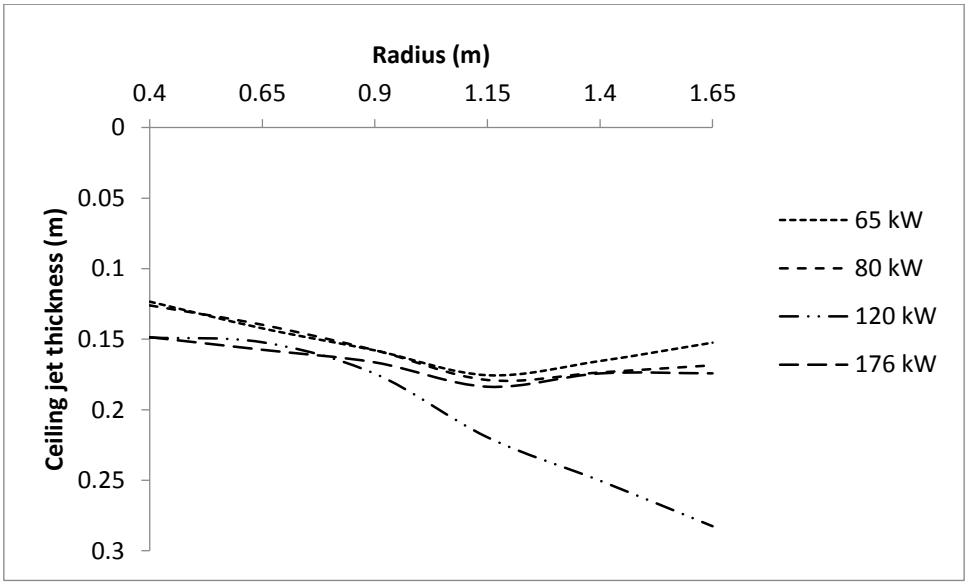

Figure 39 Ceiling jet thickness as a function of radius for a constant ceiling height of 1.94 m. Fires with HRR of 65 kW, 80 kW, 120 kW and 176 kW are burnt beneath a constant ceiling height of 1.94 m. The ceiling jet is measured over a radius of 1.25 m starting at 0.4 m.

Figure 39 shows that the ceiling jet thickness increases as the heat release is increased.

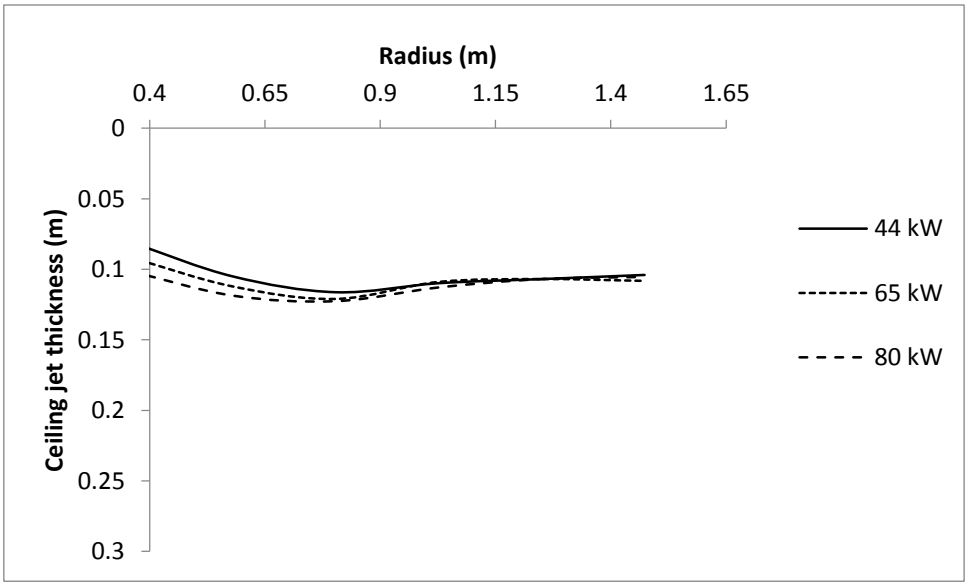

Figure 40 Ceiling jet thickness as a function of radius for a constant ceiling height of 1.12 m. Fires with HRR of 44 kW, 65 kW and 80 kW are burnt beneath a constant ceiling height of 1.12 m. The ceiling jet is measured over a radius of 1.25 m starting at 0.4 m.

Figure 40 shows that the result from ceiling height of 1.12 m the change in heat release rate does not affect the ceiling jet thickness largely.

A.1.2.1 Effect of heat release rate vs. the work of Motevalli & Marks

Burner size 0.5×0.5 m

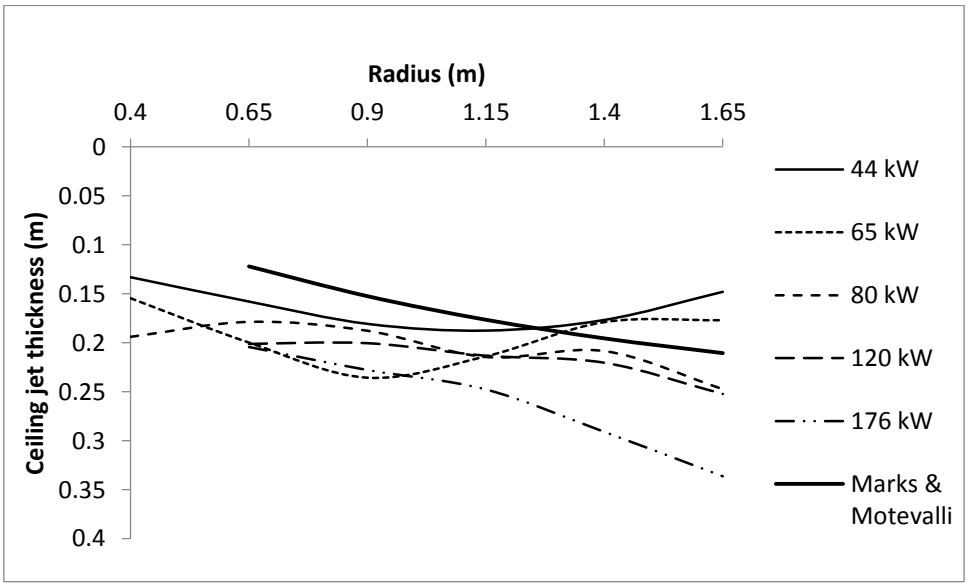

Figure 41 Ceiling jet thickness as a function of radius for the given ceiling height of 2.39 m is compared to the ceiling jet thickness from Motevalli and Marks [6].

Figure 41 show that the ceiling jet thickness approximated by Motevalli and Marks [6] underestimates the result from experiments of the strong driven ceiling jet thickness. The experimental ceiling jet thickness at 1.94 m ceiling height is affected by change in heat release rate.

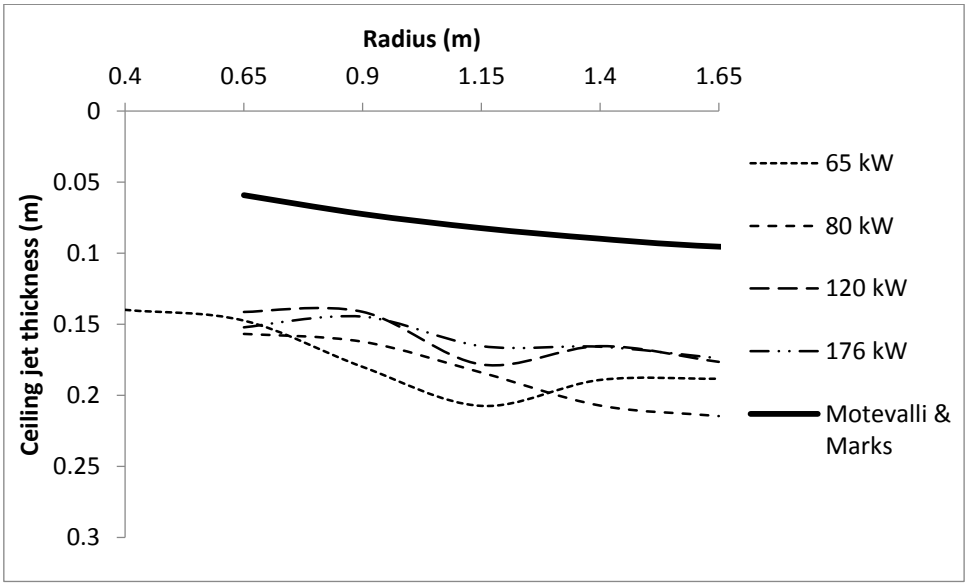

Figure 42 Ceiling jet thickness as a function of radius for the given ceiling height of 1.94 m is compared to the ceiling jet thickness from Motevalli and Marks [6].

Figure 42 show that the ceiling jet thickness approximated by Motevalli and Marks [6] underestimates the result from experiments of the strong driven ceiling jet thickness. The experimental ceiling jet thickness at 1.94 m ceiling height is affected by change in heat release rate.

Burner size 0.3×0.3 m

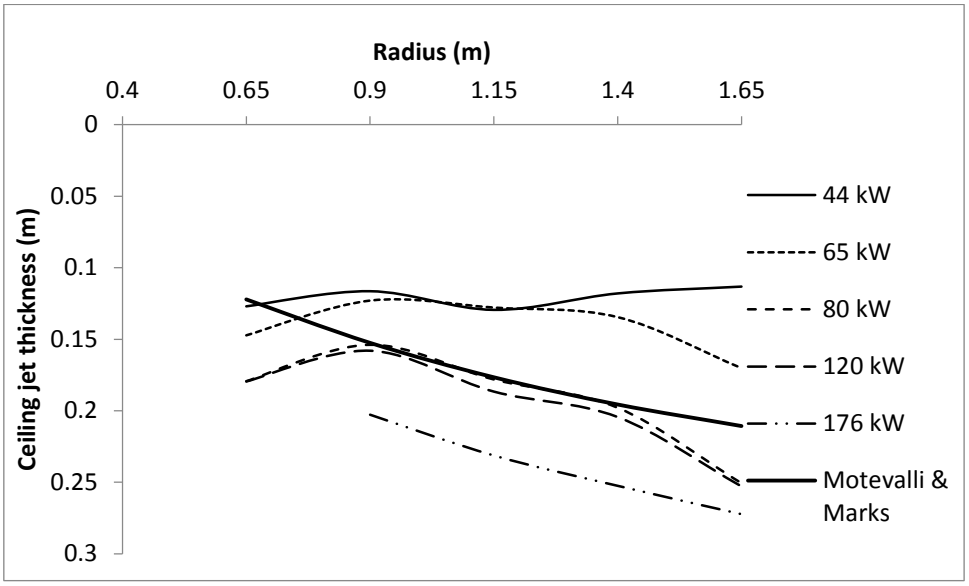

Figure 43 Ceiling jet thickness as a function of radius for the given ceiling height of 2.39 m is compared to the ceiling jet thickness from Motevalli and Marks [6].

Figure 43 show that the ceiling jet thickness approximated by Motevalli and Marks [6] compared to results from experiments of the strong driven ceiling jet thickness. The experimental ceiling jet thickness at 1.94 m ceiling height is affected by change in heat release rate.

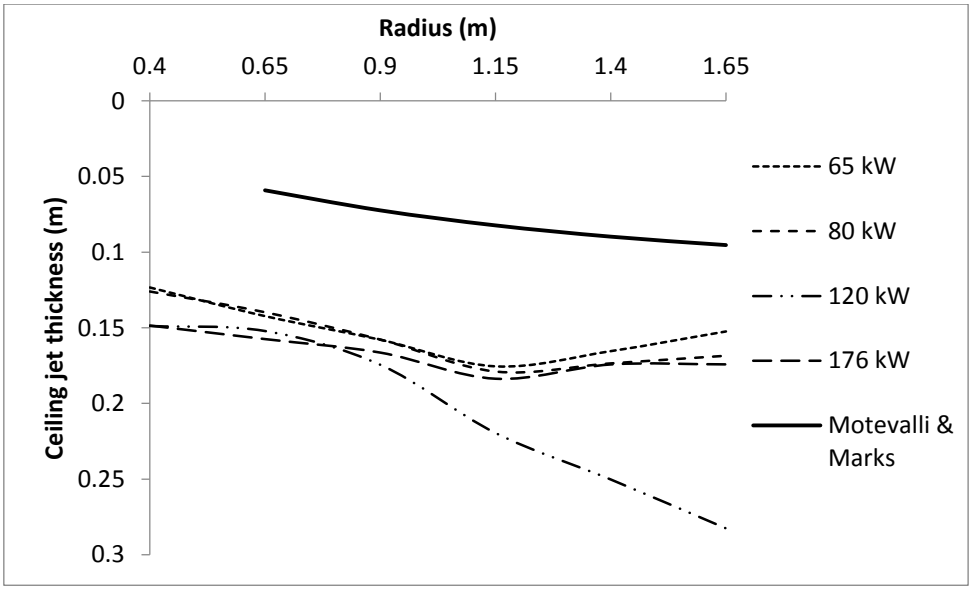

Figure 44 Ceiling jet thickness as a function of radius for the given ceiling height of 1.94 m is compared to the ceiling jet thickness from Motevalli and Marks [6].

Figure 44 show that the ceiling jet thickness approximated by Motevalli and Marks [6] underestimates the result from experiments of the strong driven ceiling jet thickness. The experimental ceiling jet thickness at 1.94 m ceiling height is affected by change in heat release rate.

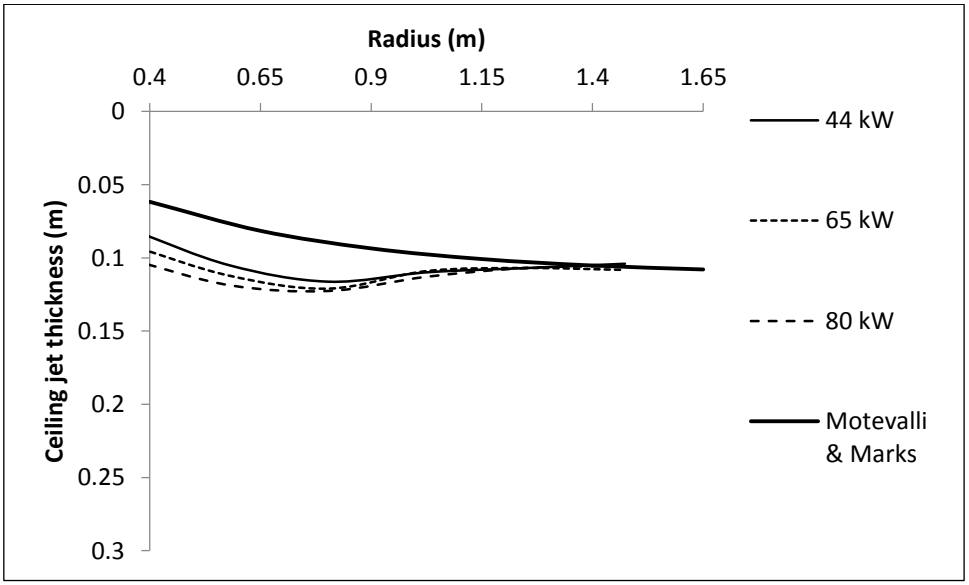

Figure 45 Ceiling jet thickness as a function of radius for the given ceiling height of 1.12 m is compared to the ceiling jet thickness from Motevalli and Marks [6].

Figure 45 show that the ceiling jet thickness approximated by Motevalli and Marks [6] underestimates the result from experiments of the strong driven ceiling jet thickness. The ceiling jet thickness under 1.12 m ceiling height, is not affected by change in heat release rate.

B.1 RESULTS FROM SIMULATION

B.1.1 Effect of ceiling height

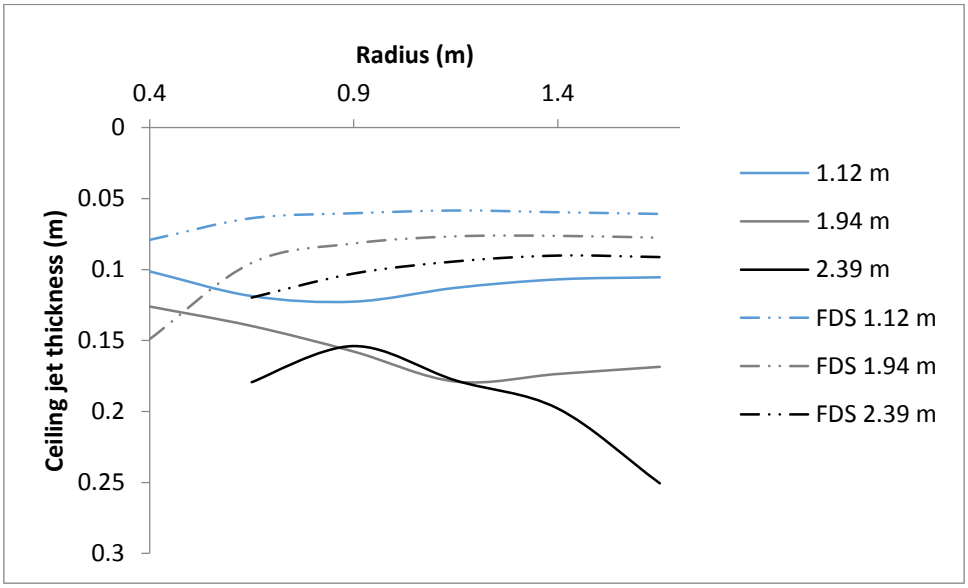

Figure 46 Ceiling jet thickness as a function of radius. A constant HRR of 80 kW fire is under ceiling heights of 1.12 m, 1.94 m and 2.39 m. The ceiling jet is measured over a radius of 1.25 m starting at 0.4 m. The dotted result represents the result from simulation in FDS.

Figure 46 show that the simulated results give the same trend as experimental results, increasing ceiling jet thickness with increase in ceiling height. The ceiling jet thickness simulated in FDS underestimates the results from experiments.

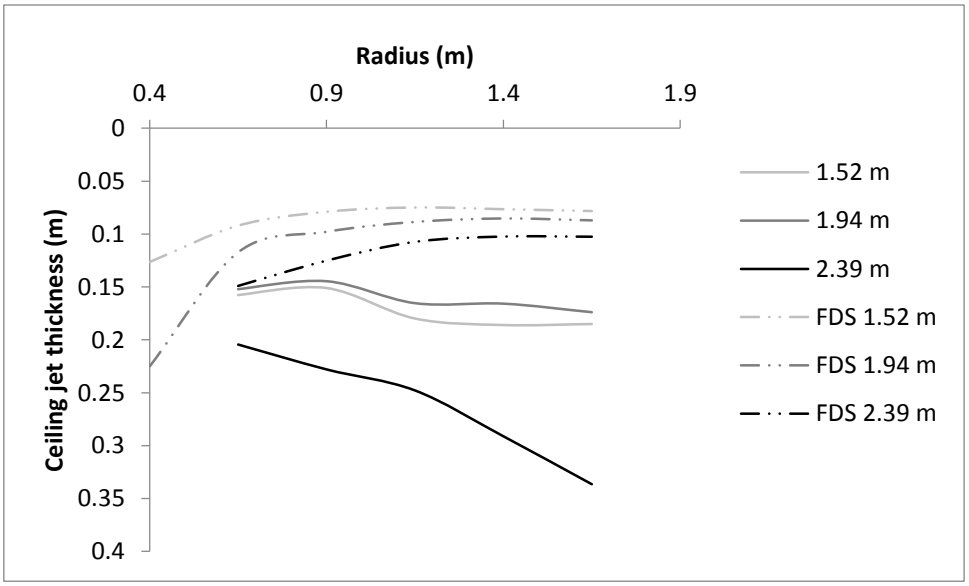

Figure 47 Ceiling jet thickness as a function of radius. A constant HRR of 176 kW fire is under ceiling heights of 1.52 m, 1.94 m and 2.39 m. The ceiling jet is measured over a radius of 1.25 m starting at 0.4 m. The dotted result represents the result from simulation in FDS.

Figure 47 show that the simulated results give the same trend as experimental results, increasing ceiling jet thickness with increase in ceiling height. The ceiling jet thickness simulated in FDS underestimates the results from experiments.

B.1.2 Effect of heat release rate

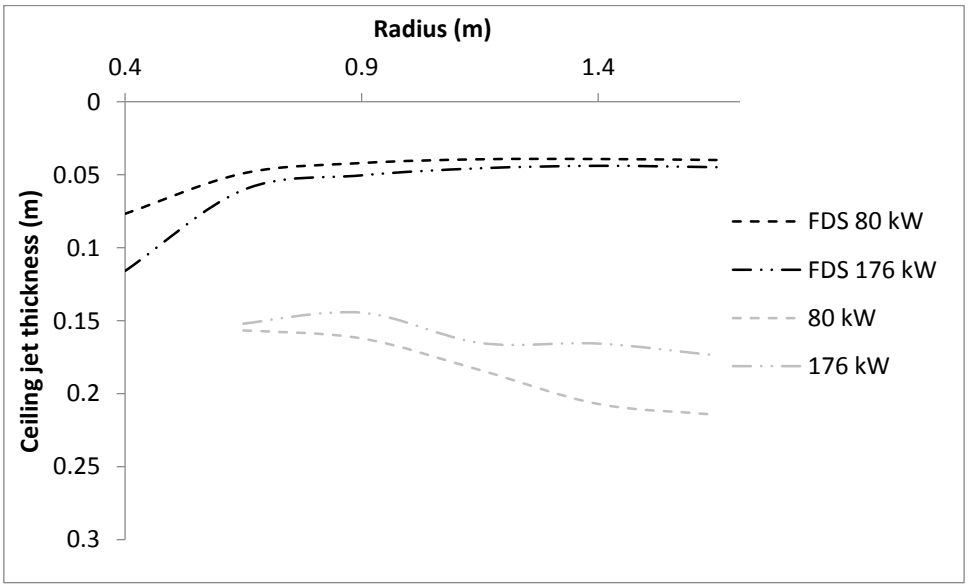

Figure 48 Ceiling jet thickness as a function of radius for a given ceiling height of 1.94 m. Fires with HRR of 80 kW and 176 kW is burnt beneath a constant ceiling height of 1.94 m. The ceiling jet is measured over a radius of 1.25 m starting at 0.4 m.

Figure 48 show that the simulated results give the same trend as experimental results, increasing ceiling jet thickness with increase in heat release rate. The ceiling jet thickness simulated in FDS underestimates the results from experiments.

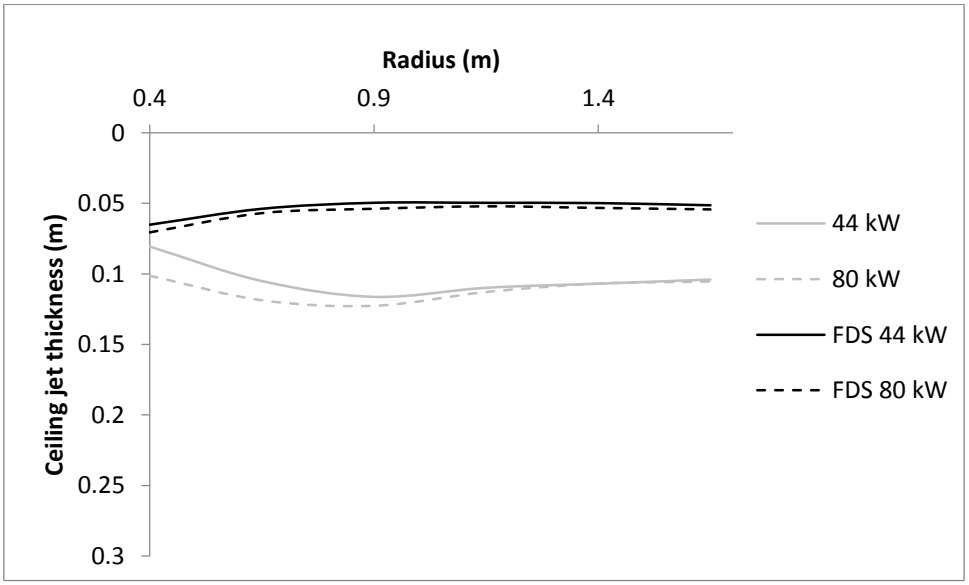

Figure 49 Ceiling jet thickness as a function of radius for a given ceiling height of 1.12 m. Fires with HRR of 44 kW, 65 kW, 80 kW and 120 kW is burnt beneath a constant ceiling height of 1.12 m. The ceiling jet is measured over a radius of 1.25 m starting

Figure 49 show that the simulated results give the same trend as experimental results, increasing ceiling jet thickness with increase in heat release rate. At a ceiling height of 1.12 m, change in heat release rate does not seem to affect the ceiling jet thickness largely. The ceiling jet thickness simulated in FDS underestimates the results from experiments.

C.1 THERMOCOUPLE PLACEMENT

The tables below show the arrangement of thermocouples from experiments. Pre- testing showed that the thermocouple needed some adjustment for some of the heat release rates, ceiling heights and burner sizes. Table 3 shows the thermocouple arrangements which were used to each experimental run.

Thermocouple arrangement 1

	0.4 m	**0.65 m**	**0.9 m**		**1.15 m**	**1.4 m**	**1.65 m**
0.02 m	■	■	■	0.02 m	■	■	■
0.13 m	■	■	■	0.15 m	■	■	■
0.155 m	■	■	■	0.175 m	■	■	■
0.18 m	■	■	■	0.20 m	■	■	■
0.205 m	■	■	■	0.225 m	■	■	■
0.23 m		■	■	0.25 m	■	■	■
0.255 m			■	0.275 m	■	■	■
0.28 m				0.30 m	■	■	■
0.305 m				0.325 m		■	■
0.33 m				0.35 m			■

Thermocouple arrangement 2

	0.4 m	**0.65 m**	**0.9 m**		**1.15 m**	**1.4 m**		**1.65 m**
0.02 m	■	■	■	0.02 m	■	■	0.02 m	■
0.08 m	■	■	■	0.10 m	■	■	0.11 m	■
0.105 m	■	■	■	0.125 m	■	■	0.135 m	■
0.13 m	■	■	■	0.15 m	■	■	0.16 m	■
0.155 m	■	■	■	0.175 m	■	■	0.185 m	■
0.18 m		■	■	0.20 m	■	■	0.21 m	■
0.205 m			■	0.225 m	■	■	0.235 m	■
0.23 m				0.25 m	■	■	0.26 m	■
0.255 m				0.275 m		■	0.285 m	■
0.28 m				0.30 m			0.31 m	■

Thermocouple arrangement 3

	0.4 m	0.65 m	0.9 m		1.15 m		1.4 m	1.65 m
0.02 m	■	■	■	0.02 m	■	0.02 m	■	■
0.05 m	■	■	■	0.06 m	■	0.07 m	■	■
0.075 m	■	■	■	0.085 m	■	0.095 m	■	■
0.1 m	■	■	■	0.11 m	■	0.12 m	■	■
0.125 m	■	■	■	0.135 m	■	0.145 m	■	■
0.15 m		■	■	016 m	■	0.17 m	■	■
0.175 m			■	0.185 m	■	0.195 m	■	■
0.2 m				0.21 m	■	0.22 m	■	■
0.225 m				0.235 m		0.245 m	■	■
0.25 m				0.26 m		0.27 m		■

Table 3 Overview of thermocouple arrangements used in each experimental run.

Run	$\dot{Q}$ [kW]	D [m]	H [m]	*Thermocouple arrangement*
1	44	0.5×0.5	2.39	Arrangement 1
2	44	0.5×0.5	1.74	Arrangement 2
3	44	0.5×0.5	1.52	Arrangement 2
4	44	0.5×0.5	1.12	Arrangement 3
5	44	0.3×0.3	2.39	Arrangement 1
6	44	0.3×0.3	1.74	Arrangement 2
7	44	0.3×0.3	1.52	Arrangement 3
8	44	0.3×0.3	1.12	Arrangement 3
9	65	0.5×0.5	2.39	Arrangement 1
10	65	0.5×0.5	2.14	Arrangement 2
11	65	0.5×0.5	1.94	Arrangement 2
12	65	0.5×0.5	1.12	Arrangement 3
13	65	0.3×0.3	2.39	Arrangement 1
14	65	0.3×0.3	1.94	Arrangement 2
15	65	0.3×0.3	1.12	Arrangement 3
16	80	0.5×0.5	2.39	Arrangement 1
17	80	0.5×0.5	1.94	Arrangement 2
18	80	0.5×0.5	1.12	Arrangement 3
19	80	0.3×0.3	2.39	Arrangement 1

20	80	0.3×0.3	1.94	Arrangement 2
21	80	0.3×0.3	1.12	Arrangement 3
22	120	0.5×0.5	2.39	Arrangement 1
23	120	0.5×0.5	1.94	Arrangement 2
24	120	0.5×0.5	1.52	Arrangement 3
25	120	0.5×0.5	1.12	Arrangement 3
26	120	0.3×0.3	2.39	Arrangement 1
27	120	0.3×0.3	1.94	Arrangement 2
28	120	0.3×0.3	1.52	Arrangement 2
29	176	0.5×0.5	2.39	Arrangement 1
30	176	0.5×0.5	1.94	Arrangement 2
31	176	0.5×0.5	1.52	Arrangement 2
32	176	0.3×0.3	2.39	Arrangement 1
33	176	0.3×0.3	1.94	Arrangement 2
34	176	0.3×0.3	1.52	Arrangement 3

D.1 SIMULATION SCRIPT

The simulation script used for the simulations performed in this study is presented here is for a 44 kW under a 2.39 m ceiling height. All simulations were simulated for 0.3 m × 0.3 m burner size.

```
/******************Miscellaneous ********************************************************************
&HEAD CHID= '44kW', TITLE= '44 kW, 0,3 burner' /
&TIME T_END= 300, /
&MISC RESTART=.FALSE./
&DUMP DT_RESTART=10/
&TMPA=17/
/****************** Computational grid ***************************************************************
&MESH IJK=128,128,122, XB= -1.6,1.6,-1.6,1.6,-0.1,2.95/
/****************** Obstructions ********************************************************************
/Floor
&OBST XB= -1.22, 1.22, -1.22, 1.22, 0.0, -0.0095, SURF_ID= 'FLOOR1'/
/Burner
&OBST XB= 0.4336038969,0.7336038969,-0.4336038969,-0.7336038969,0.0, 0.25, SURF_ID= 'BURNER'/
/Roof
&OBST XB= -1.22,1.22,-1.22,1.22,2.64,2.69, SURF_ID= 'ROOF1'/
/****************** Passive ventilations openings: ***************************************************
&VENT XB= -1.6,1.6,-1.6,-1.6,-0.1,2.95, SURF_ID='OPEN',/ Ventilation front
&VENT XB= -1.6,1.6,1.6,1.6,-0.1,2.95, SURF_ID='OPEN',/   Ventilation back
&VENT XB= -1.6,-1.6,-1.6,1.6,-0.1,2.95, SURF_ID='OPEN',/ Ventilation left side
&VENT XB= 1.6,1.6,-1.6,1.6,-0.1,2.95, SURF_ID='OPEN',/   Ventilation right side
&VENT XB=-1.6,1.6,-1.6,1.6,2.95,2.95, SURF_ID='OPEN',/   Ventilation top
/******************Fire ***************************************************************************
&REAC ID =          'PROPANE'
                    FUEL='PROPANE'
                    SOOT_YIELD = 0.01
                    C = 3.
                    H = 8.
                    HEAT_OF_COMBUSTION = 46460.
```

IDEAL = .TRUE. /

&SURF ID='FIRE1',HRRPUA=488.8888889, COLOR='RED', /

&VENT XB= 0.4336038969,0.7336038969,-0.4336038969,-0.7336038969,0.25, 0.25, SURF_ID= 'FIRE1',/

/****************** Devices **

&DEVC ID='Temperature Tree 1.1', XB=0.3007611845,0.3007611845,-0.3007611845,-0.3007611845, 2.62,2.62, QUANTITY='TEMPERATURE'/

&DEVC ID='Temperature Tree 1.2', XB=0.3007611845,0.3007611845,-0.3007611845,-0.3007611845, 2.595,2.595, QUANTITY='TEMPERATURE'/

&DEVC ID='Temperature Tree 1.3', XB=0.3007611845,0.3007611845,-0.3007611845,-0.3007611845, 2.57,2.57, QUANTITY='TEMPERATURE'/

&DEVC ID='Temperature Tree 1.4', XB=0.3007611845,0.3007611845,-0.3007611845,-0.3007611845, 2.545,2.545, QUANTITY='TEMPERATURE'/

&DEVC ID='Temperature Tree 1.5', XB=0.3007611845,0.3007611845,-0.3007611845,-0.3007611845, 2.52,2.52, QUANTITY='TEMPERATURE'/

&DEVC ID='Temperature Tree 1.6', XB=0.3007611845,0.3007611845,-0.3007611845,-0.3007611845, 2.495,2.495, QUANTITY='TEMPERATURE'/

&DEVC ID='Temperature Tree 1.7', XB=0.3007611845,0.3007611845,-0.3007611845,-0.3007611845, 2.47,2.47, QUANTITY='TEMPERATURE'/

&DEVC ID='Temperature Tree 1.8', XB=0.3007611845,0.3007611845,-0.3007611845,-0.3007611845, 2.445,2.445, QUANTITY='TEMPERATURE'/

&DEVC ID='Temperature Tree 1.9', XB=0.3007611845,0.3007611845,-0.3007611845,-0.3007611845, 2.42,2.42, QUANTITY='TEMPERATURE'/

&DEVC ID='Temperature Tree 1.10', XB=0.3007611845,0.3007611845,-0.3007611845,-0.3007611845, 2.395,2.395, QUANTITY='TEMPERATURE'/

&DEVC ID='Temperature Tree 2.1', XB=0.123984489,0.123984489,-0.123984489,-0.123984489,2.62,2.62 QUANTITY='TEMPERATURE'/

&DEVC ID='Temperature Tree 2.2', XB=0.123984489,0.123984489,-0.123984489,-0.123984489,2.595,2.595 QUANTITY='TEMPERATURE'/

&DEVC ID='Temperature Tree 2.3', XB=0.123984489,0.123984489,-0.123984489,-0.123984489,2.57,2.57 QUANTITY='TEMPERATURE'/

&DEVC ID='Temperature Tree 2.4', XB=0.123984489,0.123984489,-0.123984489,-0.123984489,2.545,2.545 QUANTITY='TEMPERATURE'/

&DEVC ID='Temperature Tree 2.5', XB=0.123984489,0.123984489,-0.123984489,-0.123984489,2.52,2.52 QUANTITY='TEMPERATURE'/

&DEVC ID='Temperature Tree 2.6', XB=0.123984489,0.123984489,-0.123984489,-0.123984489,2.495,2.495 QUANTITY='TEMPERATURE'/

&DEVC ID='Temperature Tree 2.7', XB=0.123984489,0.123984489,-0.123984489,-0.123984489,2.47,2.47
QUANTITY='TEMPERATURE'/

&DEVC ID='Temperature Tree 2.8', XB=0.123984489,0.123984489,-0.123984489,-0.123984489,2.445,2.445
QUANTITY='TEMPERATURE'/

&DEVC ID='Temperature Tree 2.9', XB=0.123984489,0.123984489,-0.123984489,-0.123984489,2.42,2.42
QUANTITY='TEMPERATURE'/

&DEVC ID='Temperature Tree 2.10', XB=0.123984489,0.123984489,-0.123984489,-0.123984489,2.395,2.395
QUANTITY='TEMPERATURE'/

&DEVC ID='Temperature Tree 2.11', XB=0.123984489,0.123984489,-0.123984489,-0.123984489,2.37,2.37
QUANTITY='TEMPERATURE'/

&DEVC ID='Temperature Tree 3.1', XB=-0.052792206,-0.052792206,0.052792206,0.052792206,2.62,2.62,
QUANTITY='TEMPERATURE'/

&DEVC ID='Temperature Tree 3.2', XB=-0.052792206,-0.052792206,0.052792206,0.052792206,2.595,2.595,
QUANTITY='TEMPERATURE'/

&DEVC ID='Temperature Tree 3.3', XB=-0.052792206,-0.052792206,0.052792206,0.052792206,2.57,2.57,
QUANTITY='TEMPERATURE'/

&DEVC ID='Temperature Tree 3.4', XB=-0.052792206,-0.052792206,0.052792206,0.052792206,2.545,2.545,
QUANTITY='TEMPERATURE'/

&DEVC ID='Temperature Tree 3.5', XB=-0.052792206,-0.052792206,0.052792206,0.052792206,2.52,2.52,
QUANTITY='TEMPERATURE'/

&DEVC ID='Temperature Tree 3.6', XB=-0.052792206,-0.052792206,0.052792206,0.052792206,2.495,2.495,
QUANTITY='TEMPERATURE'/

&DEVC ID='Temperature Tree 3.7', XB=-0.052792206,-0.052792206,0.052792206,0.052792206,2.47,2.47,
QUANTITY='TEMPERATURE'/

&DEVC ID='Temperature Tree 3.8', XB=-0.052792206,-0.052792206,0.052792206,0.052792206,2.445,2.445,
QUANTITY='TEMPERATURE'/

&DEVC ID='Temperature Tree 3.9', XB=-0.052792206,-0.052792206,0.052792206,0.052792206,2.42,2.42,
QUANTITY='TEMPERATURE'/

&DEVC ID='Temperature Tree 3.10', XB=-0.052792206,-0.052792206,0.052792206,0.052792206,2.395,2.395,
QUANTITY='TEMPERATURE'/

&DEVC ID='Temperature Tree 3.11', XB=-0.052792206,-0.052792206,0.052792206,0.052792206,2.37,2.37,
QUANTITY='TEMPERATURE'/

&DEVC ID='Temperature Tree 3.12', XB=-0.052792206,-0.052792206,0.052792206,0.052792206,2.345,2.345,
QUANTITY='TEMPERATURE'/

&DEVC ID='Temperature Tree 4.1', XB=-0.229568901,-0.229568901,0.229568901,0.229568901, 2.62,2.62,
QUANTITY='TEMPERATURE'/

&DEVC ID='Temperature Tree 4.2', XB=-0.229568901,-0.229568901,0.229568901,0.229568901, 2.595,2.595, QUANTITY='TEMPERATURE'/

&DEVC ID='Temperature Tree 4.3', XB=-0.229568901,-0.229568901,0.229568901,0.229568901, 2.57,2.57, QUANTITY='TEMPERATURE'/

&DEVC ID='Temperature Tree 4.4', XB=-0.229568901,-0.229568901,0.229568901,0.229568901, 2.545,2.545, QUANTITY='TEMPERATURE'/

&DEVC ID='Temperature Tree 4.5', XB=-0.229568901,-0.229568901,0.229568901,0.229568901, 2.52,2.52, QUANTITY='TEMPERATURE'/

&DEVC ID='Temperature Tree 4.6', XB=-0.229568901,-0.229568901,0.229568901,0.229568901, 2.495,2.495, QUANTITY='TEMPERATURE'/

&DEVC ID='Temperature Tree 4.7', XB=-0.229568901,-0.229568901,0.229568901,0.229568901, 2.47,2.47, QUANTITY='TEMPERATURE'/

&DEVC ID='Temperature Tree 4.8', XB=-0.229568901,-0.229568901,0.229568901,0.229568901, 2.445,2.445, QUANTITY='TEMPERATURE'/

&DEVC ID='Temperature Tree 4.9', XB=-0.229568901,-0.229568901,0.229568901,0.229568901, 2.42,2.42, QUANTITY='TEMPERATURE'/

&DEVC ID='Temperature Tree 4.10', XB=-0.229568901,-0.229568901,0.229568901,0.229568901, 2.395,2.395, QUANTITY='TEMPERATURE'/

&DEVC ID='Temperature Tree 4.11', XB=-0.229568901,-0.229568901,0.229568901,0.229568901, 2.37,2.37, QUANTITY='TEMPERATURE'/

&DEVC ID='Temperature Tree 4.12', XB=-0.229568901,-0.229568901,0.229568901,0.229568901, 2.345,2.345, QUANTITY='TEMPERATURE'/

&DEVC ID='Temperature Tree 4.13', XB=-0.229568901,-0.229568901,0.229568901,0.229568901, 2.32,2.32, QUANTITY='TEMPERATURE'/

&DEVC ID='Temperature Tree 4.14', XB=-0.229568901,-0.229568901,0.229568901,0.229568901, 2.295,2.295, QUANTITY='TEMPERATURE'/

&DEVC ID='Temperature Tree 4.15', XB=-0.229568901,-0.229568901,0.229568901,0.229568901, 2.27,2.27, QUANTITY='TEMPERATURE'/

&DEVC ID='Temperature Tree 5.1', XB=-0.4063455597,-0.4063455597,0.4063455597,0.4063455597,2.62,2.62, QUANTITY='TEMPERATURE'/

&DEVC ID='Temperature Tree 5.2', XB=-0.4063455597,-0.4063455597,0.4063455597,0.4063455597,2.595,2.595, QUANTITY='TEMPERATURE'/

&DEVC ID='Temperature Tree 5.3', XB=-0.4063455597,-0.4063455597,0.4063455597,0.4063455597,2.57,2.57, QUANTITY='TEMPERATURE'/

&DEVC ID='Temperature Tree 5.4', XB=-0.4063455597,-0.4063455597,0.4063455597,0.4063455597,2.545,2.545, QUANTITY='TEMPERATURE'/

&DEVC ID='Temperature Tree 5.5', XB=-0.4063455597,-0.4063455597,0.4063455597,0.4063455597,2.52,2.52, QUANTITY='TEMPERATURE'/

&DEVC ID='Temperature Tree 5.6', XB=-0.4063455597,-0.4063455597,0.4063455597,0.4063455597,2.495,2.495, QUANTITY='TEMPERATURE'/

&DEVC ID='Temperature Tree 5.7', XB=-0.4063455597,-0.4063455597,0.4063455597,0.4063455597,2.47,2.47, QUANTITY='TEMPERATURE'/

&DEVC ID='Temperature Tree 5.8', XB=-0.4063455597,-0.4063455597,0.4063455597,0.4063455597,2.445,2.445, QUANTITY='TEMPERATURE'/

&DEVC ID='Temperature Tree 5.9', XB=-0.4063455597,-0.4063455597,0.4063455597,0.4063455597,2.42,2.42, QUANTITY='TEMPERATURE'/

&DEVC ID='Temperature Tree 5.10', XB=-0.4063455597,-0.4063455597,0.4063455597,0.4063455597,2.395,2.395, QUANTITY='TEMPERATURE'/

&DEVC ID='Temperature Tree 5.11', XB=-0.4063455597,-0.4063455597,0.4063455597,0.4063455597,2.37,2.37, QUANTITY='TEMPERATURE'/

&DEVC ID='Temperature Tree 5.12', XB=-0.4063455597,-0.4063455597,0.4063455597,0.4063455597,2.345,2.345, QUANTITY='TEMPERATURE'/

&DEVC ID='Temperature Tree 5.13', XB=-0.4063455597,-0.4063455597,0.4063455597,0.4063455597,2.32,2.32, QUANTITY='TEMPERATURE'/

&DEVC ID='Temperature Tree 5.14', XB=-0.4063455597,-0.4063455597,0.4063455597,0.4063455597,2.295,2.295, QUANTITY='TEMPERATURE'/

&DEVC ID='Temperature Tree 5.15', XB=-0.4063455597,-0.4063455597,0.4063455597,0.4063455597,2.27,2.27, QUANTITY='TEMPERATURE'/

&DEVC ID='Temperature Tree 5.16', XB=-0.4063455597,-0.4063455597,0.4063455597,0.4063455597,2.245,2.245, QUANTITY='TEMPERATURE'/

&DEVC ID='Temperature Tree 6.1', XB=-0.583122292,-0.583122292,0.583122292,0.583122292,2.62,2.62, QUANTITY='TEMPERATURE'/

&DEVC ID='Temperature Tree 6.1', XB=-0.583122292,-0.583122292,0.583122292,0.583122292,2.595,2.595, QUANTITY='TEMPERATURE'/

&DEVC ID='Temperature Tree 6.1', XB=-0.583122292,-0.583122292,0.583122292,0.583122292,2.57,2.57, QUANTITY='TEMPERATURE'/

&DEVC ID='Temperature Tree 6.1', XB=-0.583122292,-0.583122292,0.583122292,0.583122292,2.545,2.545, QUANTITY='TEMPERATURE'/

&DEVC ID='Temperature Tree 6.1', XB=-0.583122292,-0.583122292,0.583122292,0.583122292,2.52,2.52, QUANTITY='TEMPERATURE'/

&DEVC ID='Temperature Tree 6.1', XB=-0.583122292,-0.583122292,0.583122292,0.583122292,2.495,2.495, QUANTITY='TEMPERATURE'/

&DEVC ID='Temperature Tree 6.1', XB=-0.583122292,-0.583122292,0.583122292,0.583122292,2.47,2.47, QUANTITY='TEMPERATURE'/

&DEVC ID='Temperature Tree 6.1', XB=-0.583122292,-0.583122292,0.583122292,0.583122292,2.445,2.445, QUANTITY='TEMPERATURE'/

&DEVC ID='Temperature Tree 6.1', XB=-0.583122292,-0.583122292,0.583122292,0.583122292,2.42,2.42, QUANTITY='TEMPERATURE'/

&DEVC ID='Temperature Tree 6.1', XB=-0.583122292,-0.583122292,0.583122292,0.583122292,2.395,2.395, QUANTITY='TEMPERATURE'/

&DEVC ID='Temperature Tree 6.1', XB=-0.583122292,-0.583122292,0.583122292,0.583122292,2.37,2.37, QUANTITY='TEMPERATURE'/

&DEVC ID='Temperature Tree 6.1', XB=-0.583122292,-0.583122292,0.583122292,0.583122292,2.345,2.345, QUANTITY='TEMPERATURE'/

&DEVC ID='Temperature Tree 6.1', XB=-0.583122292,-0.583122292,0.583122292,0.583122292,2.32,2.32, QUANTITY='TEMPERATURE'/

&DEVC ID='Temperature Tree 6.1', XB=-0.583122292,-0.583122292,0.583122292,0.583122292,2.295,2.295, QUANTITY='TEMPERATURE'/

&DEVC ID='Temperature Tree 6.1', XB=-0.583122292,-0.583122292,0.583122292,0.583122292,2.27,2.27, QUANTITY='TEMPERATURE'/

&DEVC ID='Temperature Tree 6.1', XB=-0.583122292,-0.583122292,0.583122292,0.583122292,2.245,2.245, QUANTITY='TEMPERATURE'/

&DEVC ID='Temperature Tree 6.1', XB=-0.583122292,-0.583122292,0.583122292,0.583122292,2.22,2.22, QUANTITY='TEMPERATURE'/

&SLCF PBX=0.53, QUANTITY='VELOCITY'/

&SLCF PBX=0.53, QUANTITY='VELOCITY',VECTOR=.TRUE. /

&SLCF PBZ=2.615, QUANTITY='VELOCITY',VECTOR=.TRUE. / -2.5 cm

&SLCF PBZ=2.590, QUANTITY='VELOCITY',VECTOR=.TRUE. / -5.0 cm

&SLCF PBZ=2.540, QUANTITY='VELOCITY',VECTOR=.TRUE. / -10.0 cm

&SLCF PBZ=2.490, QUANTITY='VELOCITY',VECTOR=.TRUE. / -15.0 cm

&SLCF PBZ=2.440, QUANTITY='VELOCITY',VECTOR=.TRUE. / -20.0 cm

&SLCF PBZ=2.615, QUANTITY='VELOCITY'/ -2.5 cm

&SLCF PBZ=2.590, QUANTITY='VELOCITY'/ -5.0 cm

&SLCF PBZ=2.540, QUANTITY='VELOCITY'/ -10.0 cm

&SLCF PBZ=2.490, QUANTITY='VELOCITY'/ -15.0 cm

&SLCF PBZ=2.440, QUANTITY='VELOCITY'/ -20.0 cm

&SLCF PBZ=2.615, QUANTITY='TEMPERATURE'/ -2.5 cm

&SLCF PBZ=2.590, QUANTITY='TEMPERATURE'/ -5.0 cm

&SLCF PBZ=2.540, QUANTITY='TEMPERATURE'/ -10.0 cm

&SLCF PBZ=2.490, QUANTITY='TEMPERATURE'/ -15.0 cm

```
&SLCF PBZ=2.440, QUANTITY='TEMPERATURE'/  -20.0 cm

&SLCF PBX=0.53,QUANTITY='HRRPUV'  /

/*******************MATERIAL & SURFACE ***********************************************************************

&MATL ID              = 'ASBESTOS-CEMENT'
    DENSITY          = 1400.
    CONDUCTIVITY      = 0.744
    SPECIFIC_HEAT     = 0.84 /


&MATL ID              = 'SKAMOTEC'
    DENSITY          = 1600.
    CONDUCTIVITY      = 0.69
    SPECIFIC_HEAT     = 0.84 /


&MATL ID              = 'STEEL'
    EMISSIVITY        = 0.5
    DENSITY          = 7850.
    CONDUCTIVITY      = 45.8
    SPECIFIC_HEAT     = 0.46 /


&SURF ID              = 'FLOOR1'
    COLOR            = 'BRICK'
    MATL_ID          = 'ASBESTOS-CEMENT'
    THICKNESS         = 0.05 /


&SURF ID              = 'BURNER'
    COLOR            = 'BLACK'
    MATL_ID          = 'STEEL'
    GEOMETRY                    = 'CYLINDRICAL'
    THICKNESS         = 0.005 /
&SURF ID              = 'ROOF1'
    COLOR            = 'GRAY'
```

```
    BACKING                     = 'EXPOSED'
    MATL_ID          = 'SKAMOTEC'
    THICKNESS        = 0.05 /
&TAIL /
/****************** End ***************************************************************************
```